Tampere University

ALEXANDRA SHAKUN

Low-Loss Energy Harvesting Materials from Rubber-Nanodiamond Composites

Tampere University Dissertations 270

Tampere University Dissertations 270

ALEXANDRA SHAKUN

Low-Loss Energy Harvesting Materials from Rubber-Nanodiamond Composites

ACADEMIC DISSERTATION
To be presented, with the permission of
the Faculty of Engineering and Natural Sciences
of Tampere University,
for public discussion in the auditorium FA032 Pieni sali 1
of the Festia building, Korkeakoulunkatu 8, Tampere,
on 23 June 2020, at 12 o'clock.

ACADEMIC DISSERTATION
Tampere University, Faculty of Engineering and Natural Sciences
Finland

Responsible supervisor and Custos
Assistant Professor
Essi Sarlin
Tampere University
Finland

Supervisor
Professor
Jyrki Vuorinen
Tampere University
Finland

Pre-examiners
Professor
Friedrich Kremer
University of Leipzig
Germany

Professor
James Busfield
Queen Mary University of London
United Kingdom

Opponents
Professor
James Busfield
Queen Mary University of London
United Kingdom

Professor
Dariusz M. Bieliński
Lodz University of Technology
Poland

The originality of this thesis has been checked using the Turnitin OriginalityCheck service.

Cover design: Roihu Inc.

ISBN 978-952-03-1605-1 (print)
ISBN 978-952-03-1606-8 (pdf)
ISSN 2489-9860 (print)
ISSN 2490-0028 (pdf)
http://urn.fi/URN:ISBN:978-952-03-1606-8

PunaMusta Oy – Yliopistopaino
Tampere 2020

To my family

PREFACE

The present research was conducted in the Materials Science and Environmental Engineering unit of Tampere University in 2015-2019. Moreover, the study included a research period at the Elastomer Technology group of the University of Twente, Netherlands, during June-July 2018. The research was funded by the Tampere University Graduate School and the Finnish Foundation for Technology Promotion (TES). The travelling costs were covered by the TUT on World Tour funding.

I express my sincere gratitude to my supervisors Asst. Prof. Essi Sarlin and Prof. Jyrki Vuorinen for the guidance, support, advices and time. I want to thank Prof. Anke Blume and Assoc. Prof. Wilma Dierkes for inviting me to the University of Twente and providing a lot of support and advices. Special thanks to Dr. Rafał Anyszka for the fruitful discussions, practical help, encouragement and all the nice moments. Lot of thanks to Dr. Minna Poikelispää for supporting and guiding me with the humor though the magic world of rubbers during these years. Thanks to Sarianna Palola for sharing the PhD experience and for her valuable peer support. I am grateful to all my current and former colleagues at Tampere University for the supportive atmosphere and discussions. Thanks to the colleagues from the University of Twente for their hospitality, help and a great time.

I want to thank my family, parents and in-laws for their patience, encouragement and inspiration. I am truly grateful for their interest in my work and trust in me. Thousands thanks to Sakari for being my rock despite the hard times, and to my dearests Luka, Leo and the new baby for lighting my way and giving me power to move forward.

Tampere, November 2019

Alexandra Shakun

ABSTRACT

Sustainable energy harvesting opportunities have attracted much interest in the past decades. Among the energy harvesters, dielectric elastomer generators (DEGs) offer a comparably new and very eco-efficient approach for harvesting energy from the ocean waves, human motion, vibrations and pressure. In such applications, dielectric elastomers are used instead of piezoelectrics, resulting in high energy generating potential combined with relatively low cost and weight. However, the technology related to DEGs is still at the early stage and the existing DEG prototypes cannot achieve economic profitability yet. One major reason for that is the lack of efficient low-loss elastomers. Most elastomeric materials currently used in DEGs have high dielectric and viscous losses, and others have poor mechanical properties and high cost. Moreover, none of these materials is designed for an energy harvesting application. These drawbacks significantly reduce the attractiveness and efficiency of energy harvesting. However, a significant improvement in the efficiency of DEGs can be possible by developing high performance elastomers with low dielectric and viscoelastic losses – e.g., silicone, natural rubber, or others.

The present research is focusing on material-related losses of elastomer films in order to understand the contribution of elastomer type, as well as the presence of impurities and fillers, to the potential performance of such materials in energy harvesting. The major focus of the research is set on dielectric and mechanical hysteresis losses at low frequencies and ambient temperatures. Moreover, the dynamic and mechanical properties of the materials are assessed. Furthermore, the addition of small amounts of nanodiamonds (NDs) to the elastomer is viewed as one of the opportunities of achieving the low-loss membranes, as NDs are expected to minimize dielectric and viscous losses in certain conditions. This effect is most probably related to the high structural activity of NDs and its active surface. Due to the active surface, NDs can be chemically modified to adjust their interaction with elastomer. Thus, finally, the effect of selected filler surface treatments on loss properties of the films is investigated, as a filler-matrix interface is a typical origin of high losses. Indeed, the results of this study showed that the higher amount of natural proteins caused higher dielectric losses in the latex-based compounds, but resulted in lower dynamic loss tangent. Moreover, potassium hydroxide stabilizer

used in latex compounding was found to increase the material-related losses of the materials. The described dielectric and mechanical losses of the films were reduced by the post-treatment with water or acetone. Finally, the addition of NDs containing the chemical groups able to participate in the crosslinking reactions showed a pronounced reduction of mechanical losses, especially in the PDMS composites.

The outcomes of the research help to reduce losses and gain more understanding of the key factors affecting the elastomer performance in DEGs. This knowledge can contribute to the development of energy harvesters, which are more economically preferable and easier to mass-produce than currently available prototypes. Moreover, such improvements significantly enhance economic feasibility of wave energy harvesters, and other types of dielectric energy harvesters, including wearable generators. Low-loss elastomeric films can be implemented in other industrial areas. For example, elastomers with reduced dielectric and viscous losses may enhances the performance of variable capacitors, which are used as stretchable sensors applied in sports garments, biomedical field and robotics. Finally, tire industry can benefit from the reduced dynamic mechanical losses in rubbers, which indicate the reduction of tire rolling resistance and, thus, lead to less fuel consumption.

CONTENTS

SYMBOLS AND ABBREVIATIONS

Symbols

a	fitting parameter of H-N equation
a_1	green–red color component (L*ab color scale) of an unstained sample
a_2	green–red color component (L*ab color scale) of a stained sample
A_{Load}	area under loading curve
A_{Unload}	area under unloading curve
b	fitting parameter of H-N equation
b_1	blue–yellow color component (L*ab color scale) of an unstained sample
b_2	blue–yellow color component (L*ab color scale) of a stained sample
E	electric field
E'	storage modulus
E"	loss modulus
E*	complex elastic modulus
ΔE_{ab}^*	difference between in colors before and after staining
E_b	elongation at break
F	formula weight in phr
f	frequency
G’	shear modulus (storage)
ΔH	hysteresis loss
L_1^*	lightness of an unstained sample
L_2^*	lightness of a stained sample
m_0	initial weight of ae specimen
M_{10}/ M_{50}/ M_{100}	modulus at 10%/50%/100% elongation
m_d	weight of a dried specimen
m_s	weight of a swollen specimen
1/Q	apparent crosslink density
Q	swelling value

R	universal gas constant (8.314 J/(K mol))
T	temperature
t	time
tan d	dielectric loss factor
tan δ	mechanical loss factor (DMA)
T_g	glass transition temperature
TS	tensile strength
V_H	high voltage source
V_L	low voltage source
Δε	step-like change in relative dielectric permittivity
ε	strain
ε'	relative dielectric permittivity
ε''	dielectric loss
ε*	complex dielectric permittivity
ε_0	vacuum permittivity (8.85×10^{-12} F/m)
ε_∞	high frequency (unrelaxed) dielectric permittivity
ε_s	static (relaxed) dielectric permittivity
ε_A	strain amplitude (DMA)
λ	stretch ratio
σ	stress
σ'	real part of electrical conductivity
σ''	imaginary part of electrical conductivity
σ_A	stress amplitude (DMA)
σ_{DC}	electronic (direct current) conductivity
τ	relaxation time
ω	angular frequency

Abbreviations

AC	alternating current
ATR	attenuated total reflectance
BT	barium titanite
DC	direct current
DEA	dielectric elastomer actuator
DEG	dielectric elastomer generator
DET	dielectric elastomer transducer
DMA	dynamic mechanical analysis
DMF	N,N-dimethylformamide

dNR	deproteinized natural rubber
DSC	differential scanning calorimetry
DTG	mass loss rate
ED	1,2-epoxy-9-decene
EDS	energy-dispersive X-ray spectroscopy
FTIR	Fourier-transform infrared analysis
GOPTMS	3-glycidoxypropyltrimethoxysilane
H-N	Havriliak-Negami
HTV	high-temperature vulcanizable
KOH	potassium hydroxide
LCOE	levelized cost of electricity
MBT	2-mercaptobenzothiazole
ND	nanodiamond
NR	natural rubber
ODMMS	octadecyldimethylmethoxysilane
PDMS	polydimethylsiloxane
phr	parts per hundred rubber
pNR	prevulcanized natural rubber
PU	polyurethane
RQ	research question
RTV	room-temperature vulcanizable
S	sulfur
SBR	styrene-butadiene rubber
SEM	scanning electron microscope
SMR	Standard Malaysian Rubber
TESPD	bis-3-triethoxysilylpropyldisulfide
TGA	thermal gravimetric analysis
VDMES	vinyldimethylethoxysilane
VHB	Commercial acrylic adhesive tape VHB4910, 3M
VTMS	Vinyltrimethoxysilane
WEC	wave energy converter
ZDBC	zinc dibutyldithiocarbamate
ZnO	Zinc oxide

ORIGINAL PUBLICATIONS

Unpublished manuscript

Publication I A. Shakun, E. Sarlin, J. Vuorinen, Energy dissipation in natural rubber latex films: the effect of stabilizers, leaching and acetone-treatment, pp. 1-24.

Published manuscripts

Publication II A. Shakun, E. Sarlin, J. Vuorinen, Natural rubber - nanodiamond films for the minimisation of losses in dielectric energy harvesters, International Journal of Exergy (2018) pp. 170-185.

Publication III A. Shakun, E. Sarlin, J. Vuorinen, Material-related losses of natural rubber composites with surface-modified nanodiamonds, Journal of Applied Polymer Science (2019) p. 48629.

Publication IV A. Shakun, R. Anyszka, E. Sarlin, A. Blume, J. Vuorinen, Influence of surface modified nanodiamonds on dielectric and mechanical properties of silicone composites, Polymers, (2019) p. 1104.

AUTHOR'S CONTRIBUTION

The author is responsible for the planning, experimental work, analysis of the results and writing of the manuscripts. Together with the author, Rafal Anyszka actively participated in the planning the experiments and analyzing the results reported in the Publication IV. Essi Sarlin is responsible for all SEM images and EDS analysis. All the authors participated in the planning of the experiments, commenting and writing the manuscripts.

1 INTRODUCTION

Permanent climate changes and increasing CO_2 emissions originating from the human activity have been a major concern during the past decades [1]. European statistics reveals that carbon dioxide production originating from transportation and energy production continues to increase [2]. This sets a request for the new green energy sources and related technologies. Energy harvesting from ocean waves has a high potential and, unlike wind or solar energy, wave energy harvesting can be available throughout a year without disruptions.

Currently, most of the offshore wave energy converters (WECs) contain hydraulic, pneumatic, or other heavy mechanisms that have a large size and numerous moving parts. They are also prone to corrosion in severe ocean conditions. These drawbacks are eliminated in WECs based on dielectric elastomers, which show promising results and have been used in working small- and full-scale prototypes [3; 4]. Dielectric elastomer generators (DEGs) can be very eco-efficient, as the greenhouse gas emission of a full-scale wave energy harvester based on natural rubber is estimated about 1.5 g per kWh [5], while coal-burning and photovoltaic systems produce about 975 g CO_2-eq./kWh and 36.8 g CO_2-eq./kWh, respectively [6]. Except for wave energy harvesting [5; 7-10], DEGs are known to harvest energy from human body motion [11; 12], vibrations [13] and pressure [14]. In such applications, dielectric elastomers are usually used instead of piezoelectric materials or in addition to those, showing good potential for the energy generation, as well as comparably low cost and weight.

Although we are surrounded with many potential energy sources, not all this energy is available for harvesting. The energy generated with DEGs depends on the amount of energy available for conversion and the energy lost during the conversion, as can be seen from Figure 1. For example, the wave energy available for the conversion into electricity is usually limited by the wave period and the set frequency range of the device, while the energy loss originates from many factors including the elastomer membrane, compliant electrodes, type of the harvesting cycle, etc. The ratio between the output and input energy during the conversion is known as energy efficiency. As the technology related to DEGs is still at the early stage [15], the output

energy of DEGs is generally very low and the cost of wave energy obtained by the current DEG prototypes is approximated as 0.2 USD per kWh [3], which is higher than the cost of solar energy. In addition to the development of the new DEG designs, the control over material losses is important in improving the profitability of DEGs. Any significant improvement in the efficiency of DEGs is possible only by developing a high performance elastomer – silicone, natural rubber, or other [4]. Consequently, with the use of tailor-made high-performance materials the cost of energy obtained with wave DEG can be reduced to 0.05-0.11 USD per kWh [5; 16].

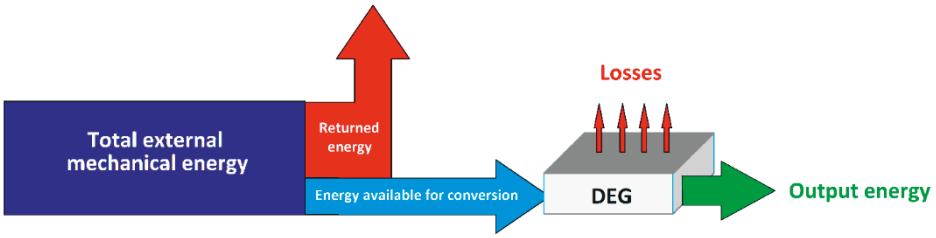

Figure 1. Scheme of the mechanical to electrical energy conversion of DEG, adapted from [17]

Despite the active ongoing research on wave energy harvesting [18], little attention has been paid to the modification of dielectric elastomer membrane used in DEGs. Many elastomeric materials currently used in DEGs have high dielectric and viscous losses, and others have poor mechanical properties and high cost. Moreover, none of these materials is designed for energy harvesting application. These drawbacks significantly reduce the attractiveness and efficiency of energy harvesting. Therefore, tailor-made dielectric elastomer membranes are in demand in order to achieve high efficiency and profitability of DEGs [4]. Moreover, more understanding of fundamental factor affecting the dielectric losses of such membranes is needed, which would contribute not only to the development of elastomeric materials for DEGs, but other application areas as well.

Outside DEG applications, elastomeric films with low material losses can be implemented in other industrial areas. For example, elastomers with reduced dielectric and viscous losses may enhance the performance of variable capacitors, which are used as stretchable sensors applied in sports garments, biomedical field and robotics. Moreover, tire industry can benefit from the reduced dynamic mechanical losses, which indicate the reduction of tire rolling resistance and, thus, lead to less fuel consumption. Thus, the findings related to the reduction of dielectric and mechanical losses in elastomers can be beneficial in the other diverse elastomer engineering applications.

2 DIELECTRIC ELASTOMER GENERATORS

Dielectric elastomer generator is a type of energy harvester transforming mechanical motion of an ambient source into electricity. The working principle of a DEG is based on changing capacitance of the dielectric elastomer membranes in-between the compliant electrodes, which occurs during stretching and charging cycles. Change in the capacitance leads to the change in electrical potential, which corresponds to the energy available for harvesting. Unlike piezoelectric generators, DEGs are passive devices and require an external energy source for charging their electrodes. Most often, a high voltage source up to 2-3 kV is used. However, other systems requiring only 240 V [19] or self-priming solutions [20; 21] are available in the literature. The need of high voltage is common for dielectric elastomer transducers (DETs) and is often related to the comparably poor electromechanical properties and high losses of the used dielectric membranes [18].

2.1 Working principle and efficiency

The basic working principle of a dielectric elastomer harvester is schematically shown in Figure 2a. A force is applied on the dielectric elastomer sheet placed between compliant electrodes, and then the "low voltage" source V_L is connected to the circuit in order to generate the charge on the electrodes while the membrane is being stretched (step A). During the step B, the membrane is disconnected from the energy source and the mechanical force is being released causing material contraction. Thus, the voltage is being build-up between the electrodes due to the change in capacitance, and is being collected to the battery ("high voltage" source V_H). After battery is disconnected from the circuit, the new cycle starts from the step A. The described working principle is based on the simplest constant charge cycle [22]. The other possible types of cycles are constant voltage and field, where the latter is the least common one. The word "constant" refers only to the state when the stretched membrane is being recovered to the initial state. The three types of harvesting cycles are shown in Figure 2b, where E is electric field and λ is the stretch

ratio. Stages 1-2 and 3-4 show the stretching and contraction of the membrane respectively, while stage 2-3 designates charging of the electrodes. [7; 23]

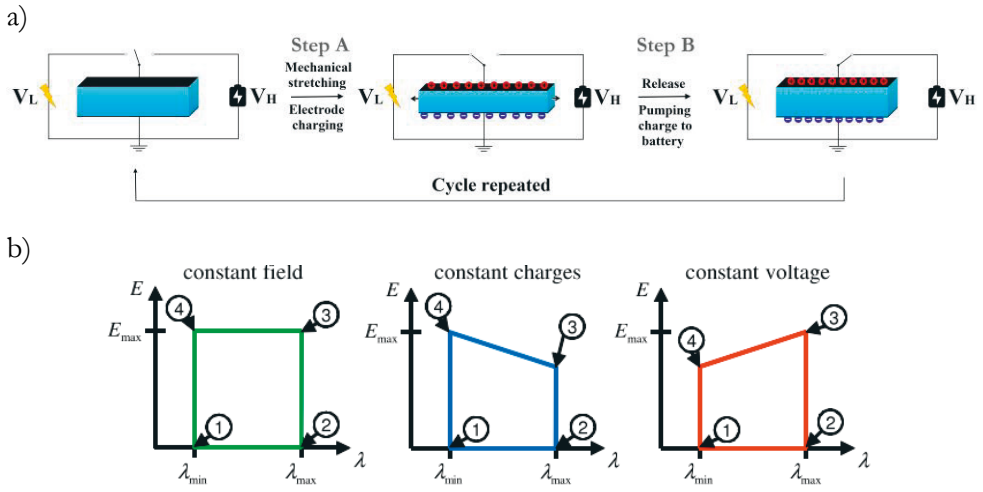

Figure 2. a) The working principle of a DEG by represented stretch-release cycle (based on [22]) and b) comparison of the three different harvesting cycles [7].

Having the same working principle, dielectric generators are available in a number of different forms and designs. Dielectric elastomers can be applied in, for example, circular diaphragm DEG with an oscillating column architecture [4], parallelogram-shaped DEGs [24], Anaconda concept [25] and others. Dielectric stretchable capacitors can be also used in electrostatic converters, as described in [26], which expectedly yield more than 60% efficiency from the low energy density sources and have a potential for wave energy harvesting. However, in most recent studies such high efficiency has never been achieved. For example, Ahnert et al. [10] estimated the possible specific energy density for the wave harvester based on Danfoss PolyPower material to be 5 mJ/g at 0.1 Hz working frequency with charging voltage about 650 V. The maximum efficiency was expected to be 42% in this case. Moreover, the authors made an assumption that return on solely material investment in such conditions would be about 10 years. Similar energy densities were obtained by Jean-Mistral and co-workers [19] for an acrylic-based harvester when using electret supplying instead of a traditional high voltage source. Thus, only 240 V charging voltage was able to yield 6 mJ/g energy at 1 Hz cycle. When using high voltage with the acrylic-based DEG, the efficiency was about 37% [22] at 2.5 kV bias voltage with energy yield of 131 mJ/g a cycle, or about 27% [27] with 560 mJ/g yield

at 2 kV for a 0.5 Hz cycle. However, only 2 - 3 % efficiency was reported by Kang et al. [12] for the acrylic-based wearable generator functioning at 1 kV charging voltage. McKay et al. [21] and Zanini et al. [20] investigated a self-priming DEG that can eliminate the need to re-supply the charge to the system, but such systems tend to have lower energy densities compared to the traditional systems.

The findings of these different studies may seem contradictory at a first glance that the same material shows so different efficiency. Due to the significant differences in DEG designs and harvesting cycle parameters, direct comparison of the efficiency and performance of DEGs from different studies is challenging. It is obvious that efficiency and energy output depends not solely on the used dielectric material but also a lot on the generator design, type and quality of electrodes, charging voltage, strain levels, cycle length, dielectric properties of the membrane and other possible factors [12]. For example, the work of Binh et al. [17] confirms the relation between the bias voltage and the amount of generated energy at the same stretch levels.

When focusing solely on the effect of dielectric elastomer type on the DEG efficiency, the control over material-related losses becomes crucial in increasing the efficiency of DEGs. With a large variety of material choices and design configurations available, no study has been able to take into account all the critical factors and create a universal model providing a tool for designing an optimal DEG from the material- and loss- viewpoint. Nevertheless, much focus has been set on studying and understanding the sources of energy dissipation in DEGs, thus contributing to the development of the best-performing elastomer harvesters. Materials utilized for an energy harvesting application should have minimal energy dissipation in order to perform well and produce sufficient amount of energy to be economically preferable.

2.2 Material-related sources of energy dissipation

In case of electrically active elastomers, sources of energy dissipation can be related to the nature of the polymer and its elasticity, as well as to current leakage. The main sources of energy dissipation originating from the elastomer itself are shown in Figure 3, and they are valid for different types of DETs. Due to the viscoelastic nature of elastomers, part of the losses arises from the chain motion, slipping and rearrangement during the stretch-release cycle. As an electric field is involved, some

energy is lost during the field-induced dipole and chain motion, as well as the current leak due to the presence of free electrons and ions in the system.

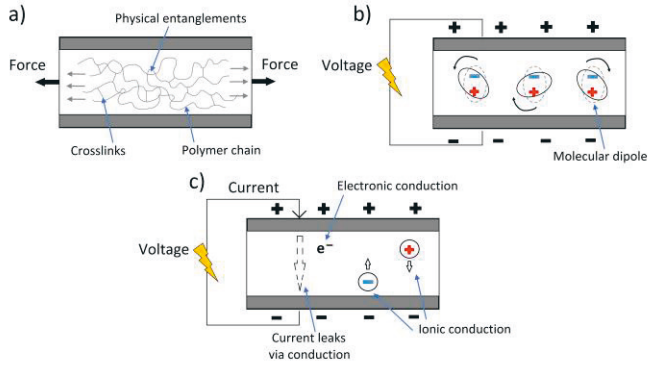

Figure 3. Scheme of relaxation-based dissipative processes due to a) sliding of polymer chains; b) re-orientation of dipoles under the applied electric field; and c) a dissipation based on charge transport (current leakage), adapted from [22; 28].

The model of energy dissipation process in DETs is developed and described in details in the work of Foo et al. [28], while other works focus also on the performance and energy outcome [17; 22; 29; 30]. The models depend a lot on the type of the transducer used. Circular film generators with biaxial stretching are the most popular ones, although a model for uniaxialy stretched elastomer strips is also available [17]. Furthermore, a large number of models describing the performance of DETs, including energy dissipation processes and prediction of the power output in DEGs, is currently available [22; 28; 29; 31; 32]. Most of these models take commercial acrylic VHB4905 tape (3M) as a reference for the calculations. Some studies concerning Danfoss PolyPower silicones [8; 10; 17; 33] and NR [34] are also known. Moreover, one should remember the dependence of these models on the type of generator and elastomeric material used. For example, due to a strongly viscous nature of the VHB acrylic film, most of acrylic-based models may not be applicable to other elastomers. Next, the selected elastomer model may be too simplified and not correspond to the real elastomer at the most real cases. Modelling of viscoelastic behaviour of the generator is typically based on the Ogden's model, as it was stated by Kofod et al. [35] to be the simple and describing the performance of DET closest to the real-life tests when compared with Neo-Hookean and Mooney-Rivlin models. However, Wissler and Mazza [36] imply that instead, Yeoh model should be used even if it fails to describe pull-in instability in dielectric transducers. Binh et al. [17] justify the use of Mooney-Rivlin model in their study by the small strain applied for silicone DEGs. Finally, Gent model can be used to

characterize the viscoelastic behaviour of elastomer showing the stiffening effect at high stretch. Nevertheless, currently available models do not take into account all possible loss sources. For example, dielectric dissipation and the effect of compliant electrodes is often excluded from the evaluation.

In case of relaxation-based processes, the relaxation times τ are important to be known in order to decide which dissipative processes should be included into the DEG model. Dielectric relaxation due to the rotation of dipoles is negligible in scale compared to the viscoelastic relaxation and the distortion it brings by the sliding and stretching of long polymer chains. Respectively, when subjected to an external force, relaxation times are about 10^{-6} for dielectric and 10^{2} for viscoelastic relaxation at room temperature [28]. It is known [37], that both dielectric and viscoelastic losses should be minimal if the corresponding relaxation times are shorter or the same range as the disturbing oscillation, meaning that the material has enough time to recover from the distortion. Otherwise, the losses are considered to be significant enough to be mentioned in the modelling of the energy dissipation. This theory is supported in the work of Foo et al. [28] for dielectric elastomer actuators (DEAs), where the dielectric dissipation process has been excluded from the model of dissipative elastomer based on its dielectric relaxation time. In another work, Foo and co-workers [22] are mostly focusing on just viscoelastic losses, contribution of Maxwell force and current leak to the energy dissipation in DETs. Indeed, dissipation of energy through the current leak is known to increase tremendously at low cycle frequencies and high strains [31]. However, in the model, the assumption is made that dielectric properties of elastomer are independent of the strain, which is not true in most cases [38; 39].

2.2.1 Dielectric energy dissipation

All materials respond to the external disturbance in the way compensating its effects. On a macroscopic level, material responds to an applied electric field by becoming polarized. The response to the applied electric field can be instantaneous or time-dependent. Instantaneous response occurs at very high frequencies or very short times and is associated with the atomic and electronic displacements in the dielectric material [40]. At the same time, dipoles and polymer chains in a dielectric material cannot respond instantaneously with the applied electric field and require some time τ (relaxation time) for the alignment.

The dielectric response is usually obtained as complex permittivity:

$$\varepsilon^*(\omega) = \varepsilon'(\omega) - i\varepsilon''(\omega) \ , \qquad (1)$$

where $\omega = 2\pi f$ is the angular frequency, ε' is the real part of the complex dielectric permittivity and the dielectric loss (ε'') is the imaginary part. Relative dielectric permittivity ε' describes the ability of the molecules in a material to polarize under an applied electric field and also presents the energy stored in cycle. Dielectric loss ε'' is a part of the energy dissipated and transferred, for instance, into heat build-up. The example of dielectric spectra is shown in Figure 4. Relaxation peaks in ε'' spectra correspond to the step-like change in ε' ($\Delta\varepsilon$) and are associated with different polarization and relaxation mechanisms acting in the material. Moreover, each relaxation can be expressed by a specific τ. Havriliak and Negami (H-N) theory is often used to describe the dielectric relaxation process [40]:

$$\varepsilon^*(\omega) = \varepsilon_\infty + \frac{\varepsilon_s - \varepsilon_\infty}{[1+(i\omega\tau)^a]^b} \ , \qquad (2)$$

where ε_∞ is high frequency (unrelaxed) permittivity and ε_s is static (relaxed) permittivity. By changing the values of fitting parameters a and b, the H-N equation can be simplified to Cole-Cole and Cole-Davidson formulas. Phase lag existing between ε' and ε'', also known as the loss angle, can be expressed by dissipation factor tan delta (tan d) showing how much energy was lost in a cycle compared to the energy stored [41]:

$$\tan d = \frac{\varepsilon''}{\varepsilon'} \qquad (3)$$

Dielectric permittivity of material depends on its chemical composition and structure, while loss factor is also influenced by the peculiarities of molecular motion and purity of the polymer [42].

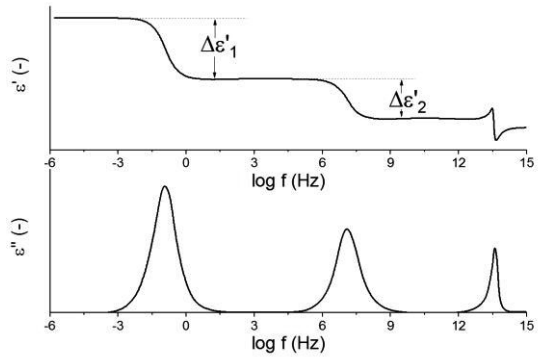

Figure 4. Dielectric spectra example, adapted from [43].

An ideal dielectric material is an insulator containing no free charge carriers that can move in electric field, but real dielectrics are able to conduct electricity due to the impurities and imperfections within the material, and their conductivity is ranging from 10^{-18} to 10^{-6} S/m [41; 44]. Thus, every dielectric also has sources of current leak. The electrical conductivity of the dielectric material can be expressed from dielectric permittivity and loss [43]:

$$\sigma'(\omega) = \omega\varepsilon_0\varepsilon''(\omega);\ \sigma''(\omega) = \omega\varepsilon_0\varepsilon'(\omega) \quad , \qquad (4)$$

where σ' and σ'' are real and imaginary part of the electrical conductivity respectively, and ε_0 = 8.854 pF/m is the dielectric permittivity of vacuum. A pure electronic conduction has no effect on dielectric permittivity ε', and ε'' increases linearly with frequency:

$$\varepsilon''(\omega) = \frac{\sigma_{DC}}{\varepsilon_0\,\omega} \quad , \qquad (5)$$

where σ_{DC} is the electronic (direct current) conductivity independent of frequency. Therefore, conductivity contribution is detected at low frequencies as a linear portion of a dielectric loss curve increasing as frequency decreases, while dielectric permittivity curve is not affected, as can be seen from Figure 5a. Finally, a dramatic increase in dielectric loss is possible at low frequency due to the parasitic effect known as electrode polarization, which is related to the blocking charges at the sample-electrode interface. Electrode polarization is more common for the complex and electrically conducting systems, especially for thin samples. Additionally, electrode polarization affects the dielectric permittivity of the sample and can mask the actual relaxation processes. [43]

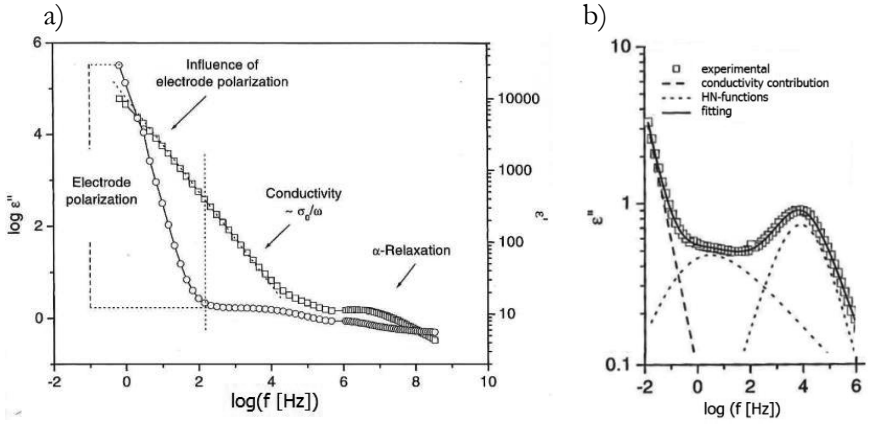

Figure 5. a) An example of the contribution of electrode polarization and electrical conductivity to ε'(circles) and ε'' (squares); and b) ε'' data analysis and fitting of a two-component system involving two Havriliak-Negami functions and conductivity contribution function. Adapted from [43].

The dielectric loss curve of a real polymeric sample can be more complex than is shown in this theoretic representation. An example of a two-component system is depicted in Figure 5b, where both equations (2) and (5) are used to model the dielectric loss response. The curve is relatively common for rubbers studied around room temperature, where the increase in dielectric loss at the frequencies above 10^4 Hz is usually associated with the segmental dynamics of the sample (α-relaxation)[45]. In such materials, the additional relaxations and the conductivity contribution are usually related to the impurities and compounding ingredients, which are present in most rubbers. Moreover, most rubbers contain different fillers aiming to enhance the properties of the elastomer. In case of such rubber composites, especially those utilizing electrically conductive fillers, charge accumulated at the material interfaces can move through the material in electric field thus leading to the increase in dielectric losses and electrical conductivity. This happens due to Maxwell-Wagner, or interfacial, polarization originating from the charge built up and accumulation at the filler-matrix interface because of significant difference in their conductivities. Moreover, when using stretchable composites under applied electric field, conduction paths have to be avoided. Even when material show no percolation in the initial state, relocation of polymer chains, filler particles moved closer to each other by external pressure and reduction of thickness during the electromechanical cycle may create percolation paths or increase current leakage before percolation. This generally leads to a short circuit and material breakdown.

2.2.2 Mechanical energy dissipation

In an ideally elastic system, all the applied mechanical energy will be returned without losses. However, in most of the real systems some part of applied energy is dissipated. Figure 6a gives a good representation of the phenomenon: when a ball is dropped from a height, it never bounces back to the same height. The saved energy can be described by the elastic storage modulus E', and the dissipated energy – by the loss modulus E". For example, rubbers are viscoelastic by nature, combining the features of both elastic and viscous behaviour. While the elastic response is instantaneous, the viscous response is dependent on time. Moreover, viscous deformation is not reversible. Therefore, viscoelastic nature of elastomers leads to unavoidable energy dissipation upon application of mechanical energy. Furthermore, the viscoelastic nature of elastomers is seen from the strain response to stress, as

shown in Figure 6b. When stress σ is applied to the rubber, the strain response ε is delayed thus causing a phase lag δ. The complex modulus of the rubber can be expressed as [46]:

$$E^* = \frac{\sigma}{\varepsilon} = \frac{\sigma_A}{\varepsilon_A}(cos\delta + i\, sin\delta) = \frac{\sigma_A}{\varepsilon_A}\cos\delta + i\frac{\sigma_A}{\varepsilon_A}sin\delta = E' + iE'', \quad (6)$$

where σ_A is stress amplitude and ε_A is strain amplitude.

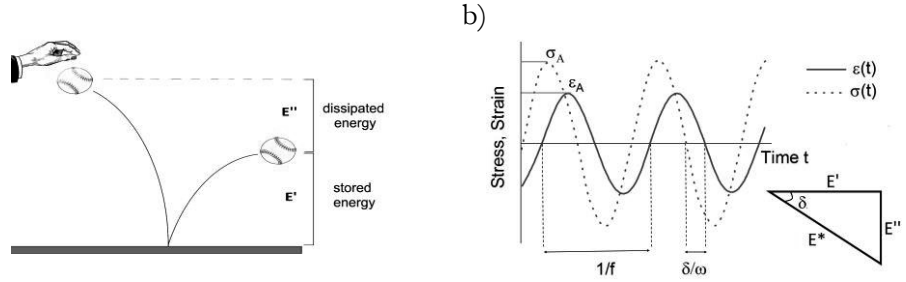

Figure 6. a) Representation of viscoelastic energy loss; and b) viscoelastic response of a material as revealed by DMA. Adapted from [45].

Energy dissipation during mechanical disturbance of rubbers can be observed in micro- and macro-scale and is governed by different phenomena [47]. The cause for the energy loss during the mechanical loading can be internal friction between the polymer chains, slippage and rearrangement of the chain position, break-up of a filler network, which can also lead to the release of occluded rubber [48]. As a result, the material exhibits creep, stress relaxation, heat build-up, as well as Mullin's and Payne effects. Mullins effect is an instantaneous and irreversible softening of the material related to the slipping and rearrangement of the rubber chains along each other and the filler particles, while the Payne effect is observed by the reduction of storage modulus of filled rubbers under sufficient strain, which is related to the breakage of the filler-filler network. Accordingly, chain dynamics of the filled rubber is affected by the three main interaction types: filler-filler network, filler-polymer interactions and polymer-polymer network created by vulcanization and physical entanglements. The schematic interactions are shown in Figure 7.

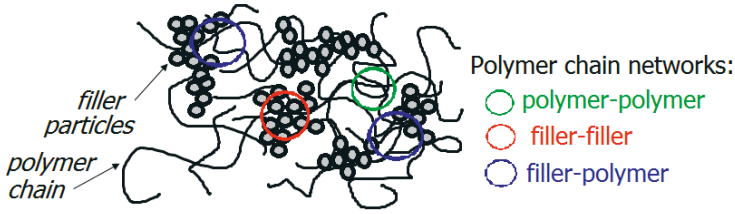

Figure 7. Schematic polymer chain network interactions in elastomer composites.

Dynamic properties of rubbers are dependent on temperature, time and strain. An efficient method of studying the mechanical energy dissipation on micro-level is dynamical mechanical analysis (DMA), while cyclic loading, creep and stress relaxation can be useful for the approaching the macro-scale effects of energy mechanical energy loss. Mechanical energy dissipation studied by DMA further allows to assess the mechanical damping properties of rubbers. Similarly to the dielectric analysis, the DMA loss tangent (tan δ) expresses the ratio of energy lost to energy stored in the cycle and describes energy dissipation, as seen from Figure6b. Moreover, the loss tangent may be a representation of a hysteresis loss at strains below 1% [49]. DMA can also be used to assess the effect of fillers to the rubber chain dynamics similar to the dielectric analysis.

Rubbers experience hysteresis due to their viscoelastic nature. Hysteresis loss describes the energy lost during this loading-unloading cycle, which is the case in most DEGs, and it is found important to address this source of the energy dissipation. The mechanical hysteresis measurement is performed by subjecting the sample to stretch-release cycles to a fixed present of elongation for a number of times. The example of hysteresis behavior of NR is shown in Figure 8a. This commercial NR film is used as reference in the present study and is known to contain a small amount of a non-black filler. The first several cycles always show higher hysteresis loss than the further cycles due to the Mullins effect. The energy loss during the loading-unloading cycle can be calculated from the area of the hysteresis loop, as shown in Figure 8b.

a) b)

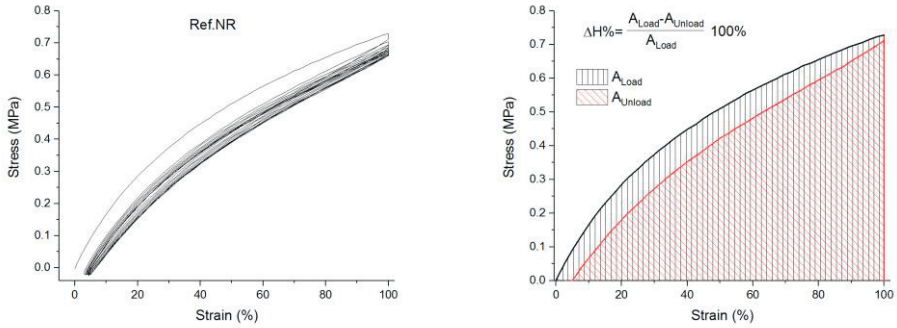

Figure 8. a) An example of a cycling loading test results showing Mullins effect; and b) a calculation example of an energy lost during one cycle.

3 DIELECTRIC ELASTOMERS

Despite of more than 15 years of research, the most used materials for DEGs are commercial acrylic adhesive tapes (VHB4905/VHB4910 and F9460PC [50], 3M). The convenience of utilizing the VHB acrylic tape is clear - it is well-studied [51; 52], with proven DEG suitability and readily available with the consistent quality. The material parameters and constants of the VHB tape have been reported in many publications, and its behavior under applied stress and electric field is well-predicted. Moreover, the viscoelastic behavior of the VHB tape is well-described, which makes the modeling process of a new DEG more convenient. Finally, the VHB tape is an adhesive that can ease the device assembly and electrode application. These factors may explain why most of the researchers focus solely on design of the generator and compliant electrodes, on modeling and optimizing DEGs rather than on modifying the electroactive polymer itself. This problem is pointed out, for example, in the works of Yin et al. [53] and Graf et al. [54].

VHB tape is considered in literature to have high dielectric losses [18], as many sources report dielectric permittivity and loss only at 1 kHz, which is well above the actual operating frequency of most DEGs. Moreover, dielectric properties of VHB are dependent on stretching. [55] VHB is known for the discrepancy of the dielectric permittivity (4.2 - 6) and loss values reported in the literature [18; 56], which can be related to the softness and high adhesiveness of the material and difficulty to eliminate air between sample and electrode without compressing and disturbing the sample. However, when only frequencies below 10 Hz are considered, the dielectric properties of the VHB tape are well suitable for the DEGs due to low dielectric losses and comparably high dielectric permittivity, which is always beneficial for a capacitor. The study of Vu-Cong et al. [57] has indicated that the dielectric losses of VHB below 10 Hz are lower than most of the silicones, which are successfully applied in DEGs.

The most serious problem of using VHB tape, according to [5; 27], is severe stress relaxation after few cycles. This means that a harvester is capable of generating energy just for a comparably short time. Moreover, acrylic rubber is more expensive compared to other general rubbers. Furthermore, a high dynamic loss tangent is expected, as VHB is a very lightly crosslinked material showing a high portion of a

viscous flow [58]. Therefore, it also shows considerably high mechanical energy dissipation during the loading-unloading cycle [4]. Nevertheless, other elastomer materials used in DEGs have their own drawbacks.

After acrylic adhesive tape, silicone materials are probably the next widely used material group for DEGs. A few commercial silicone materials are specially designed for DEGs. For example, silicone dielectric transducer produced by former Danfoss Polypower offered good performance both as DEA and DEG application [8; 10]. Danfoss PolyPower produced not solely dielectric material (silicone Elastosil RT 625 by Wacker containing silicone oil softener [59]), but the whole assembly including the compliant silver-based electrodes with a specially designed surface profile. More recently, LEAP technology company offered sensor and energy harvesting solutions based on Elastosil 2030 silicone film by Wacker involving carbon-filled silicone electrodes [60]. Some studies offer custom-formulated polyurethane (PU) [54], which is stated to have better performance than silicone.

Since 2011, new NR-based harvesting solutions started to emerge [61]. For example, according to Li et al. [29] and the original study of Kaltseis et al. [5], commercial soft NR ZruElast sheets showed better properties for energy harvesting application than the VHB acrylic tape. To be precise, the material studied by Li et al. is not solely a natural rubber, but a blend of NR and styrene-butadiene rubber (SBR) that is compounded with fillers, as seen from the manufacturer's datasheet [62]. Indeed, such material over-performs acrylic VHB tape in energy harvesting properties, but NR latex-based Oppo Band seems to be even more preferable. According to the author [5], viscoelastic hysteresis losses after 100's cycle decrease in the row VHB > NR/SBR > NR (19.3% > 7.0% > 2.3%), as well as dielectric losses at 1 kHz follow the same trend: $2.5 \times 10^{-2} > 5.6 \times 10^{-3} > 2.0 \times 10^{-3}$. This may be related to the differences in the glass transition temperature. Electric breakdown field of VHB is also the lowest compared to NR/SBR [34]. Thus, NR has a significant advantage over the VHB 4910, but both VHB- and NR/SBR-based generators can show very similar efficiency, when the design and the material parameters are adjusted properly. However, according to the theoretical works of Koh et al. [61; 63], NR performs better than VHB only at strains lower than 15%. Remarkably, this theoretical model does not include the effect of energy dissipation in the system and does not consider the different nature of elastomeric films.

Altogether, the acrylic adhesive, silicones and NR are the most used materials in DEGs. The material costs and the estimated levelized cost of electricity (LCOE) of these optimized elastomers are compared to the already functioning steel-based WEC Pelamis in Table 1 [5]. According to this comparison, natural rubber-based

DEG is expected to have the most suitable power/material cost ratio, which would result in the final energy cost close to the more traditional energy sources.

Table 1. Economic data (2013) calculated for WECs based on different materials based on [5].

WEC material type	Material cost (US $/kg)	LCOE (US cent/kWh)
Steel	4.15	26.5 – 61.7
Natural rubber	7.6	4.8 – 11.1
Silicone	20.0	11.8 – 27.5
Acrylic	105.0	12.3 – 28.5

3.1 Natural rubber

Natural rubber is a unique natural polymer with superior mechanical properties. NR is originally obtained in a latex form from *Hevea Brasiliensis*. The outstanding properties of NR are related to the presence of the insoluble rubber constituents, mostly natural proteins, which normally comprise about 2.2% of rubber mass [64]. Proteins, phospholipids and other insoluble non-rubber constituents account for the higher modulus and strength, faster scorch and pronounced strain-induced crystallization in NR compared to the synthetic polyisoprene [65]. Another function of proteins in NR is emulsification of a rubber fraction. The water-soluble proteins present in NR are also known as allergens [66; 67]. The structure of the natural rubber polymer is cis-1,4-polyisoprene with two trans-1,4-isoprene units at the ends containing α- and ω-chain ends. These α- and ω-chain ends are responsible for bonding possibility with phospholipids and proteins, which leads to branching of NR and is responsible for its green strength and gel formation [68; 69]. The general structure of NR, proteins and phospholipids, as well as the schematic representation of NR structure and the related branching is shown in Figure 9.

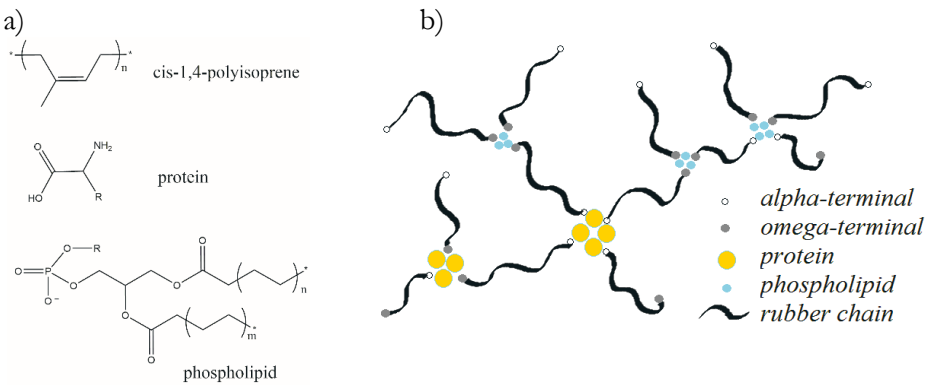

Figure 9. a) General structure of NR, proteins and phospholipids, where -R is an organic group; and b) a schematic structure of NR chains and branching associated with the presence of proteins and phospholipids.

NR contains two different types of proteins: water-soluble proteins, and insoluble proteins strongly bound to the rubber molecule [67]. Water-soluble components of rubber, including some naturally occurring proteins and phospholipids, are known to migrate to the surface of a dry latex film with time [70; 71]. For prevulcanized latexes the amount of the migrating extractable proteins are known to be considerably higher than for a post-vulcanized ones, and the amount of extractable proteins correlate with the increase in drying temperature, porosity and thickness of films. Moreover, some leaching processes may increase the amount of extractable proteins instead of decreasing it [72]. Insoluble rubber proteins are usually strongly bond to the rubber particle and are evenly distributed throughout the latex film unless they are solubilized, denaturated or degraded [73; 74]. For example, washing latex with surfactants results in denaturation of proteins and eases their removal with water. Also the use of strong alkali can hydrolyze phospholipids and degrade proteins into smaller fragments thus allowing them to be removed by washing. While water does not affect the rubber itself, acetone is known to dissolve some non-crosslinked rubber chains. Application of acetone has also been found to degrade some proteins and break the established hydrogen bonds [75]. Moreover, small fragments of degraded proteins are able to create ionic linkages to the rubber particles. Therefore, not only water-soluble, but also insoluble proteins can be expected to migrate in the latex films as a consequence of a specific treatment.

In deproteinized natural rubber (dNR), most of the proteins are removed by the enzymatic treatment. [74]. As a result of such treatment, the branching points associated with ω-terminals are removed, but the existing phospholipids maintain

the long-chain branching in the dNR through the junctions at α-terminals, which contain two types of functional groups [76; 77]. Therefore, deproteinization of NR results in similar mechanical properties as the standard NR. When compounded with an efficient vulcanization system, dNR is expected to have low hysteresis, creep and stress relaxation [78]. However, the use of conventional vulcanization system lowers mechanical properties of dNR and increases dynamic loss tangent [79]. Generally, rubber compounding chemicals are known to affect also the dielectric losses of NR. For instance, ZnO and stearic acid cause an increase in dielectric losses [80]. Moreover, some surfactants can increase dielectric losses of unvulcanized dNR [81].

From the dielectric loss point of view, natural proteins and phospholipids, as well as compounding ingredients in NR can be considered as impurities, which can increase dielectric dissipation, especially at low frequencies. Presence of impurities contributes to the ionic conductivity, which produces an increase in dielectric loss. [82] As deproteinized rubber contains about 80% less proteins than the standard NR, and the remaining proteins are much smaller in size [74], dNR is expected to show reduced dielectric losses without compromising the outstanding tensile properties of NR [83; 84].

Both NR latex and dNR latex [39; 45; 80; 81; 85], as well as their synthetic analogue polyisoprene [86-88] are well-studied in terms of dielectric behavior, including the relation of dielectric properties to material pre-stretch [55], but not in terms of protein and ingredients migration with time. As the protein migration is a time-dependent process, it is important to analyze the time-dependency of the dielectric losses of the various rubber samples, also considering the effect of compounding ingredients, vulcanization process, amount of natural proteins and the post-treatment methods.

3.2 Silicone

Silicones, also known as polysiloxanes, belong to an inorganic polymer group and consist of the repeating -Si(R,R')O- units, where -R and -R' are organic groups of different nature. The most frequently used silicone material is polydimethylsiloxane (PDMS), where both -R- and -R' are methyl groups. Silicones grades can be divided into two groups: high-temperature vulcanizable (HTV) and room-temperature vulcanizable (RTV) silicones. In the first case, crosslinking in silicones can be achieved through a radicals from organic peroxides. In case of RTV, crosslinks can be created with a condensation reaction, e.g. through a specially added crosslinker

groups via metal-catalyzed process, or in anhydrous one-component systems. Crosslinker groups often contain double bonds, and curing is achieved through hydrosilylation reaction. [89]

Silicones are generally insulators, unless filled with conductive particles or chemically modified [59]. Silicones are known for their excellent heat and cold resistance, as well as ozone, weather and salt water resistance [89]. However, most silicones have poor mechanical properties. Therefore, reinforcing fillers, such as silica, titania and calcium carbonate, are often added to them. However, these reinforcing materials usually result in the creation of unwanted electrical conduction paths which increase dielectric losses. Moreover, the presence of fillers usually increase mechanical energy dissipation on micro- and macro-levels through the arising Payne and Mullin's effects.

Silicones are well-studied in terms of their dielectric behavior, also for the DET application [59; 90-93] and in relation to the pre-stretch [94; 95]. A large number of different silicone types, commercial and newly synthetized, have been discussed in the extensive review by Madsen et al. focusing on the potential of silicones for actuation and energy harvesting [96]. Moreover, aging properties of silicones [97] and the effect of plasticizers [98] on dielectric properties have been studied.

4 FILLERS FOR DIELECTRIC ELASTOMER COMPOSITES

For the improvement of the performance of dielectric elastomers, compounding with fillers and plasticizers is often utilized. Importantly, the interface between filler particles and the matrix must be taken into consideration when designing a dielectric elastomer. The addition of fillers usually aims to modify the elastic modulus and increase the dielectric permittivity of rubbers used as dielectric actuators, but the presence of fillers often increases the dielectric losses. [99] In case of elastomeric generators, the composite needs to show low hysteresis and reduced viscoelastic relaxation time at the temperature and frequency of interest. Moreover, increased dielectric permittivity and decreased loss are desirable, while electrical conductivity should be avoided.

The rubber composites used in DETs can be divided into several groups based on the fillers added: composites with ceramic fillers, clays, conductive fillers and core-shell fillers. However, new filler types are constantly being investigated for their suitability for DET application. For example, detonation-produced nanodiamonds are believed to have suitable properties for successful DET composites due to their low dielectric losses, high electrical resistivity and outstanding tribological properties, such as ability to reduce friction that can result in low mechanical hysteresis of the composites [100].

4.1 Conventionally used fillers

Most of the filled dielectric elastomers are developed for the use in DEAs rather than DEGs. Therefore, the viscous losses are not reported in many cases, but much attention is paid to the dielectric permittivity and elastic moduli of the composites. As for ceramic filler-based composites applied in DEGs, Yin et al. [53] developed PU-based films filled with barium titanate ($BaTiO_3$, BT) nanoparticles and N,N-dimethylformamide (DMF). The developed composite over-performed VHB acrylic tape, as well as pure PU. As mentioned in the study, the improvements are achieved by increased dielectric permittivity of such composites combined with reduced

elastic modulus. However, as expected for any composite material, material-related losses increased drastically, thus leading to only 0.45% efficiency (electrical-to-mechanical energy ratio). Generally low energy density and efficiency may be related to the harvesting cycle parameters, e.g. comparable low strain and frequency. Finally, when comparing pure PU to the VHB acrylic tape, the latter one was shown to be more efficient.

In contrast, some research groups [101; 102] achieved low dielectric losses by adding BT to silicones, also with a plasticizer [103]. Moreover, Yu et al. [104] estimated that a number of commercially available liquid silicone rubbers filled with titanium dioxide can be suitable for energy harvesting applications due to their good mechanical properties, increased dielectric permittivity and high dielectric breakdown strength.

Although titanium dioxide (TiO_2) can be successfully applied for increasing dielectric permittivity of elastomer composites, electrical conductivity increases as well as dielectric loss [105; 106]. The results are similar if TiO_2 is used with a plasticizer [107].

The addition of clays, such as montmorillonite, could be useful in achieving a combination of increased dielectric permittivity, low dielectric loss and relatively low elastic moduli [108; 109]. Moreover, the same goal can be achieved with conductive fillers, such as multiwall carbon nanotubes, in concentrations well below the percolation threshold [91; 110; 111], or a combination of BT with carbon black [112]. Due to the limitations of conductive fillers related to the possible short circuit and challenges is long-term stability, encapsulation approach has been applied by some researchers leading to the application of core-shell type fillers. The most successful core-shell dielectric composites are based on silica (SiO_2), silver and polydopamine in silicone matrix [113-115].

4.2 Nanodiamonds

Detonation nanodiamonds (NDs), also known as ultradispersed diamonds, possess excellent mechanical properties, low electrical conductivity, high thermal conductivity and a highly reactive surface due to a large amount of reactive chemical groups on the surface [116-118]. NDs are mostly applied for biomedical, electronic and tribology applications and in different polymer-based composites [118-120]. However, similar to other nanomaterials, the fabrication of ND-elastomer composites is associated with some challenges. They can be related to the poor ND-

elastomer interactions and strong agglomeration of NDs, resulting in poor dispersion and reduced composite strength.

Detonation NDs are produced by explosive decomposition of a combination of carbon-containing explosives, for example 2,4,6-trinitrotoluene and 1,3,5-trinitro-1,3,5-triazacyclohexane, under controlled conditions in oxygen-deficient atmosphere. Single ND particles are about 4 - 6 nm in diameter consisting of a sp^3-carbon core, thin sp^2–carbon transitional layer and an active surface. [121] The surface of a pristine ND is hydrophilic and mostly contains carboxyls, hydroxyls, lactones, ketones and ethers, but it can be modified and homogenized through a large number of methods [122]. Due to the presence of carboxyl and hydroxyl groups, NDs form strong aggregates and agglomerates, which are difficult to break down. Thus dispersing NDs to small aggregates and single particles is very challenging even with an ultrasonic energy. For example, due to the high surface energy of NDs, breaking up ND aggregates into primary particles cannot be achieved by direct ultrasonication [123]. In some cases, high-energy ultrasonication may even lead to a higher aggregation of ND particles due to the induced changes on the ND surface [124]. Moreover, a direct mixing of the ND powder with the polymer results in filler agglomeration and inadequate dispersion [125-127]. However, surface modification could decrease interactions between the ND particles by introducing complex moieties onto the ND surface preventing strong inter-particle bonds.

4.2.1 Nanodiamond surface modification

Although NDs are considered easily reactive compared to other carbon materials, a surface modification often requires several steps, strong chemicals and/or high temperatures [128]. While a simple oxidation in air at about 425 °C can be employed in order to increase the amount of oxygen-containing groups, especially –COOH, on a ND surface [129; 130], any further modification may be a challenge. During the oxidation in air, ketones, aldehydes, and esters on the ND surface are converted into carboxylic acids, anhydrides, or cyclic ketones, and some sp^2-carbon is removed from the surface giving an access to the formation of oxygen-containing groups. When heated above 600 °C in an inert atmosphere, unmodified ND first loses its oxygen-containing groups and then undergoes graphitization and sintering above 800 °C resulting in a mass loss up to 10 - 20% [131]. Another traditional route of ND functionalization often includes a reduction of a pristine ND surface to hydroxyls followed by introduction of amine groups, e.g. by silanization, which

enables further modifications [132; 133]. Other common ND surface modification routes are presented in Figure 10.

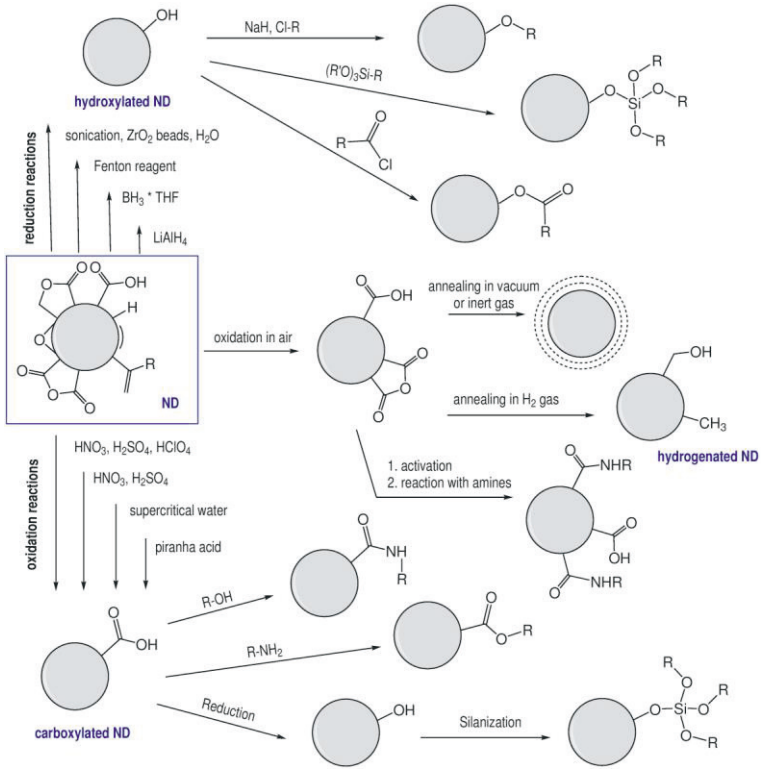

Figure 10. Schematic ways of ND surface modification based on [134; 135].

Due to the presence of sp^2-carbon layer in NDs, many surface modification routes suitable for carbon nanotubes can be applied to nanodiamonds as well. As an example, different silanization reactions are possible involving carboxyl and hydroxyl surface groups created after oxidation of the nanofiller in air, as well as silylation processes on unoxidized surface [136].

Organosilanes are known as coupling agents enabling attachment between polymers and fillers. The common formula of organosilane is R-Si(-R')$_3$. A treatment with silanes creates a hydrophobic ND surface and, therefore, improves the dispersion of NDs in nonpolar organic media. If a vinyl-containing silane is used, it is reported that the dispersion is improved both in nonpolar and polar organic media [124]. However, an increase in the agglomerate size can be observed after silanization due to the condensation reaction between treated particles [137] or a self-

condensation of the silane [138]. Owing to the self-condensation reaction, a siloxane shell is formed around the ND particle, which can further bond particles into very large aggregates. Basic conditions and elevated temperature facilitate the condensation of silanol groups [139]. A minimum condensation rate for tri-, di- and monosilanols can be achieved at pH 4, pH 6 and pH 6.5 – 7, respectively, which allows minimizing the siloxane shell formation [140].

Several works report a direct one-step functionalization of NDs by organosilanes. Zhang et al. [141] have applied (3-mercaptopropyl)trimethoxysilane for the modification of NDs with unknown surface. According to the provided FTIR (Fourier transform infrared analysis) data, however, high amount of hydroxyl groups on the ND surface can be suggested. A direct functionalization of carboxylated NDs with a vinyl-containing silane has been reported in the work of Hajiali et al. [142], and a possibility of such reaction was mentioned in the latest review of Zhang et al.[119]. However, no strong evidence has been provided for the existence of ND-silane bonds as the result of such modification. The goal of the modification was to create polysiloxane shell on ND surface. A polysiloxane coating is usually achieved through a Stöber process, which involves a silane hydrolysis in basic conditions followed by the reaction between hydrolysed silane and hydroxyl groups on the ND surface and further polycondensation via creation of Si-O-Si bonds [143]. When ND surface contains COOH- groups instead of OH- groups, a hydrolyzed silane can most probably react with –OH group of other silane molecules rather than with the -COOH group of the ND. Therefore, a probability of the reaction between carboxylated nanodiamond and hydrolyzed silane needs to be evaluated.

Another direct functionalization of carboxylated NDs through the reaction with the epoxy group can be applied [138; 144] based on the esterification reaction discussed in literature [145; 146]. The reaction with an epoxy-group containing compound can easily attach various chemical groups to the ND surface, for example, silanes and vinyls. As organosilanes are widely used in rubber technology to improve rubber-filler interactions, especially in silica-filled systems [147], they can be used for other filler systems to induce chemical bonding to the polymer through the crosslinking sites. At the same time, double bond in vinyl-containing compounds can also react with the crosslinking system used for the rubbers resulting in lower filler-filler and improved rubber-filler interactions. Thus, the loss properties of such compounds are expected to be improved.

5 AIMS OF THE STUDY

The aim of this thesis is to reduce losses and gain more understanding of the key factors affecting the performance of elastomer films in DEGs. Therefore, the material-related losses of elastomer films are investigated in order to understand the contribution of elastomer type, as well as the presence of impurities and fillers, to the expected performance of such elastomers in DEGs. Moreover, the present research focuses on evaluation of the effect of the filler surface treatment on the loss properties of the rubber films. This knowledge contributes to the development of energy harvesters, which are more economically preferable and easier to mass-produce than currently available prototypes. Achievement of the stated goal will remarkably increase the attractiveness of alternative energy sources and its economical favorability. The study is based on the following hypotheses:

- Natural proteins present in natural rubber (NR) increase the dielectric losses of the elastomer, and the removal of the large portion of those proteins by deproteinization should reduce these losses.

- Post-treatment of elastomer films by acetone and water leaching partly removes non-rubber constituents responsible for the higher dielectric loss.

- Nanodiamonds (NDs) have an active surface that can interact with proteins and other impurities in rubber, thus decreasing the material-related losses at low frequencies. NDs are expected to be more effective for the complex systems and their effectiveness is suggested to decrease in a row latex NR → dry NR → deproteinized NR and silicone.

- Surface modification of NDs improves the interaction between rubber and filler by creating chemical or physical bonding, and facilitates the loss reduction by reducing the interfacial effect.

Based on the abovementioned hypotheses, the following research questions (RQ) are stated:

1. How the presence of naturally occurring proteins in natural rubber films, and system complexity in general, affect material-related losses? (*Publications I and II*)

2. Can the material–related losses of natural rubber be lowered by the post-treatment methods (leaching with water and acetone)? (*Publications I and II*)

3. Can the material-related losses be lowered by the incorporation of nanodiamond filler, and what is the effect of the nanodiamond surface treatment on its performance? (*Publications II-IV*)

The practical approach is divided into 1) enhancing the theoretical base related to the dielectric losses in rubbers, and 2) a practically oriented research utilizing the obtained knowledge to overcome the current issues with the materials used in DEGs. The fundamental study addresses the factors within elastomer membrane, which contribute to the dielectric losses, and their dependency on time. The application-oriented study offers solutions for minimizing the material-related losses in elastomer films. The structure of the study is presented in Figure 11.

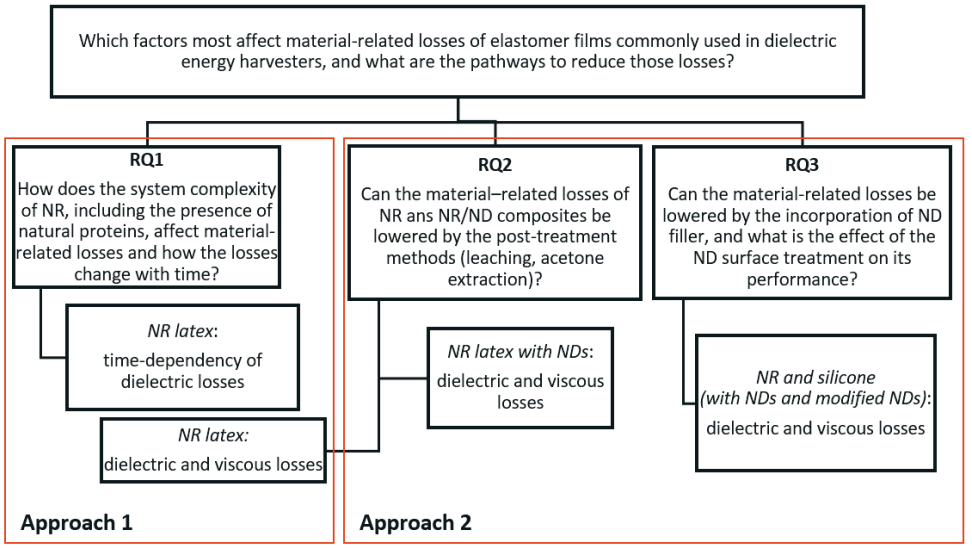

Figure 11. The summary of the study.

6 EXPERIMENTAL

The materials and methods used in the study are discussed in this section. First, the elastomers used as matrix are introduced followed by the necessary compounding ingredients, then nanodiamond types and their surface modifiers are discussed. Finally, the sample preparation and characterization methods are described.

6.1 Materials

Natural rubber latex (NR, Full Ammonia grade), deproteinized natural rubber latex (dNR, Vytex grade), and prevulcanized natural rubber latex (pNR, Revultex MR) all containing about 60% of polymer, were used in the study. Prevulcanized latex was used as received, while the other latex types required compounding. Latex compounding ingredients included water-based dispersions of 50% zinc dibutyldithiocarbamate (ZDBC) and 68% sulfur (S) supplied by Akron Dispersions Ltd, as well as 50% nano zinc oxide (ZnO) from Sigma Aldrich. Two different conventional latex stabilizers - 1N potassium hydroxide (KOH, VWR) and 10% ammonium caseinate (Akron) were used in compounding. The compounding ingredients for the dry NR (Standard Malaysian Rubber, SMR10) included sulfur, 2-mercaptobenzothiazole (MBT), stearic acid and ZnO, all of standard industrial grade. The amount of the additives is based on dry phr (parts per hundred rubber) content of the ingredients.

Two-component room temperature curable silicone (PDMS) with Pt catalyst (Elastosil 601 RT, Wacker) was used in the study. Silicone oil (Rhodorsil 47 V 50, VWR) was used as plasticizer in 0/1/5/10 phr amounts. Commercial acrylic adhesive tape VHB (VHB4910, 3M) and 0.35 mm thick physiotherapeutic natural rubber band with medium stiffness (Green, Duke Fitness) were used as reference.

The study utilized NDs with carboxylated surface (uDiamond Molto Vox, Carbodeon Oy) both as-received and surface-modified, and NDs with hydrogenated surface (Molto Nuevo, Carbodeon Oy) were used as received. Vinyltrimethoxysilane

(VTMS, Sigma Aldrich), bis-3-triethoxysilylpropyldisulfide (TESPD, Sigma Aldrich) as well as 1,2-epoxy-9-decene (ED, abcr GmbH) and

3-glycidoxypropyltrimethoxysilane (GOPTMS, abcr GmbH) were used as surface modifiers for the carboxylated NDs. Moreover, additional surface modifications were performed with monoalkoxysilanes (vinyldimethylethoxysilane (VDMES) and octadecyldimethylmethoxysilane (ODDMS), abcr GmbH). Structures of the used surface modifiers are shown in Figure 12. Glacial acetic acid (Sigma Aldrich) was used for the pH adjustment of the silanization reaction. The full range of used materials is presented in Table 2.

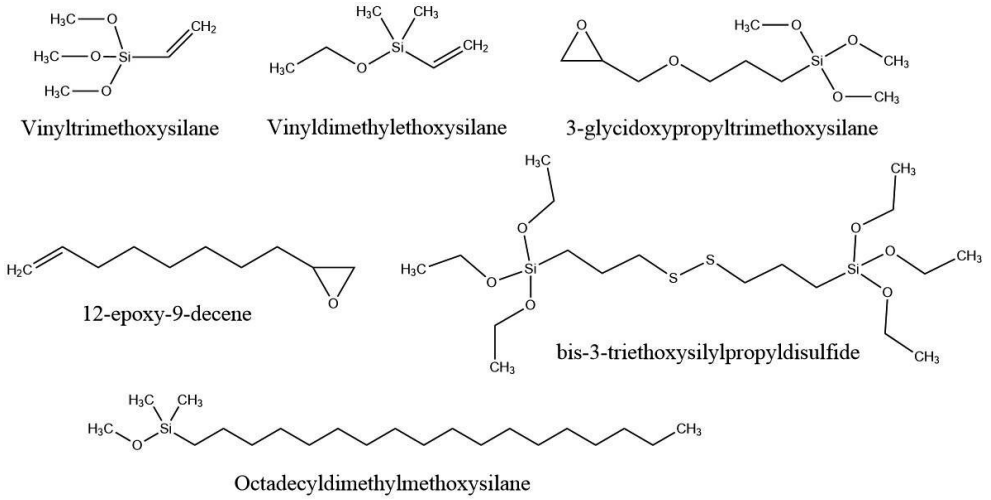

Figure 12. Chemical structure of the surface modifiers used in the study.

Table 2. Summary of the samples and their abbreviations used in the study (where ***x*** = phr amount)

Matrix				Additives		ND filler			Post-treatment		Abbreviation
Type		Details	Supplier	Plasticizer	Protein-containing stabilizer	Amount, phr	Type of surface	Surface modifier	Leach	Acetone	
NR		Prevulcanized latex (Revultex MR)	Algol Chemicals Oy	-	-	0 - 10	-COOH	-	-	-	pNR/COOH_ ***x***
									+	-	pNR/COOH_ ***x***-L
									-	+	pNR/COOH_ ***x***-A
		Full ammonia latex	Centrotrade Deutschland	-	-	-	-	-	-	-	NR_KOH
									+	-	NR_KOH-L
									-	+	NR_KOH-A
					+	-	-	-	-	-	NR_a.c.
									+	-	NR_a.c.-L
									-	+	NR_a.c.-A
		Deproteinized latex (Vytex)		-	-	-	-	-	-	-	dNR_KOH
									+	-	dNR_KOH-L
									-	+	dNR_KOH-A
					+	-	-	-	-	-	dNR_a.c.
									+	-	dNR_a.c.-L
									-	+	dNR_a.c.-A
		Standard Malaysian Rubber	KSK Globalink Manufacturing	-	-	0, 1	-COOH	-	-	-	SMR/COOH
							-COOH	-vinyltrimethoxysilane			SMR/VTMS
							-COOH	-triethoxysilylpropyldisulfide			SMR/TESPD
							-H	-			SMR/H
Silicone		RTV (Elastosil 601 RT)	Wacker	0- 10 phr	-	-	-	-	-	-	PDMS_oil***x***/0
				10 phr	-	0.1, 1	-COOH	-vinyltrimethoxysilane	-	-	PDMS_oil10/VTMS_***x***
								-vinyldimethylethoxysilane			PDMS_oil10/VDMES_***x***
								-octadecyldimethylmethoxysilane			PDMS_oil10/ODDMS_***x***
								-1,2-epoxy-9-decene			PDMS_oil10/ED_***x***
								-3-glycidoxypropyltrimethoxysilane			PDMS_oil10/GOPTMS_***x***
Reference	**Acrylic**	VHB 4910 tape	3M	-	-	-	-	-	-	-	Ref.VHB
	NR	Physiotherapy band (green)	Duke fitness	-	-	-	-	-	-	-	Ref.NR

6.1.1 Nanofiller modification

As-received, carboxylated NDs were oxidized in air at 425 °C for 4 hours in order to increase the amount of surface carboxyl groups available for the further modification by oxidizing the existing oxygen-containing groups, such as lactones. The amount of oxygen-containing surface groups was determined by Boehm titration performed according to the procedure described elsewhere [148]. The total amount of the surface groups, which can be identified by the Boehm titration, was determined by the reaction with NaOH. The amount of carboxylic groups was determined by the reaction with $NaHCO_3$, lactones - from the difference between NaOH and $NaHCO_3$ tests, and the amount of phenolic groups from the difference between Na_2CO_3 and $NaHCO_3$ reacted with the functional groups of the carbon material.

The silane-based modification was performed as described in [30], with ND to silane mass ratio of 1:5. After the modification, the powder was washed with acetone, filtered, purified in Soxhlet extractor with toluene and dried in oven for 24 h at 120 °C. The schematic chemical modification reactions are shown in Figure 13. In order to understand the probability of the reaction between the carboxylic groups of ND and the silanol groups of the modifier, additional surface modifications were performed with monoalkoxysilanes following the same procedure as for VTMS and TESPD. Vinyldimethylethoxysilane was chosen due to its similarity to VTMS. However, the characteristic FTIR peak of a vinyl group is often small, and it could remain unnoticed. Therefore, octadecyldimethylmethoxysilane was chosen as the second modifier due to the distinctive FTIR peak of a long aliphatic chain that could identify the presence of the modifier on the ND surface.

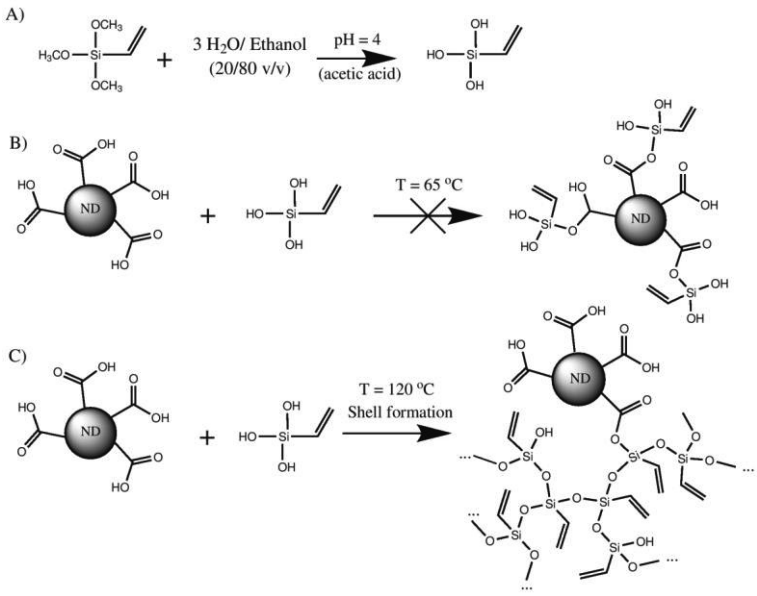

Figure 13. Modification process of carboxylated ND by silanization (example of vinyltrimethoxysilane, applies for other silanes). *[Publication IV]*

For the epoxy-based modification, 0.3 g of oxidized NDs were placed into a three-neck flask, dispersed in 80 ml toluene and brought to a constant temperature (40 °C). After temperature stabilization, ED was added slowly in excess molar amount (5:1 based on the amount of surface carboxyl groups on NDs). The reaction was allowed to proceed for 24 hours, followed by filtration and washing with toluene. The obtained fillers were further purified in a Soxhlet extractor with toluene for 24 hours and dried in an air-ventilated oven at 120 °C for 12 hours. The schematic chemical modification reactions are shown in Figure 14. The modification of NDs with GOPTMS was performed following the same procedure as for ED.

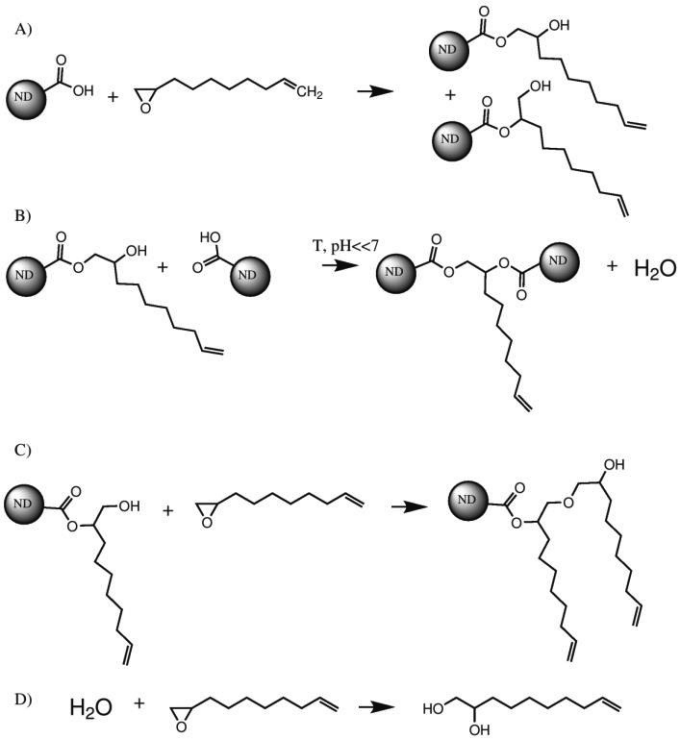

Figure 14. Possible reactions between the epoxy-group containing modifier (example of 1,2-epoxy-9-decene, applies for other epoxy-containing compounds) and carboxylated ND. Only one carboxyl group is depicted on ND surface for clarity. *[Publication IV]*

6.2 Preparation of elastomer films

Latex was mixed with curatives by magnetic stirrer according to the recipe shown in Table 3. The obtained solutions were poured into the molds, degassed in vacuum for 30 minutes and left for 24 hours for drying. The dried samples were gently removed from the molds and cured in the ventilated oven at 120 °C for 15 and for 30 minutes. Leaching treatments were performed on dried unvulcanized samples by washing in deionized water at 35 °C for 20 minutes. The samples were vulcanized after drying at room temperature for 24 hours. Acetone treatment was performed on vulcanized samples by immersing them into acetone for 30 minutes at room temperature. After the treatment, the samples were washed in deionized water and dried for 24 hours at room temperature.

Table 3. Formulation for unfilled NR latex samples

Ingredient	Role	Amount (phr-dry)			
		NR_KOH	dNR_KOH	NR_a.c.	dNR_a.c.
Full ammonia NR latex	Elastomer	100	-	100	-
Deproteinized NR latex		-	100	-	100
KOH, 1N	Stabilizer	0.1	0.1	-	-
Ammonium caseinate		-	-	0.5	0.5
ZDBC	Accelerator	2	2	2	2
S	Curative	1	1	1	1
ZnO	Activator	1	1	1	1

The dry NR samples were compounded with the needed ingredients in a laboratory scale mixer (Brabender W 50 driven by Brabender Plasti-Corder) according to the recipe presented in Table 4. The rotor speed was 60 rpm and the starting temperature 50 °C. The materials were cured at 150 °C in hot press to form 1 mm thick sheets.

Table 4. The recipe of dry NR compounds.

Ingredient	Role	Amount (phr)
SMR10	Elastomer	100
ZnO	Activator	3
Stearic acid	Activator	1
S	Curative	1.75
MBT	Accelerator	1
ND powders	Filler	0/1

For the preparation of ND-PDMS composites, ND powder was first dispersed in silicone oil by ultrasonication (FinnSonic m03) for 30 minutes at room temperature. ND-containing oil was then added to the part A of a two-component silicone containing the catalyst and stirred for 5 minutes, then combined with part B silicone containing the crosslinker and stirred for another 2 minutes. The material was poured into molds to form both 1 mm and 0.5 mm thick sheets, and then degassed in vacuum for 30 minutes to eliminate air bubbles. The samples were left to cure for 24 hours at ambient conditions.

6.3 Characterization methods

Characterization methods used in the study are divided into three sub groups according to the nature of the analysis.

6.3.1 Dielectric characterization

Dielectric characterization was performed for about 0.5 mm thick samples at room temperature (23 ± 1 °C) and ambient relative humidity 35% ± 3%. Moreover, temperature dependency of the dielectric properties was evaluated in -80 – 70 °C range with 10 °C steps. Dielectric permittivity, dielectric loss and electrical conductivity were measured with a Novocontrol Alpha-A dielectric analyzer. The frequency sweep was done from 0.5 Hz to 1 MHz. The thickness of each sample was carefully measured prior to the test. The samples were placed between 2 mm thick rigid gold-plated electrodes 20 mm in diameter. Both samples and electrodes were wiped with isopropanol prior to the test to remove any impurities from the surface and to improve the contact between the sample and electrodes, thus reducing possible electrode polarization and the surface contact effect. Three specimens of each sample were tested, and the average value was calculated.

6.3.2 Mechanical characterization

Mechanical characterization methods included dynamic mechanical analysis (DMA), stress relaxation test, cyclic loading at two different rates and maximum elongations and tensile testing at two rates used for the determination of elastic moduli of the materials.

DMA, stress relaxation and low rate tensile cyclic loading of the samples were performed with Pyris Diamond DMA (Perkin Elmer) using about 1 mm thick samples. DMA samples were measured in the tension mode at 1 Hz with 0.1% displacement amplitude and 3 °C/min heating rate. For the stress relaxation measurement, samples were stretched to 10% and the change in force was recorded. Three specimens of each sample were tested, and the average value was calculated. The low rate cyclic loading was performed at ambient conditions, when samples with 10 mm test length were stretched to 45 ± 1% at 6 mm/min rate. Three specimens of each sample were tested, and the average value was calculated. The high rate tensile cyclic loading was performed on Z1.0 testing machine (Zwick/Roell) at ambient conditions at 500 mm/min rate and 100% maximum elongation. The test length was 35 mm. Pre-stress of 0.1 N was applied to avoid buckling of the samples. The hysteresis loss was calculated by subtracting integrated loading and unloading curves and dividing the value by the area under the corresponding loading curves, as was presented in Figure 8b. Three specimens of each sample were tested, and the average value was reported. Tensile testing of dumb-bell specimen was performed

at ambient conditions on Messphysik Midi 10-20 universal tester at 200 mm/min rate with 10 mm test length. The stress values at 10, 50 and 100 % elongation were recorded as moduli at 10, 50 and 100 % respectively. Average of three parallel measurements was taken and respectively designated as $M_{10\%}$, $M_{50\%}$ and $M_{100\%}$.

6.3.3 Structural and thermal characterization

Characterization methods included electron microscopy, infrared spectroscopy, swelling tests, colorimetry and thermal analysis for the determination of structural, chemical and thermal properties and behaviour of the samples.

The cryo-fracture surfaces of ND powders and ND-filled rubbers were studied with a scanning electron microscope (SEM, Zeiss ULTRAplus) equipped with an energy dispersive X-ray spectroscopy detector (EDS, Oxford Instruments X-MaxN 80). The samples were coated with a thin carbon layer to prevent charging during SEM analysis. In the EDS analysis, the average of two point measurements were reported. Fourier transform infrared spectra (FTIR) were obtained with Bruker Tensor 27 in the attenuated total reflectance (ATR) mode in the range from 500 to 4000 cm^{-1} with a diamond crystal background and 4 cm^{-1} resolution.

Curing characteristics of the latex materials were studied with DMA 861e (Mettler Toledo). Uncured samples were tested with 0.5% shear amplitude at 120 °C and 1 Hz frequency for 30 minutes, and the change in shear modulus was recorded. Temperature pre-equilibration step took 8 minutes before the actual test. The optimum curing time was determined as time of pre-equilibration plus the time the shear modulus (G') reached the maximum (plateau) value. Curing behavior of dry NR samples was studied with Advanced Polymer Analyzer APA 2000 (Alpha Industries) for 20 minutes at 150 °C. The apparent crosslink densities 1/Q were calculated from the swelling values Q, which is defined as grams of solvent per gram of rubber hydrocarbon [149]:

$$Q = \left(\frac{m_s - m_d}{m_0}\right)\frac{F}{100}, \qquad (7)$$

where m_s and m_d are the weight of the swollen and dried specimen, respectively, m_o is the initial weight of the specimen, and F is formula weight, meaning total weight of rubber together with compounding ingredients based on hundred parts of rubber. For the determination of apparent crosslink density, three specimens (about 10x10x1 mm) of the sample were weighed and then immersed in toluene for 72 hours. The solvent was renewed every 24 hours. The saturated swollen specimens were removed from solvent, wiped quickly with filter paper and weighed. Specimens were weighed

again after 48 hour drying in air at room temperature. Three parallel measurements were conducted and the average values were reported.

Staining was performed on dry latex samples by immersing them in amido-black staining solution (Sigma Aldrich) for 2 minutes, blotting the samples dry and de-staining for 30 minutes in acetic acid/isopropanol/water solution (10%/25%/65% by volume). The de-staining solution removed all unreacted stain. The colorimetric analysis was performed with Minolta CR-300 in the L*ab scale, where color is expressed as three numerical values: *L* for the lightness, a and b for the green–red and blue–yellow color components, respectively. Difference between colors before and after the staining ΔE^*_{ab} was calculated based on formula:

$$\Delta E^*_{ab} = \sqrt{(L_2 - L_1)^2 + (a_2 - a_1)^2 + (b_2 - b_1)^2}, \quad (8)$$

where index 1 stands for an unstained sample, and index 2 for the stained one. Due to their transparency, all samples were evaluated against a white background. Three parallel measurements were conducted, and the average value reported

Thermogravimetry (TGA) was performed for ND powder samples with TG 209 F3 Tarsus (Netzsch) in nitrogen gas (N_2) flow. Samples were heated to 125 °C with 20 K/min rate, kept at 125 °C for 10 minutes to remove humidity, and then heated to 850 °C with 20 K/min rate. Differential scanning calorimetry (DSC) was used to study the effect of NDs on the crystallinity of PDMS with DSC 214 Polyma (Netzsch) in N_2 flow with 10 K/min heating (cooling) rate.

7 RESULTS

The most important findings from the four publications and some unpublished data are presented and analyzed in this section. First, the effectiveness of the ND surface treatment is evaluated. The further results are organized based on the types of testing. Furthermore, the section includes data related to the time-dependency of the dielectric losses and the effect of proteins and compounding ingredients.

7.1 Surface-treated nanodiamonds

Special attention was paid to accessing the efficiency of the surface treatment of the nanodiamonds and the determination of the chemical groups on their surface. First, the probability of the attachment of silane-groups to the ND surface over silane self-condensation was approached by applying the silanes with only one reactive site (monoalkoxysilanes), which cannot form a shell around NDs. The presence of these silanes on the ND surface would indicate that the reaction between carboxylic and silanol groups is possible. Unreacted silanes and the silanes condensed with another silane molecules are removed by the filtration, as such molecules are not attached to the ND surface.

The NDs modified with monoalkoxysilanes were studied with FTIR and TGA methods. The resulting curves are shown in Figure 15. For both modified samples, an increase in all peak intensities, especially the ones related to the presence of –OH group, was noticed. In ND-VDMES sample, the peak at 1620 cm^{-1} (-OH) is especially pronounced. In ND-ODMMS, the peak shifts to 1624 cm^{-1}, which, together with an increased broad peak at 3400 cm^{-1}, is indicative of the presence of water or solvent. Moreover, in ND-ODMMS sample, the peaks at 2944, 2875 and 1455 cm^{-1} corresponding to $–CH_2-$, and 1745 cm^{-1} corresponding to C=O group of lactones become more apparent. However, no sharp and intensive characteristic band for a long aliphatic chain appeared at 720 - 725 cm^{-1} in ND-ODMMS. Furthermore, no vinyl group bands can be seen around 3080/2997 cm^{-1} and 909 cm^{-1} in ND-VDMES, and both spectra look very similar to the untreated ND-COOH. Next, the TGA data of both ND-ODMMS and ND-VDMES shown in

Figure 15b is very similar to ND-COOH, although ND-VDEMS contains some adsorbed water. No degradation peaks are seen in the DTG curves at the temperatures below 500 °C. Finally, no traces of Si were revealed in the samples by the EDS analysis. These findings imply the absence of ODMMS and VDMES on the ND surface. Therefore, the reaction between the alkoxy and carboxylic group is considered improbable in the used reaction conditions.

a) b)

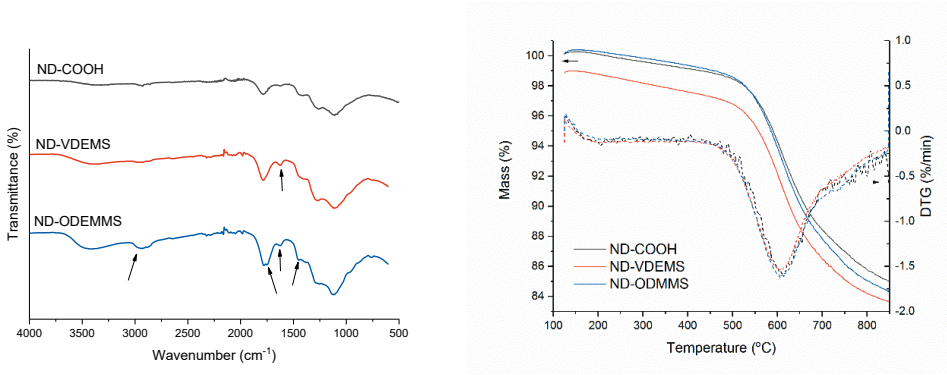

Figure 15. a) FTIR spectra, where the differences in spectra are marked with arrows; and b) TGA mass loss and mass loss rate (DTG) curves for the mono-silanol group modified NDs. [*Publication IV]*

The EDS analysis of ND particles was performed and the results are presented in Table 5. It confirms that new elements were introduced to the fillers upon modification, and the ratio of the elements was changed. Exceptionally high silicon and oxygen content in ND-VTMS and also sulfur in ND-TESPD confirms the extensive shell formation. The presence of a similar shell formation in the ND-GOPTMS sample is unlikely, as both the Si content and the Si : O ratio are low. This suggests that the reaction between the epoxy and -COOH groups is much more pronounced, and that the GOPTMS molecule is bounded to the ND surface and was less likely to condense due to restricted mobility.

Table 5. EDS analysis of the filler particles.

Sample	Element content (%)				
	C	O	Si	S	others
ND-COOH	96.0	3.2	-	<1	<1
ND-H	97.2	1.9	<1	<1	<1
ND-VTMS	54.6	18.0	27.3	-	<1
ND-TESPD	42.5	14.3	20.5	22.5	<1
ND-ED	96.0	4.0	-	-	-
ND-GOPTMS	90.8	6.6	2.6	-	-

The modification of ND particles by multifunctional silanes and epoxy-containing compounds is further confirmed by FTIR and TGA analysis presented in Figure 16. The reference ND-COOH shows characteristic carbonyl weak peaks around 1780cm^{-1} and number of broad peaks at 1300 - 900 cm^{-1} as a combination of overlapping C-O stretch peaks from multiple oxygen-containing groups, e.g. lactones and phenols [150]. The same peaks are present in all modified materials, but epoxy-modified materials have more pronounced carbonyl peaks. Peaks at 3100 – 3600 cm^{-1} and 1625 cm^{-1} appear due to stretching and bending of –OH groups respectively [151]. Upon both silane modifications, a characteristic broad peak around 1020 cm^{-1} corresponding to Si-O-Si bond appeared due to the condensation of hydrolyzed alkoxy groups. Moreover, a notable shoulder around 1100-1150 cm^{-1} is seen. These peaks are characteristic for silica, indicating overlapping Si-O-Si and Si-C peaks with the contribution from C-O bond [152; 153]. The intensity of the peaks suggests an extensive shell formation around ND clusters especially for ND-TESPD powder. Peaks at 1275 cm^{-1} correspond to a Si-C stretching, and are present in all fillers modified with the silane-containing group [151; 154]. Moreover, ND-TESPD spectra showed multiple peaks for –CH_3 and –CH_2- groups in the range 1340 - 1412 cm^{-1} and more pronounced presence of –OH and -COOH groups. Modification with ND-VTMS is confirmed by the appearance of peaks at 3062cm^{-1}, 1601 cm^{-1} and 985 cm^{-1} due to the C=C bond, and 749 cm^{-1} due to the C-H bend of the vinyl group [155]. However, the peak at 3080 cm^{-1} of ND-ED powder is somewhat smaller. Moreover, ND-ED has double peaks corresponding to the different antisymmetrically coupled C=O stretches (1780 cm^{-1} and 1750 cm^{-1}), which probably indicate two different reaction A products (see Figure 14) in epoxy-modification.

a) b)

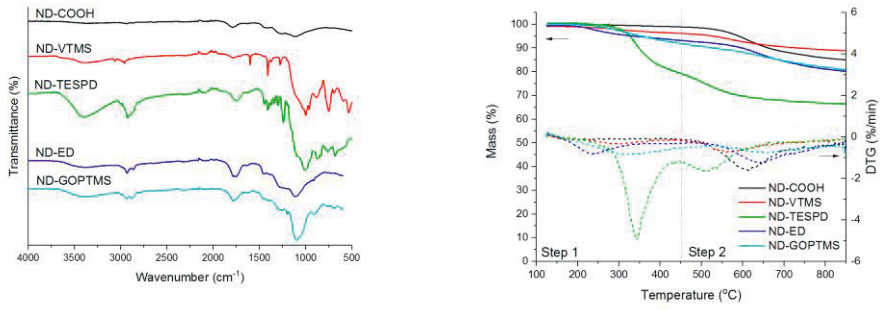

Figure 16. a) FTIR-ATR spectra; and b) TGA mass loss and mass loss rate curves for the silanol- and epoxy- group modified NDs. Combined from [*Publication III]* and [*Publication IV]*

Thermogravimetric analysis in Figure 16b reveals that, unlike ND-COOH, all modified samples show a mass loss in the range of 200 – 360 °C related to the removal of strongly bound water and decomposition of organic groups attached upon the surface modification. The second mass loss step corresponds the removal of lactonic and other oxygen-containing surface groups, as when heated above 600°C in inert atmosphere, ND surface usually loses its oxygen-containing groups and then undergoes graphitization and sintering above 800 °C resulting in a mass loss up to 10-20% [131]. The numerical data of TGA results is shown in Table 6. Less than 1% mass loss of ND-VTMS and ND-ED samples during the isothermal step could be related to the presence of water or solvent residues. Among all the modified samples, ND-ED has the lowest DTG_{max} temperature during the first decomposition step, which is related to the absence of Si in the structure. The higher residual mass of ND-VTMS than ND-COOH and the other samples is related to the significant amount of Si in the sample. Both the highest mass loss during the first and second step, and the lowest residual of ND-TESPD sample is related to the large size of the molecule with relatively lower Si content in it, as well as to the extensive shell formation around the ND. The increase in the DTG_{max} temperature during the second decomposition step of the ND-ED and ND-GOPTMS samples compared to ND-COOH can be an indication of the reduction of the original oxygen-containing groups on the ND surface as the result of a successful chemical attachment of the new groups.

Table 6. Thermogravimetric data for ND powders.

Sample	Mass loss at isothermal step (%)	Temperature at DTG_{max} (°C)		Mass loss (%)		Residual mass (%)
		1st step	2nd step	1st step	2nd step	
ND-COOH	-	-	614.0	1.2	13.9	85.0
ND-VTMS	0.9	302.2	557.6	2.9	7.4	88.9
ND-TESPD	-	343.3	512.9	20.7	13.1	66.5
ND-ED	0.7	234.5	644.9	6.7	12.4	80.2
ND-GOPTMS	-	312.1	660.0	10.3	8.9	80.8

The SEM images of the filler particles are shown in Figure 17. The microscopy reveals that all the modified NDs are more agglomerated than ND-COOH. Among the modified fillers, ND-TESPD and ND-VTMS samples have the largest agglomerates, which can be related to the silanol condensation and shell formation around the ND clusters. At the same time, ND-ED and ND-GOPTMS are comparable in agglomerate size and distribution with the untreated ND-H powder.

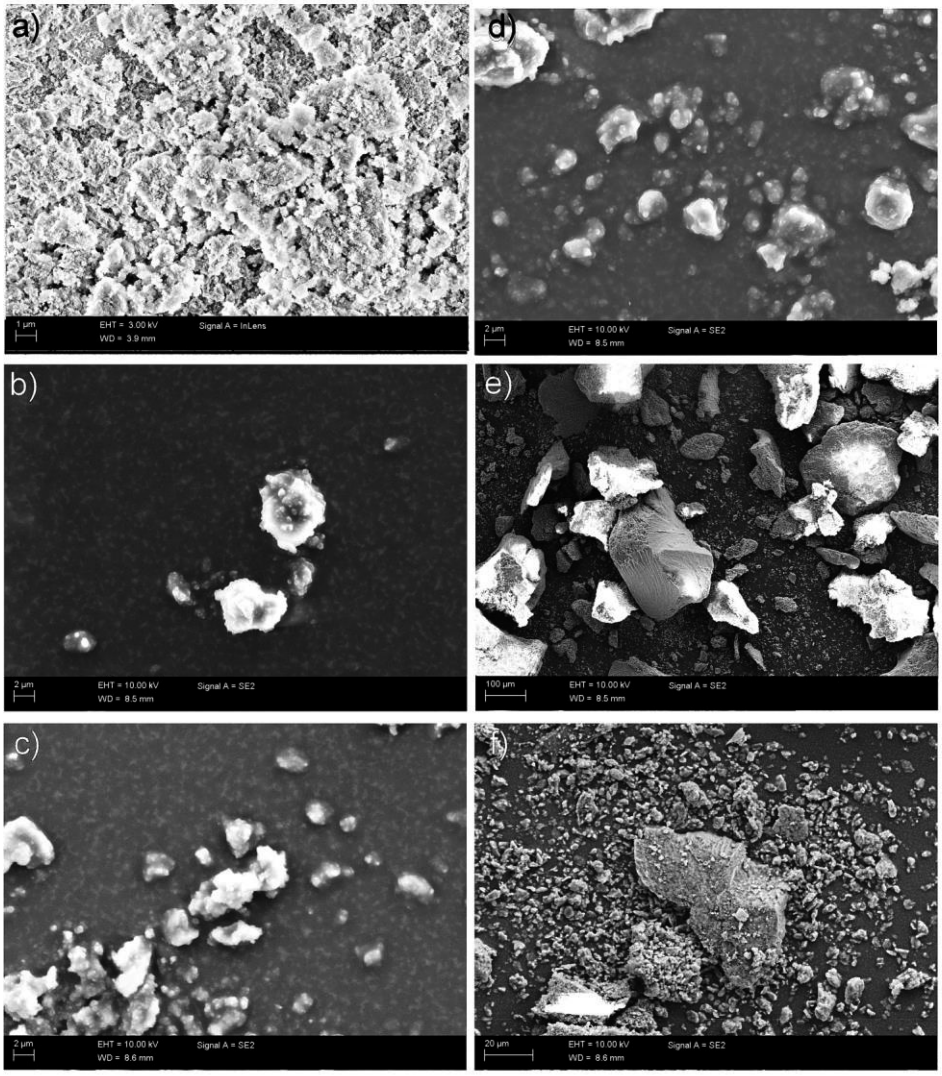

Figure 17. SEM images of ND powders: (a) ND-COOH; (b) ND-ED; (c) ND-GOPTMS; (d) ND-H; e) ND-TESPD; and f) ND- VTMS. Note the difference in the magnification. The magnifications were selected to make the single particle agglomerates distinguishable and emphasize the significant size difference between them. *[Publication IV]*

7.2 Curing behavior

The curing behavior was evaluated for the latex samples and SMR, where the effect of NDs was also seen. As can be seen from Figure 18a, dNR samples show some

reversion – decrease in modulus after the optimum curing was reached, which is related to the breakage of some sulfur bonds. Reversion is common for NR compounds, and in this case can be related to the decreased amount of proteins [156]. According to Figure 18b, the addition of NDs to the SMR compound results in minor reduction of curing times. Moreover, addition of ND-COOH and ND-VTMS increases maximum torque and reduces the scorch times, which is probably related to the high thermal conductivity of NDs, effective crosslinking reactions and presence of carboxylic groups on the surface [157]. Addition of ND-TESPD leads to an opposite effect on curing and shows no reversion. Moreover, TESPD-modified sample have the lowest torque and increased scorch time. This effect may be explained by less efficient crosslinking reaction and deactivation of curatives due to the presence of some silanol groups on the modified filler, as these groups are known to interact with accelerator [158]. Moreover, unwanted bubble formation may be responsible for the effect. Finally, hydrolysis of the alkoxy groups of silanes and self-condensation creates a shell around ND particles [136], which may affect its surface properties and thermal conductivity.

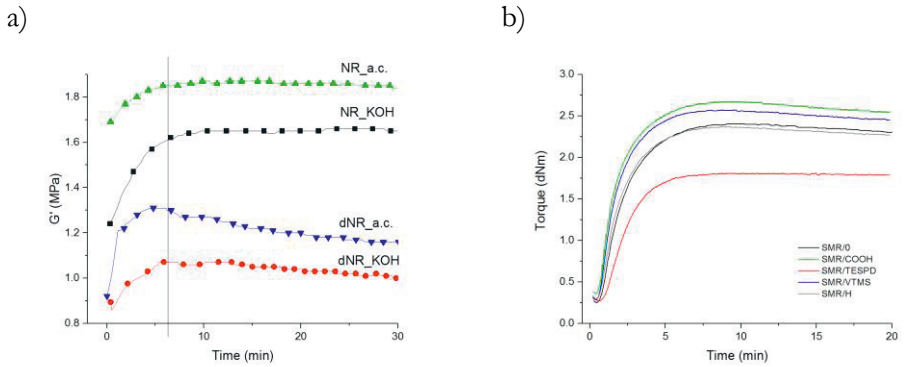

Figure 18. Curing curves of a) unfilled latex samples; and b) SMR samples with 1 phr NDs. *[Publication I]* and *[Publication III]*

7.3 Dielectric properties

Dielectric properties of the elastomers suggested for the DEG application, especially the dielectric loss at low frequency area and ambient temperatures, are the first priority of the study. The dielectric permittivity, loss and conductivity results of the unfilled elastomers used in the study, as well as the reference materials, are presented in Figure 19. In terms of dielectric permittivity, Ref.VHB has the highest ε' (5.1 at

low frequency range) among the samples, which is related to the presence of polar groups in its structure. At the same time most NR and PDMS samples, being non-polar, show almost constant values of ε' (2.8 – 3.4) in the whole frequency range. However, prevulcanized pNR exhibits an increase in ε', which is associated with the onset of electrode polarization, as also the corresponding dielectric loss curve suggests (Figure 19b). As can be seen from Figure 19b and 19c, both dielectric loss and electrical conductivity curves of the materials are significantly different. Some similarities are found between pNR/0 and Ref.NR, except for the latter one exhibiting additional relaxation around 10 Hz. Moreover, a strong segmental relaxation is seen for the Ref.VHB resulting in a comparable high dielectric losses at frequencies above 10 Hz. However, below 1 Hz, its losses are among the lowest and are comparable to SMR/0. As for PDMS samples, no significant change is seen upon the addition of a plasticizing oil (0 - 10 phr). The samples show increased dielectric losses and frequency-independent electrical conductivity below 1 kHz, which was same regardless of the amount of the plasticizer. The further focus is set only on PDMS samples containing 0 and 10 phr of silicon oil as the boundary samples.

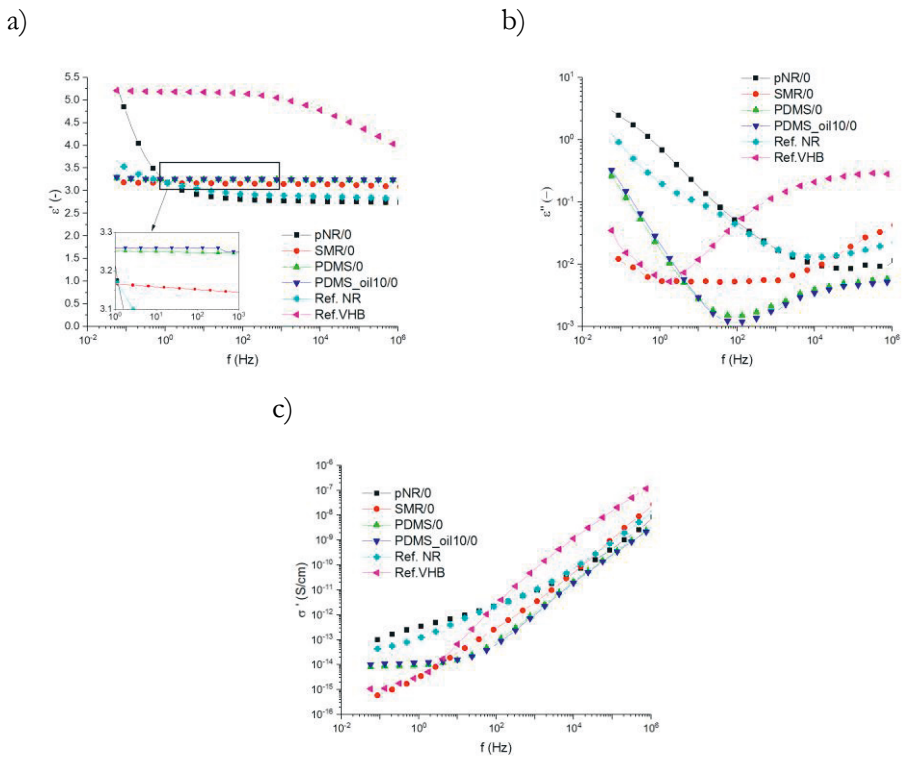

Figure 19. a) Dielectric permittivity; b) dielectric loss and c) AC conductivity of unfilled and reference samples.

The difference in temperature-related dielectric losses of latex-based NR compounds compared to the Ref.NR and the changes in dielectric losses of SMR sample upon the addition of 1 phr of NDs with different surfaces, are presented in Figure 20a and 20b respectively. The relaxation peaks associated with the glass transition T_g are clearly seen for all the samples. Both pNR/0 and Ref.NR have lower T_g peak and temperature, which implies less chain restriction. Other samples show much broader relaxation peaks suggesting more chain interactions. Remarkably, differences in the latex stabilizer type seem not to affect the T_g area, while a small decrease in T_g peak height and temperatures is noticed for the deproteinized samples. This can be related to less polymer-polymer interactions due to the reduced protein amount. Addition of 1 phr of NDs to the SMR results in increased dielectric losses after the T_g, as can be expected upon addition of any filler. Less pronounced increase from ND-VTMS and ND-TESPD can be related to better filler-polymer interface.

For all the samples, an increase in dielectric losses in seen with increasing temperature. In addition, Ref.NR is showing an additional relaxation near the room temperature, which can be related to the presence of inorganic filler or some other compounding ingredients not present in the other samples. This event is related to the contribution of increased ionic conductivity, similarly to isothermal low frequency events, resulting in the increased dielectric losses [43].

a) b)

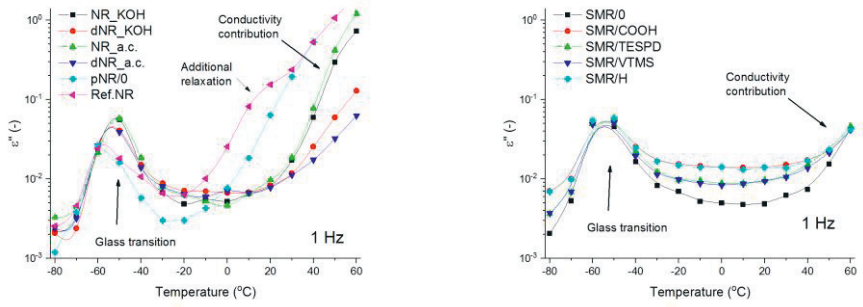

Figure 20. Temperature dependency of the dielectric loss of a) unfilled NR samples and Ref.NR; and b) SMR containing 1 phr of NDs.

Similarly to the SMR, the addition of small amounts of NDs to the prevulcanized NR latex results in no significant changes in either dielectric permittivity or losses, as seen from Figure 21. However, as the ND amount increases from 2 to 10 phr, the shapes of the curves change implying the reduced electrode polarization, but an appearance of the loss increase associated with the filler-polymer interface. Moreover, the added NDs change the shape of the AC conductivity curve to a more linear, which supports the suggestion about reduced charge transport after the addition of up to 10 phr NDs.

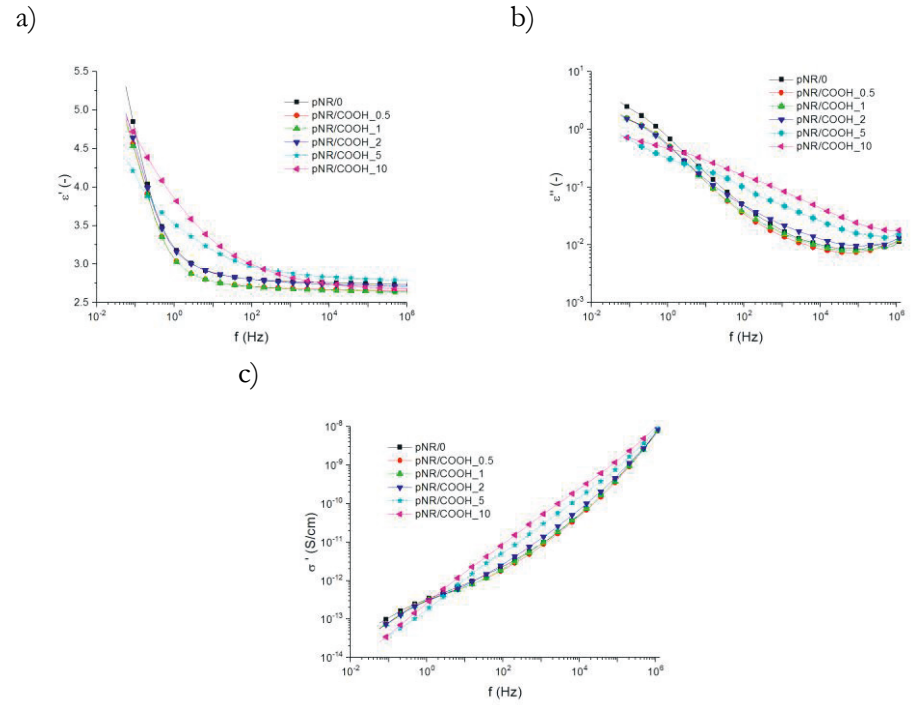

Figure 21. a) Relative dielectric permittivity, b) dielectric loss, and c) electrical conductivity of prevulcanized NR latex containing various amounts of ND-COOH. [*Publication II]*

In PDMS, as seen in Figure 19b, the addition of oils results in no significant difference in dielectric losses. However, the addition of 0.1 phr NDs results in reduced dielectric losses below 10 Hz (Figure 22a). This effect can be related to the reduction of the contribution from electrical conductivity, as can be seen also from Figure 22b. Such losses may be related to the impurities and mobile ions within the matrix that could be trapped and demobilized on the ND surface. Furthermore, the addition on even small amounts of filler results in the increased dielectric loss below 1 kHz occurring due to the permittivity and conductivity differences at the matrix-filler interface known as Maxwell-Wagner, or interfacial polarization. As this interfacial effect is less pronounced for the modified ND samples compared to ND-COOH, a stronger filler-matrix bond and a more uniform interface is suggested as explanation for this phenomenon. Finally, when 1 phr ND-COOH, ND-ED and ND-GOPTMS was added to PDMS, the losses associated with the interfacial effect become more pronounced (Figure 22c), but the electrical conductivity is reduced further and the curve becomes more linear (Figure 22d). These fillers were selected for the comparison due to the differences in their dielectric behavior at the

frequencies below 10 Hz in the composites containing 0.1 phr NDs. The effect was very similar to the NR compounds, and due to the increased losses at low frequencies of the mentioned compounds, it is decided to focus further on the composites containing 0.1 phr NDs.

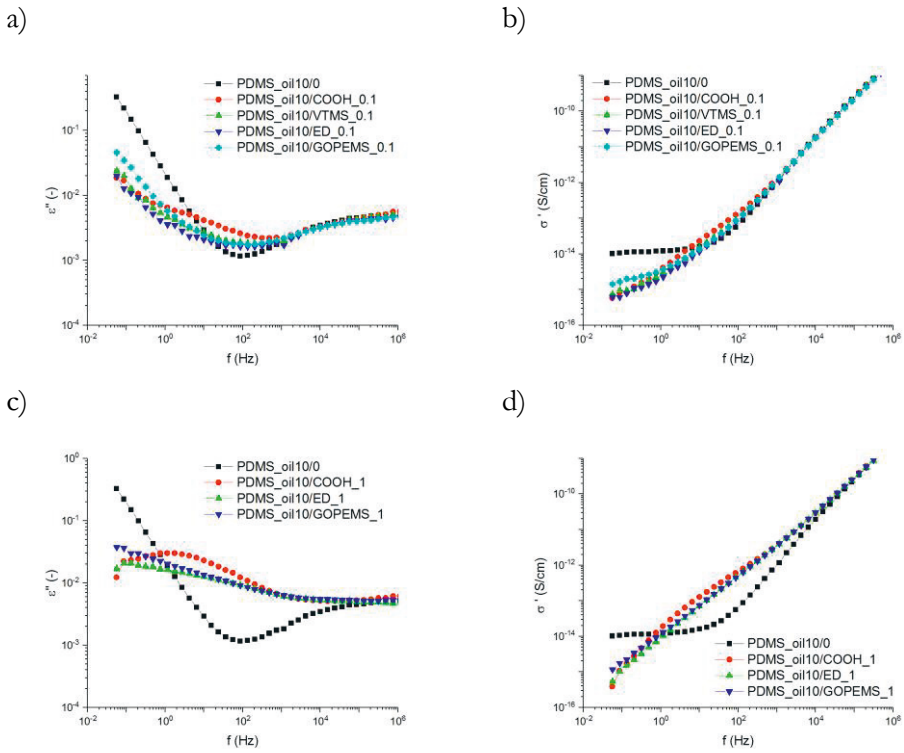

Figure 22. a, c) Dielectric loss; and b, d) AC electrical conductivity of PDMS samples containing 0.1 phr and 1 phr of NDs, respectively. [*Publication IV]*

7.3.1 Effect of proteins, compounding ingredients and post-treatment of latex films

The differences in dielectric loss of cured materials with different compounding ingredients and protein content are not that pronounced, as it was seen in Figure 20a. Figure 23 shows that the compounds containing KOH stabilizer shows generally higher dielectric losses at frequencies below 100 Hz than the compounds containing ammonium caseinate. Moreover, as expected, the losses of deproteinized dNR were lower than the standard NR.

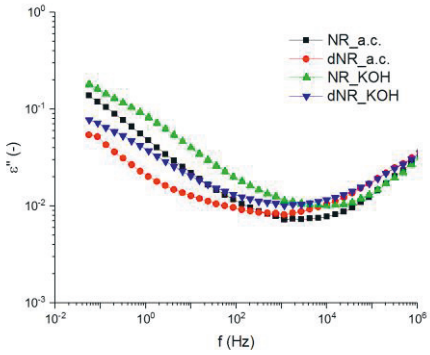

Figure 23. Comparison of dielectric loss of NR latex samples with different stabilizers and protein content. [*Publication I]*

In order to estimate the content of the protein-based substances and phospholipids on the sample surface, the FTIR absorbance peaks normalized by 1664 cm^{-1} peak (C=C, characteristic for NR) were analyzed at 3300 cm^{-1} (-OH, characteristic for proteins) and 1739 cm^{-1} (C=O ester stretching characteristic for phospholipids) [83]. According to Figure 24, deproteinized NR has less proteins, but more phospholipids than standard NR. However, due to the nature of different stabilizers, this evaluation may be incorrect, as the presence of OH^- from KOH contribute to the intensity of the peak used for the identification of proteins.

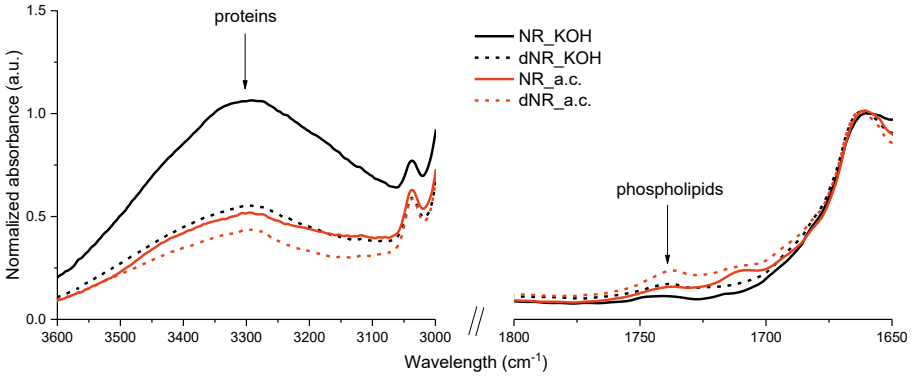

Figure 24. Normalized FTIR spectra of NR and dNR samples with different stabilizers. [*Publication I]*

Another method applied for the evaluation of the amount of proteins on the rubber surface is staining. The stain reacts with the water-soluble rubber proteins resulting

in more intense color change [70]. Therefore, a relative surface protein content can be compared between the samples. However, such method cannot be correlated to the absolute quantity of the proteins, and also may include some of the insoluble rubber proteins [159]. As can be seen from Table 7, pNR compound shows the highest surface protein content according to the staining method, and this is supported by the literature [72]. The phenomenon may be related to the specific ingredients used in the production of commercial prevulcanized latex, for instance, surfactants, which can solubilize insoluble rubber proteins. Among the unvulcanised latex samples, the results are also predictable: deproteinized NR shows much lower color change ΔE^*_{ab} compared to the normal samples, and the addition of protein-based stabilizer (ammonium caseinate) increases ΔE^*_{ab}.

Table 7. Crosslink density and colorimetric data of the uncured* latex samples.

Property	NR_KOH	dNR_KOH	NR_a.c.	dNR_a.c.	pNR
ΔE^*_{ab} (-)	10.1 ± 0.5	5.5 ± 0.4	21.0 ± 0.5	12.0 ± 0.5	33.7 ± 0.4
1/Q (-)	0.056 ± 0.023	0.069 ± 0.001	0.044 ± 0.005	0.100 ± 0.003	0.187 ± 0.002

* except for prevulcanized pNR

In addition to the compounding ingredients, the degree of crosslinking can also affect the dielectric properties of the materials. The existence of the crosslinks in unvulcanized samples is partly explained by the developing branching points due to the presence of proteins and/or phospholipids [160]. Moreover, as the samples are compounded with the curatives, the curing process proceeds slowly during the film formation and drying [161]. The high crosslinking and deviation of NR_KOH over NR_a.c. shown in Table 7 can be explained by the presence of protein fragments appeared due to the addition of strong alkali, which are able to link to the ω-terminals in NR chain [74]. The highest 1/Q of unvulcanized dNR can be related to the largely reduced amount of the proteins on the rubber particle surface, resulting in more active adsorption of the compounding ingredients and the stabilizers to the surface of the rubber particle. As a result, the sample with the highest 1/Q show the lowest dielectric losses at low frequencies. Furthermore, high 1/Q of the dNR_a.c. sample can be explained by accelerating action of ammonium caseinate due to the presence of ammonia ion.

Regardless of the post treatment, the dNR_a.c. samples had the lowest dielectric loss at low frequencies, and when the post-treatment was involved, small changes were noticed to other samples as well. For example, the post-treatment of the samples by leaching shows only a little positive effect on reducing the dielectric losses of NR_KOH sample, not affecting the deproteinized samples (Figure 27a). At the

same time, Figure 27b indicates that the acetone-treatment seems to be successful only in reducing the dielectric losses of the NR_a.c. sample, which can be related to the ability of acetone to remove the insoluble proteins [162]. In case of prevulcanized NR filled with different amounts of NDs (Figure 25c and Figure 25d), the difference in the dielectric loss reduction between leaching and acetone treatment is very small, and both methods equally lower the losses compared to the untreated materials. The loss reduction is most likely related to the removal of the surfactant from the system and lowering the conductivity contribution.

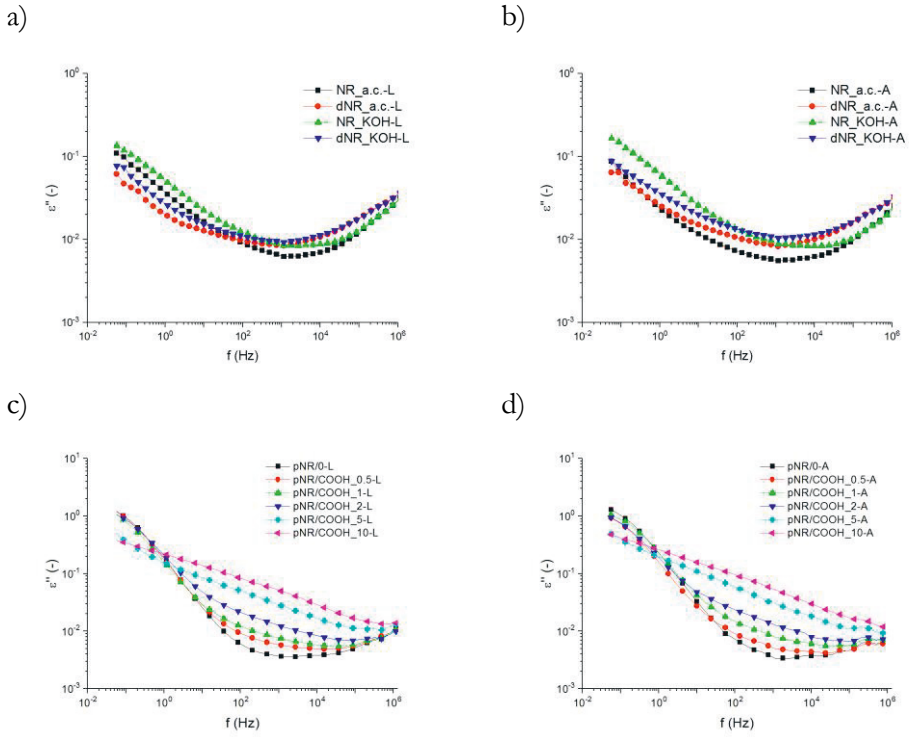

Figure 25. Comparison of dielectric losses of a, c) leached; and b, d) acetone-treated latex NR samples. [*Publication I]* and [*Publication II]*

7.3.2 Time-dependency of the dielectric properties

As a common practice, e.g. for the tensile tests ISO 37:2017 and electrical resistivity tests ASTM D991-89(2010), testing of rubber materials is performed between 16 hours and four weeks after vulcanization. However, despite the existing set of recommendations for testing of DETs developed by Carpi et al. [163] aiming to

make the testing results comparable within the field of application, no limits are mentioned for the times between the curing and dielectric testing of such materials. As was noticed previously, when the conditions of the dielectric testing, such as humidity and temperature, are maintained constant, the amount of proteins, different stabilizers and the degree of crosslinking can have a small effect on the dielectric losses of the materials. Moreover, these material properties may change with time and upon the post-treatment within this given timeframe. Therefore, it is important to study the dependency of dielectric loss on time after curing and evaluate the possible cause of such change in order to determine the optimum time intervals for the testing.

As seen from Figure 26, the dielectric losses seem to stabilize after 3 weeks and 2 weeks after curing for NR and dNR latex samples, respectively. Furthermore, the post-treatment methods have an effect on the time-dependency of the dielectric losses, as seen from Figure 27 and Figure 28. In both cases of post-treatment, the samples can be considered stable already at 2 weeks after curing.

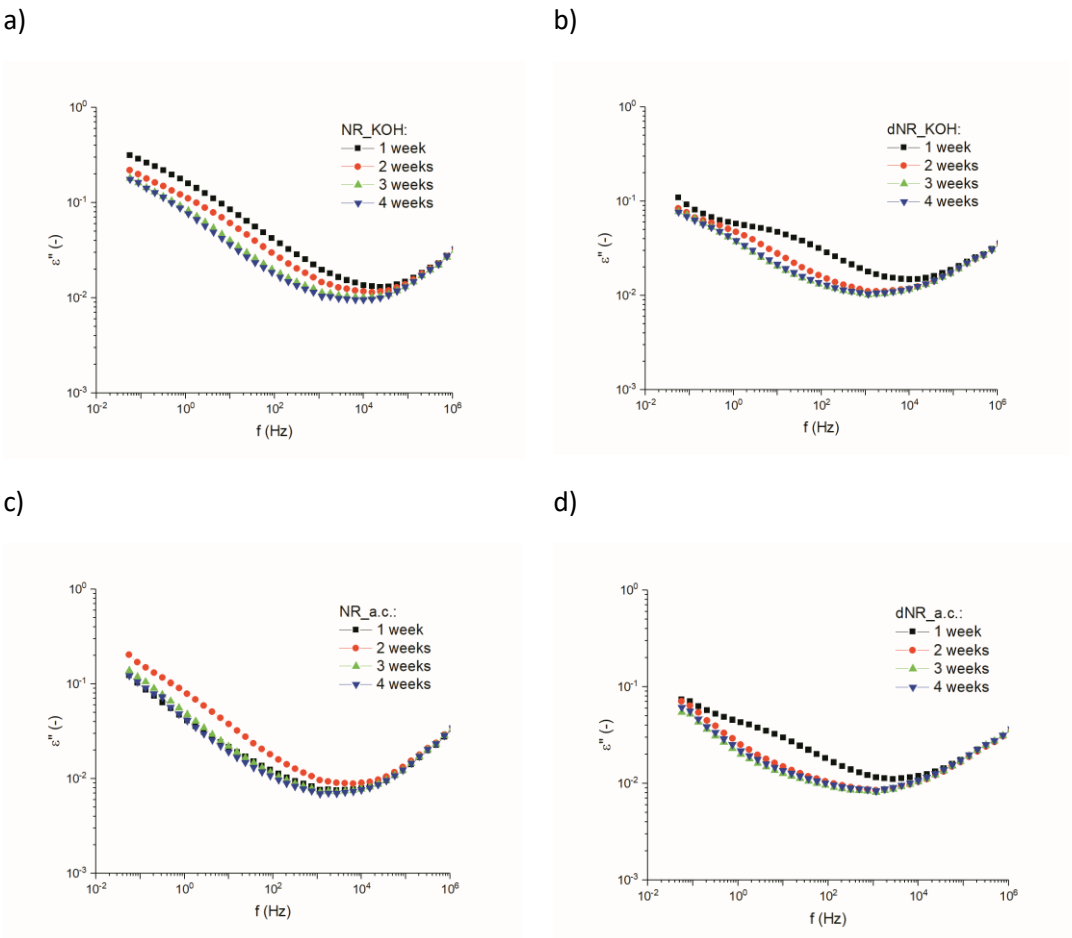

Figure 26. Time-dependency of dielectric loss properties of (a, c) NR and (b, d) deproteinized NR films. *[Publication I]*

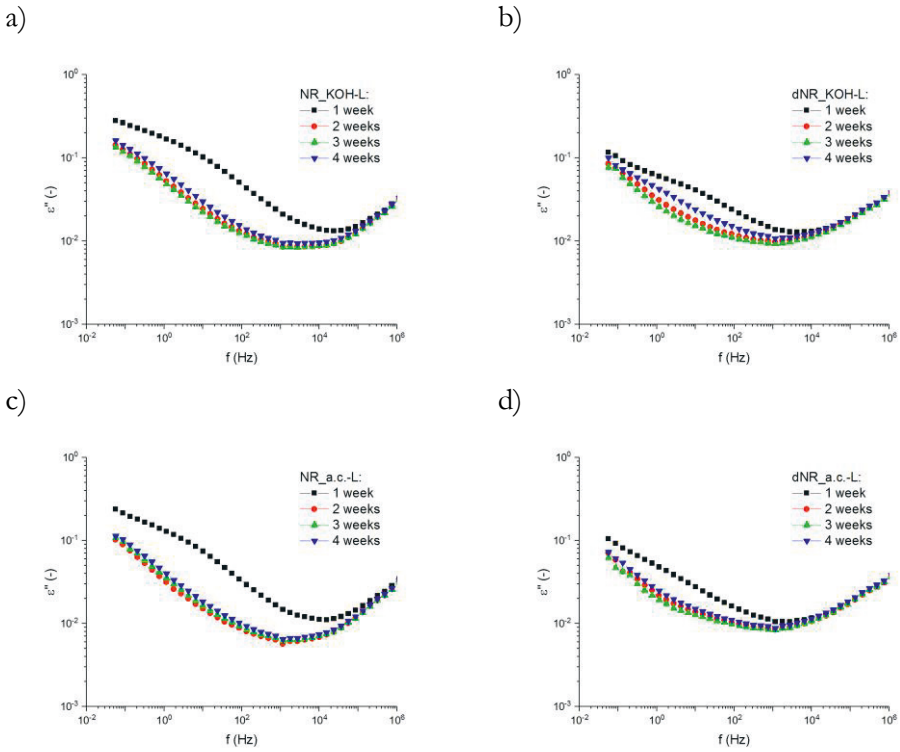

Figure 27. Time-dependency of dielectric loss properties of leached (a, c) NR and (b, d) deproteinized NR films. *[Publication I]*

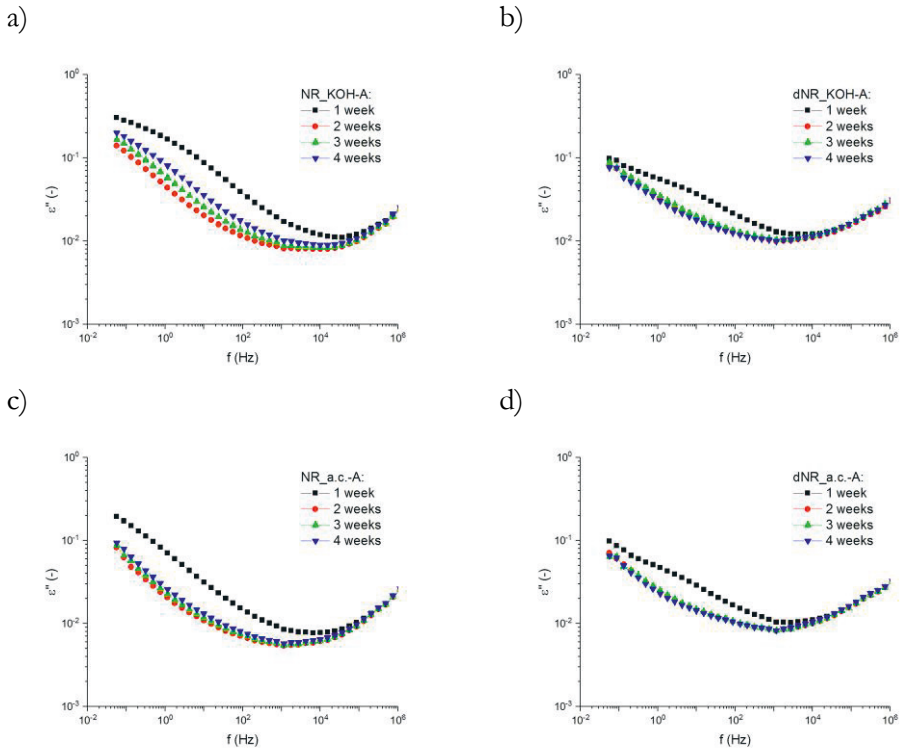

Figure 28. Time-dependency of dielectric loss properties of acetone-treated (a, c) NR and (b, d) deproteinized NR films. *[Publication I]*

According to the colorimetry results at different times after cure presented in Figure 29, the untreated samples containing ammonium caseinate have higher content of the surface proteins compared to KOH-stabilized compound. As the uncured NR_a.c. sample show almost twice higher color difference than at one day after cure (Figure 29b), most of the protein-containing stabilizer was expected to be migrated to the surface during the film drying phase. Thus, the increase in color difference seen in the NR_KOH and the NR_a.c. at three weeks after cure can be related to the migration of the natural proteins. The finding is also consistent with the dielectric data, where the minimum losses were achieved after two weeks after curing. At the same time, dNR samples as well as post-treated dNR-L and dNR-A samples show little dependency on time regardless of the stabilizer type. Generally, leaching was an efficient method to reduce the amount of water-soluble proteins in all the samples, and these samples show little dependency of the protein content on time after cure, same as the dielectric changes over time after cure were small. Furthermore, the acetone treatment of all NR samples results in significantly increased color

difference. As acetone is known to cause denaturation and precipitation of proteins, it probably allows extracting some insoluble proteins from the bulk of the sample, which can be detected by colorimetric method [164]. Moreover, acetone can dissolve a small portion of rubber thus exposing rubber from under the surface. Finally, acetone treatment is found to decrease the apparent crosslink density of the NR compounds regardless of the NR stabilizer type (Figure29 c and Figure 29d). As acetone cannot break the crosslinks created during the vulcanization process, the results can be explained by elimination of the crosslinking points related to the protein interactions. As these proteins are not connected to the NR chains, they are expected to be prone to migration, which is consistent with the high surface protein concentration of the same compounds. This also explains little effect of the acetone-treatment on the dNR_a.c. samples.

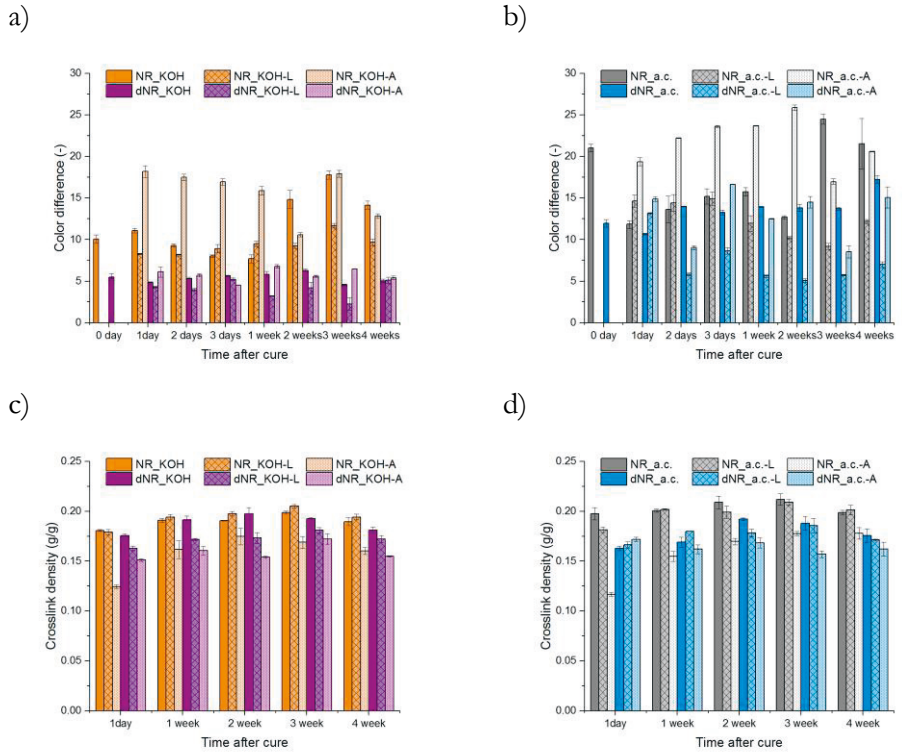

Figure 29. Changes in colorimetric data of the post-treated samples containing a) KOH; and b) ammonium caseinate stabilizer with time, and the changes in colorimetric data of the post-treated samples containing c) KOH; and d) ammonium caseinate stabilizer with time. Time scale is based on the curing moment of the untreated samples. Time scale is based on the curing moment of the untreated samples. *[Publication I]*

In general, it is evident that crosslinking continued developing a little with time. However, the change was minor and could not have caused any significant change in dielectric losses. As expected, dNR samples had somewhat lower crosslink densities due to the reduced amount of natural proteins that could have created branching points and served as cure activators [65].

Prevulcanized NR samples also show some time dependency of dielectric loss on the time after sample preparation, as seen from Figure 30. Here, a reduction of losses is clearly associated with lowered electrode polarization and electrical conductivity contribution related to the possible migration of the surfactant from the bulk of the material. Similarly to other latex materials, both losses and dielectric permittivity stabilize at 3 weeks after the sample preparation day.

a) b)

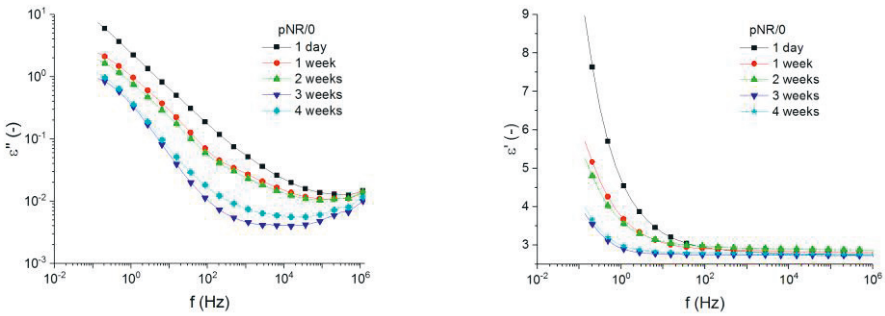

Figure 30. Time dependency of a) dielectric losses; and b) relative dielectric permittivity of pNR/0 sample starting from the sample preparation day.

Not only NR latex samples showed the dependency of dielectric properties on time after vulcanization. The dependency of dielectric losses on time after cure for PDMS compounds is seen in Figure 31. The most significant difference in ε" is observed after two weeks after cure. The changes are related to the reduction of conductivity contribution. The PDMS samples filled with NDs show the same tendency of decreasing ε" with time after cure, but it is a little less pronounced than in case of unfilled PDMS (Figure 31b).

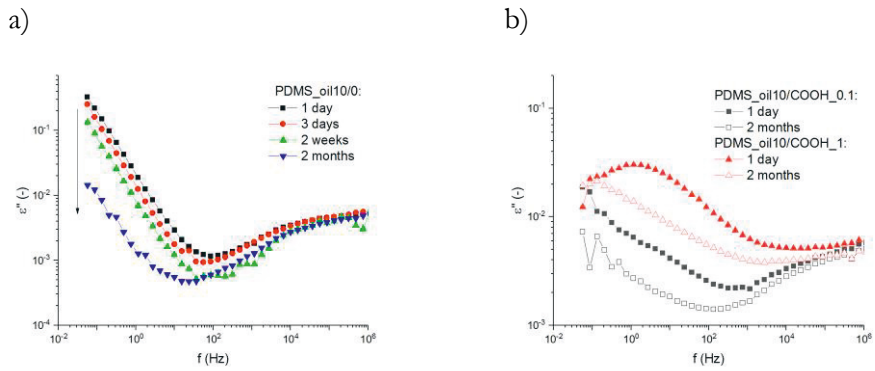

Figure 31. Time-dependent dielectric loss of a) PDMS_oil10/0; and b) PDMS_oil10 with 0.1 and 1 phr of ND-COOH. *[Publication IV]*

7.4 Mechanical properties

The mechanical properties of the compounds were determined with the tensile test, and are represented by the stress-strain curves and the modulus values (stresses at 10, 50, and 100 % elongation). Stress-strain curves of the unfilled and reference materials are shown in Figure 32. In can be seen that PDMS samples have low mechanical strength and elongation at break compared to the other samples. Reference VHB tape has the lowest tensile strength, but high elongation at break. Among the other materials, pNR shows the highest tensile strength, while NR latex stabilized with KOH possesses the highest elongation at break. Moduli values of the samples are presented in Table 8. It can be seen that Ref.VHB has the lowest modulus. Moreover, the post-treatment has very little effect on the moduli values of the latex samples. Finally, Ref.NR and pNR/0 have the highest moduli among the NR samples, which is not desired for the DEG application.

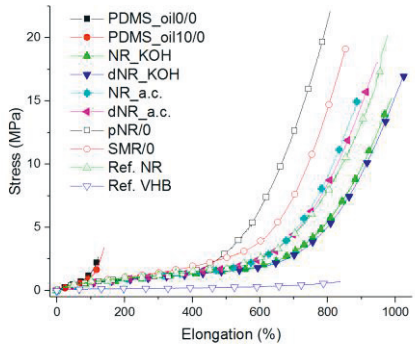

Figure 32. Stress-strain curve of the unfilled and reference materials.

Table 8. Modulus values of unfilled and reference samples including the effect of post-treatment (leach, acetone)

Sample	M_{10} (MPa)			M_{50} (MPa)			M_{100} (MPa)		
	-	leach	acetone	-	leach	acetone	-	leach	acetone
NR_KOH	0.12 ± <0.01	0.12 ± <0.01	0.12 ± 0.01	0.37 ± 0.01	0.39 ± <0.01	0.37 ± 0.01	0.52 ± 0.02	0.55 ± 0.01	0.52 ± 0.02
dNR_KOH	0.12 ± 0.01	0.13 ± <0.01	0.12 ± 0.01	0.36 ± 0.01	0.40 ± 0.01	0.39 ± 0.02	0.51 ± 0.03	0.58 ± 0.01	0.55 ± 0.03
NR_a.c.	0.13 ± <0.01	0.14 ± <0.01	0.13 ± <0.01	0.46 ± 0.01	0.46 ± 0.01	0.39 ± <0.01	0.55 ± 0.01	0.66 ± 0.01	0.54 ± 0.01
dNR_a.c.	0.13 ± <0.01	0.12 ± <0.01	0.12 ± 0.01	0.39 ± 0.02	0.39 ± 0.01	0.37 ± 0.03	0.55 ± 0.03	0.56 ± 0.02	0.53 ± 0.04
pNR/0	0.20 ± 0.01	0.14 ± 0.01	0.16 ± 0.01	0.49 ± 0.02	0.42 ± 0.01	0.48 ± 0.02	0.66 ± 0.03	0.60 ± 0.02	0.68 ± 0.02
SMR/0	0.12 ± <0.01	-	-	0.43 ± <0.01	-	-	0.63 ± 0.01	-	-
PDMS/0	0.12 ± 0.01	-	-	0.49 ± 0.03	-	-	1.34 ± 0.11	-	-
PDMS_oil 10/0	0.12 ± 0.01	-	-	0.45 ± 0.01	-	-	1.38 ± 0.09	-	-
Ref.NR	0.17 ± <0.01	-	-	0.51 ± <0.01	-	-	0.72 ± <0.01	-	-
Ref.VHB	0.05 ± 0.01	-	-	0.11 ± 0.01	-	-	0.13 ± 0.01	-	-

The effect of the addition of different amounts of carboxylated NDs on mechanical properties of the prevulcanized NR latex can be seen in Figure 33a. At the same time, the moduli values of the compounds are presented in Table 9. It can be noted that the addition of more than 2 phr of ND-COOH resulted in significantly increased moduli but decrease in the tensile strength and the elongation at break, which suggests the hydrodynamic effect and ND agglomeration rather than the reinforcement.

a) b)

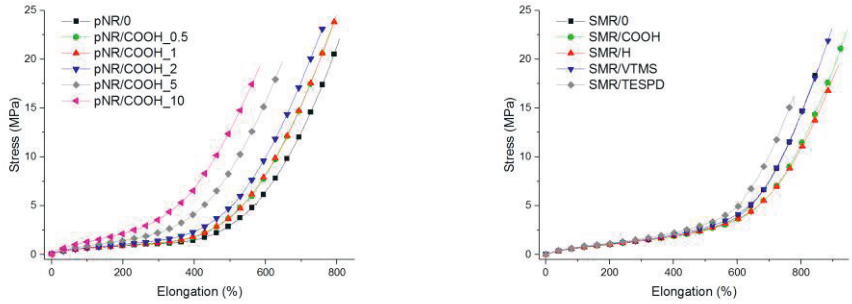

Figure 33. Stress-strain curves of a) pND filled with ND-COOH; and b) SMR filled with 1 phr of NDs.

Table 9. Modulus values of prevulcanized NR latex filled with various amounts of ND-COOH.

Sample	M_{10} (MPa)	M_{50} (MPa)	M_{100} (MPa)
pNR/0	0.20 ± 0.01	0.49 ± 0.02	0.66 ± 0.03
pNR/COOH_0.5	0.17 ± 0.01	0.45 ± 0.02	0.66 ± 0.01
pNR/COOH_1	0.19 ± 0.01	0.47 ± <0.01	0.67 ± 0.01
pNR/COOH_2	0.18 ± <0.01	0.48 ± 0.02	0.71 ± 0.03
pNR/COOH_5	0.18 ± 0.03	0.59 ± <0.01	0.89 ± <0.01
pNR/COOH_10	0.33 ± 0.01	0.89 ± 0.01	1.33 ± 0.02

As can be seen in Figure 32b, addition of 1 phr of ND-TESPD to SMR leads to a significant reduction of both tensile strength and elongation at break, which is related to the presence of large ND agglomerates in the rubber. Both addition of ND-COOH and ND-VTMS results in increased tensile strength, while addition of ND-H increases only elongation at break. According to the Table 10, the presence of fillers has no significant effect on moduli, which is consistent with the results for pNR.

Table 10. Modulus values of SMR filled with 1 phr of NDs.

Sample	M_{10} (MPa)	M_{50} (MPa)	M_{100} (MPa)
SMR/0	0.12 ± <0.01	0.43 ± <0.01	0.63 ± 0.01
SMR/COOH	0.12 ± <0.01	0.43 ± 0.03	0.63 ± 0.04
SMR/TESPD	0.11 ± 0.01	0.39 ± 0.03	0.57 ± 0.05
SMR/VTMS	0.14 ± 0.01	0.46 ± 0.01	0.69 ± 0.01
SMR/H	0.13 ± 0.01	0.45 ± 0.01	0.67 ± 0.01

Next, the effect of oil and 0.1 phr of different NDs on mechanical properties of PDMS is evaluated in Figure 34. As expected, addition of oil increases elongation at break a little, but the mechanical properties stay relatively poor. The addition of

NDs, except for ND-COOH, somewhat decreases elongation at break without much change in the tensile strength and increases the moduli (Table 11). Only ND-COOH has a drastic negative effect on both tensile strength and elongation at break of the PDMS sample.

a) b)

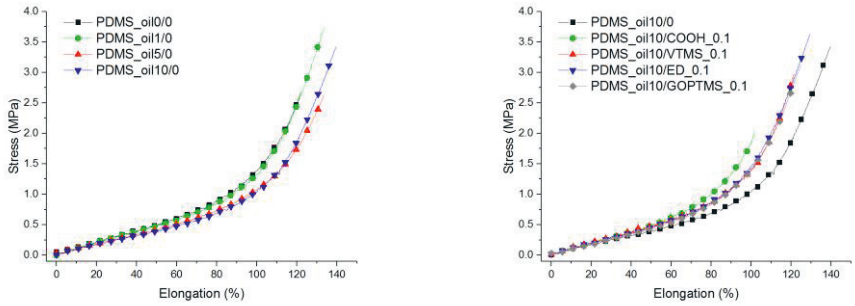

Figure 34. Stress-strain curves of PMMS containing a) different amounts of oil; and b) 0.1 phr of NDs with different surface modifications.

Table 11. Modulus values of PDMS rubbers with different oil content and 0.1 phr of NDs.

Sample	M_{10} (MPa)	M_{50} (MPa)	M_{100} (MPa)
PDMS/0	0.12 ± 0.01	0.49 ± 0.03	1.34 ± 0.11
PDMS_oil1/0	0.10 ± 0.01	0.46 ± 0.03	1.21 ± 0.12
PDMS_oil5/0	0.11 ± 0.01	0.44 ± 0.02	1.09 ± 0.02
PDMS_oil10/0	0.12 ± 0.01	0.45 ± 0.01	1.08 ± 0.09
PDMS_oil10/COOH_0.1	0.11 ± 0.01	0.49 ± <0.01	1.13 ± 0.22
PDMS_oil10/VTMS_0.1	0.10 ± 0.01	0.47 ± 0.01	1.39 ± 0.02
PDMS_oil10/ED_0.1	0.10 ± 0.02	0.44 ± 0.01	1.38 ± 0.10
PDMS_oil10/GOPTMS_0.1	0.11 ± 0.01	0.45 ± 0.01	1.39 ± 0.03

7.5 Stress relaxation

Stress relaxation for the unfilled and reference materials is presented in Table 12. The stress loss is evaluated at 1, 5 and 60 minutes after the start of the test. Among the samples, PDMS has the lowest stress relaxation, and Ref.VHB – the highest. These outcomes can be explained by the chain structure of the materials and the chemical crosslinking, as Ref.VHB is very lightly crosslinked, which enables the possibility of the irreversible flow resulting in decreasing stress. When comparing

the NR materials, SMR/0 sample is found to show a little less stress relaxation than the Ref.NR, but all the latex-based samples are more prone to the stress loss. However, deproteinization and the use of ammonium caseinate stabilizer seems favorable in reducing the stress loss in NR latex samples. Furthermore, both leaching and acetone treatments were found useful for the stress loss reduction in case of the latex samples stabilized with KOH.

Table 12. Stress relaxation of the unfilled latex compounds with different post-treatments.

Sample	Stress loss at 1 minute (%)			Stress loss at 5 minutes (%)			Stress loss at 60 minutes (%)		
	-	leach	acetone	-	leach	acetone	-	leach	acetone
NR_KOH	5.8 ± 0.3	5.3 ± 1.4	4.0 ± 0.6	9.7 ± 1.4	9.4 ± 2.1	6.8 ± 0.7	13.3 ± 1.9	13.1 ± 2.1	10.3 ± 1.0
dNR_KOH	4.9 ± 1.2	4.1 ± 0.6	4.1 ± 0.5	7.5 ± 0.9	7.1 ± 1.4	7.2 ± 2.5	10.4 ± 0.7	10.4 ± 1.8	10.4 ± 3.3
NR_a.c.	5.6 ± 1.9	4.4 ± 1.1	4.2 ± 0.4	10.1 ± 1.8	7.6 ± 1.5	6.7 ± 1.1	13.8 ± 1.6	10.6 ± 2.9	9.5 ± 2.2
dNR_a.c.	3.6 ± 1.1	4.2 ± 0.6	3.8 ± 0.1	5.9 ± 1.9	6.7 ± 1.1	5.9 ± 0.2	8.0 ± 2.2	9.1 ± 2.6	8.4 ± 0.2
pNR	5.0 ± 0.1	5.8 ± 0.2	4.4 ± 0.2	10.18 ± 0.1	10.0 ± 0.6	8.6 ± 1.6	20.1 ± 0.1	14.2 ± 0.9	16.2 ± 4.9
SMR/0	2.4 ± 0.1	-	-	3.7 ± <0.1	-	-	6.2 ± 0.6	-	-
PDMS/0	1.1 ± <0.1	-	-	1.8 ± 0.1	-	-	2.8 ± 0.5	-	-
PDMS_oil10/0	0.8 ± 0.1	-	-	1.3 ± 0.3	-	-	2.3 ± 0.4	-	-
Ref.NR	2.8 ± 0.2	-	-	4.5 ± 0.4	-	-	7.0 ± 0.7	-	-
Ref.VHB	19.2 ± 1.6	-	-	28.6 ± 2.9	-	-	37.1 ± 4.8	-	-

Addition of small amounts of carboxylated NDs to the prevulcanized NR latex resulted in significantly increased stress losses, as seen from Table 13. Generally, only samples containing 5 and 10 phr of ND-COOH show lower stress relaxation than the unfilled pNR/0. The results for the untreated samples are correlating with the increased modulus of the compounds, while the enhancement in the stress loss behavior of the acetone-treated samples can be related to the improvements in the rubber-filler interface.

Table 13. Stress relaxation of pNR-ND composites.

Sample	Stress loss at 1 min (%)	Stress loss at 5 min (%)	Stress loss at 1 hour (%)
pNR/0	5.0 ± <0.1	10.2 ± <0.1	20.1 ± <0.1
pNR/COOH_0.5	7.9 ± <0.1	14.9 ± <0.1	25.2 ± <0.1
pNR/COOH_1	6.2 ± <0.1	11.9 ± <0.1	20.2 ± <0.1
pNR/COOH_2	6.1 ± <0.1	11.4 ± <0.1	18.1 ± <0.1
pNR/COOH_5	4.9 ± <0.1	9.6 ± <0.1	17.8 ± <0.1
pNR/COOH_10	3.6 ± <0.1	6.7 ± <0.1	12.1 ± <0.1

However, when dry SMR rubber is used with 1 phr of NDs, some reduction of stress relaxation is noticed (Table 14). This can be related to the absence of the stabilizers and surfactants in the system which would lower the filler-rubber interactions. Moreover, it can be seen that the samples containing surface-modified ND-VTMS and ND-TESPS, which can contribute to the rubber curing process, show even more reduced stress losses.

Table 14. Stress relaxation of SMR composites containing 1 phr of NDs with different surface treatments.

Sample	Stress loss at 1 min (%)	Stress loss at 5 min (%)	Stress loss at 1 hour (%)
SMR/0	2.40 ± 0.08	3.67 ± 0.02	6.20 ± 0.61
SMR/COOH	2.05 ± 0.26	3.27 ± 0.26	4.22 ± 0.72
SMR/TESPD	1.83 ± 0.38	2.98 ± 0.67	4.90 ± 1.56
SMR/VTMS	1.58 ± 0.40	2.72 ± 0.66	4.11 ± 1.11
SMR/H	2.00 ± 0.10	3.35 ± 0.23	4.63 ± 0.37

Similar effect of even smaller amount of the NDs on stress relaxation is seen for the PDMS composites, presented in Table 15. Such improvement can be related to the enhanced interfacial interaction between matrix and filler upon the filler surface modification.

Table 15. Stress relaxation of PDMS compounds.

Sample	Stress loss at 1 min (%)	Stress loss at 5 min (%)	Stress loss at 1 hour (%)
PDMS/0	1.08 ± 0.04	1.77 ± 0.11	2.83 ± 0.47
PDMA_oil10/0	0.78 ± 0.13	1.30 ± 0.28	2.26 ± 0.38
PDMS_oil10/COOH_0.1	0.61 ± 0.17	0.96 ± 0.23	1.98 ± 0.38
PDMS_oil10/VTMS_0.1	0.56 ± 0.09	0.86 ± 0.06	1.47 ± 0.16
PDMS_oil10/ED_0.1	0.69 ± 0.04	1.22 ± 0.28	2.50 ± 0.41
PDMS_oil10/GOPTMS_0.1	0.62 ± 0.12	1.07 ± 0.21	2.41 ± 0.37

7.6 Dynamic mechanical behaviour

DMA analysis results for the unfilled and reference materials are presented in Table 16. The glass transition temperatures T_g show a small shift towards lower temperatures for the deproteinized NR latex samples, which can be related to the higher chain mobility due to the reduced NR-protein interactions. Moreover, dNR samples showed higher maximum values of tan δ than, indicating that the motion of the molecules is less restricted. While leaching seems not to cause significant changes in the chain mobility, the acetone-treatment reduces the T_g of NR latex compounds much more. This may mean that some rubber-associated proteins were removed from the system upon the treatment, rubber-protein linkages were broken, thus giving more freedom to the rubber chains.

Table 16. DMA loss tangent numerical data for the unfilled and reference samples.

Sample	Temperature at tan δ_{max} (°C)			tan δ_{max} (-)			tan δ at 20 °C (-)		
	-	leach	acetone	-	leach	acetone	-	leach	acetone
NR_KOH	-53.5	-54.7	-55.0	1.94	2.42	2.15	0.076	0.067	0.076
dNR_KOH	-55.7	-54.5	-55.5	2.41	2.40	2.43	0.084	0.069	0.082
NR_a.c.	-55.9	-56.2	-57.6	2.29	2.36	2.25	0.073	0.079	0.083
dNR_a.c.	-56.9	-55.1	-55.7	2.33	2.42	2.45	0.106	0.085	0.092
pNR	-56.6	-57.0	-56.4	2.42	2.64	2.45	0.085	0.074	0.079
SMR/0	-55.0	-	-	2.62	-	-	0.065	-	-
PDMS/0	-119.7	-	-	0.68	-	-	0.058	-	-
PDMS_oil10/0	-120.9	-	-	0.64	-	-	0.043	-	-
Ref.NR	-63.6	-	-	1.98	-	-	0.173	-	-
Ref.VHB	-0.9	-	-	1.21	-	-	0.956	-	-

The effect of different loads of NDs on the prevulcanized NR samples containing various amounts of carboxylated NDs on the energy damping properties are further compared. As shown in Figure 35, the addition of up to 2 phr of NDs leads to both a small decrease of T_g and an increase in the tan δ peak, while the addition of higher amounts of filler results in the opposite effect. Dry lubricating phenomenon of NDs at low concentration may be responsible for the effect [100]. An increase in T_g at higher filler loads is very small, and the decrease of loss tangent peak is probably due to the domination of decreased free volume. Furthermore, all the composites, especially samples with low ND content (up to 2 phr), show lower loss tangent than SMR/0 in the 0 - 20 °C range. This can be possibly explained by better rubber-filler

interaction, as an improvement of tensile properties was also observed for the same compounds.

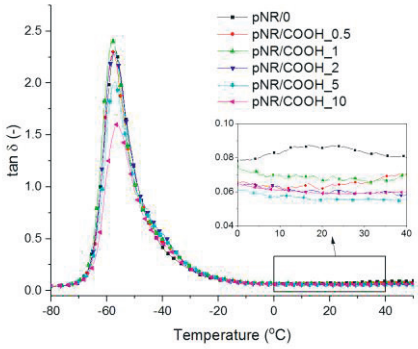

Figure 35. DMA loss tangent curves of pNR-ND composites as a function of temperature.

When the SMR samples containing 1 phr of NDs with different surface chemistry were studied with DMA, the addition of ND-COOH shifted the glass transition at the maximum tan δ of NR towards lower temperatures and increased maximum tan δ, which is similar to the pNR compound. However, loss tangent at room temperature is marginally increased implying that no strong interaction was introduced between SMR and ND-COOH, which is not surprising due to the polarity differences. The addition of modified NDs has an opposite effect on both T_g and loss tangent at room temperature. This small positive effect of VTMS-modified and hydrogenated NDs on the loss tangent could mean better affinity between the filler and rubber.

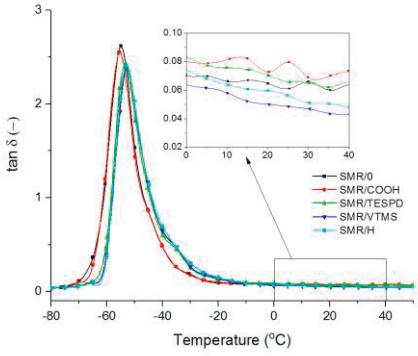

Figure 36. Temperature dependence of DMA loss tangent of SMR samples containing 1 phr of NDs. *[Publication III]*

For the PDMS compounds, the T_g determined at maximum tan δ has lowered upon the addition of oil, as seen in Figure 37. However, the addition of fillers results in a small shift of the T_g towards higher temperatures, and also lowers and broadens the transition peaks which is related to the restriction of chain mobility and the differences in the amount of amorphous phase, which was further confirmed by the DSC study. In the DMA curves, melting is observed for all the PDMS samples as a drop in tan δ around -50 °C. Furthermore, some decrease in tan δ is seen in 0 - 20 °C temperature range upon the addition of 0.1 phr of modified NDs. PDMS_oil10/COOH_0.1 and PDMS_oil10/VTMS_0.1 compounds show the lowest tan δ indicating the lowest loss.

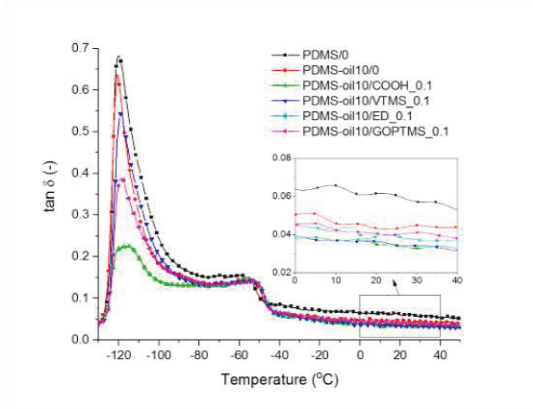

Figure 37. DMA loss tangent curves of PDMS-ND composites as a function of temperature. *[Publication IV]*

The mentioned effect of NDs on the chain orientation and behavior is seen from the DSC curves presented in Figure 38. Significant melting peaks are seen for all compounds containing NDs, while the PDMS_oil10/0 compound is almost fully amorphous. Degree of crystallinity of the compounds containing NDs increases significantly, as shown in Table 17. This implies the NDs behave as crystallization centers and affect the chain orientations in polymer, which can consequently be responsible for the dry lubrication action seen in DMA. Finally, the observed reduction in tan δ of ND-filled PDMS compounds can be related to the increased apparent crosslink density of all filled samples except for PDMS_oil10/GOPTMS_0.1 (Table 17). The increase in 1/Q also implies some increased filler-rubber interactions.

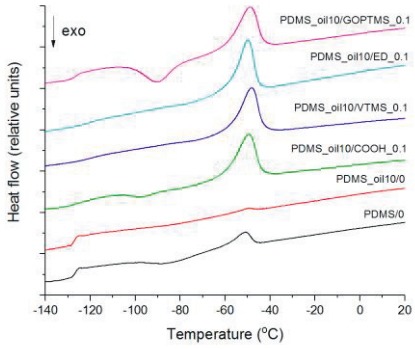

Figure 38. DSC curves of PDMS-ND compounds. The curves are shifted vertically for clarity. *[Publication IV]*

Table 17. Glass transition temperature, crystallinity and apparent crosslink densities of silicone compounds.

Sample	DSC T_g (°C)	Enthalpy (J/g)		Degree of crystallinity* (%)	1/Q (-)
		cold crystallization	melting		
PDMS/0	-127.0	3.26	3.84	0.9	0.689 ± 0.005
PDMS_oil10/0	-127.3	0.78	0.92	0.2	0.614 ± 0.003
PDMS_oil10/COOH_0.1	-124.8	1.45	15.37	22.7	0.683 ± 0.003
PDMS_oil10/VTMS_0.1	-120.6	-	15.47	25.2	0.674 ± 0.004
PDMS_oil10/ED_0.1	-121.6	-	14.90	24.3	0.679 ± 0.003
PDMS_oil10/GOPTMS_0.1	-126.6	9.57	13.58	6.5	0.554 ± 0.047

*Based on the enthalpy of fusion of 100% crystalline PDMS = 61.3 J/g [165]

7.7 Hysteresis loss

Hysteresis loss is evaluated at low testing rate for all the samples. Moreover, the effect of increasing the testing rate and elongation is compared for the unfilled and some filled materials. For the Ref.VHB experiencing severe stress relaxation, and for the PDMS samples having generally low elongation at break, only low-rate test at 45% elongations were performed. It can be seen from Table 18 and Table 19 that the differences between the low- and high-rate results are mostly determined by the different elongation – the hysteresis loss approximately doubles as the elongation changes from 45 to 100%. Nevertheless, the rate also affects the losses, as at slower rate stress relaxation is present to some extent.

Among the tested unfilled and reference materials, Ref.VHB has the highest hysteresis losses, which can be explained by the low crosslink density. At the same time, PDMS samples show the lowest hysteresis loss, which is mostly related to the structure and flexibility of the polymer chain. Among the NR latex materials, NR_KOH and pNR/0 have the highest hysteresis losses at 10th cycle, while deproteinized samples have reduced hysteresis losses. Leaching with water reduces the losses further and it is most efficient for NR samples and dNR-KOH-L. Nevertheless, the commercial Ref.NR shows somewhat lower hysteresis loss than NR latex samples. Acetone-treatment also has a positive effect on the hysteresis loss reduction, but not as pronounced as leaching with water. Remarkably, acetone-treatment is more efficient in reducing hysteresis at low rate than the high rate. The difference is most likely related to the significant reduction of the stress relaxation effect upon such treatment.

Table 18. Hysteresis loss at low rate of the unfilled and reference compounds including the post-treatment (leach, acetone).

Sample	ΔH at 1st cycle (%)			ΔH at 10th cycle (%)		
	-	leach	acetone	-	leach	acetone
NR_KOH	8.2 ±1.2	7.3 ± 1.4	7.6 ± 2.7	3.2 ± 1.3	2.7 ± 1.5	2.2 ± 1.4
dNR_KOH	9.5 ± 0.3	7.7 ± 0.7	8.6 ± 1.5	2.7 ± 1.6	1.5 ± 0.4	1.2 ± 0.7
NR_a.c.	8.5 ± 0.7	6.8 ± 1.4	9.2 ± 1.4	1.9 ± 0.1	1.4 ± 0.7	2.5 ± 0.6
dNR_a.c.	7.8 ± 1.3	7.5 ± 0.5	6.8 ± 1.9	2.8 ± 1.3	2.7 ± < 0.1	1.1 ± 0.9
pNR	9.3 ± 0.3	8.2 ± 1.1	9.6 ± 0.2	3.2 ± 0.3	2.7 ± 0.3	2.9 ± 0.2
SMR/0	5.4 ± 0.8	-	-	1.6 ± 0.3	-	-
PDMS/0	1.5 ± 0.2	-	-	0.6 ± 0.2	-	-
PDMS_oil10/0	2.2 ± 0.3	-	-	0.6 ± 0.2	-	-
Ref.NR	8.1 ± 0.1	-	-	3.1 ± 0.2	-	-
Ref.VHB	19.5 ± 2.9	-	-	12.9 ± 1.3	-	-

Table 19. Hysteresis loss at high rate of the unfilled and reference compounds including post-treatment (leach, acetone).

Sample	ΔH at 1st cycle (%)			ΔH at 10th cycle (%)		
	-	leach	acetone	-	leach	acetone
NR_KOH	19.2 ± 1.4	16.4 ± 1.3	17.9 ± 0.2	9.1 ± 0.5	7.2 ± 0.4	7.0 ± 0.2
dNR_KOH	19.3 ± 1.4	16.3 ± 0.8	16.1 ± 0.6	7.9 ± 0.3	5.7 ± 0.2	6.7 ± 0.2
NR_a.c.	19.2 ± 1.9	14.1 ± 0.7	16.7 ± 1.7	9.1 ± 0.1	5.6 ± 0.5	7.8 ± 0.8
dNR_a.c.	16.3 ± 1.7	16.4 ± 1.8	16.2 ± 1.1	7.1 ± 1.0	6.3 ± 0.3	6.1 ± 0.1
pNR	17.8 ± 0.1	18.4 ± 0.7	15.5 ± 0.1	8.2 ± 0.1	8.0 ± 0.2	6.5 ± 0.1
SMR/0	10.9 ± 0.4	-	-	3.2 ± 0.2	-	-
PDMS/0	N/A	-	-	N/A	-	-
PDMS_oil10/0	N/A	-	-	N/A	-	-
Ref.NR	16.2 ± 0.6	-	-	6.7 ± 0.1	-	-
Ref.VHB	N/A	-	-	N/A	-	-

As prevulcanized NR was found to have relatively high hysteresis losses compared to the other NR samples, the effect of different amounts of NDs on hysteresis losses was assessed. From Table 20, it is seen 2 phr of ND-COOH is needed to reduce the hysteresis losses of pNR at first cycle a little, which is consistent with the results from mechanical testing. Nevertheless, the losses at 10th cycle stay comparable high regardless of the filler content.

Table 20. Hysteresis loss at low rate of pNR filled with various amounts of ND-COOH.

Sample	Hysteresis loss at low rate (%)	
	1st cycle	10th cycle
pNR/0	9.5 ± 2.6	2.0 ± 0.5
pNR/COOH_0.5	9.8 ± 0.4	2.2 ± 0.6
pNR/COOH_1	11.1 ± 1.9	2.6 ± 0.8
pNR/COOH_2	9.1 ± 1.4	2.3 ± 1.1
pNR/COOH_5	11.3 ± 0.5	4.3 ± 1.7
pNR/COOH_10	20.0 ± 2.1	5.6 ± 0.8

In SMR samples, no clear trend in hysteresis loss is seen upon the addition of 1 phr of NDs in both low- and high-rate cycles (Table 21). Nevertheless, in both cases at 10th cycle, SMR/H shows some hysteresis reduction. High deviations in hysteresis loss data, especially for SMR/TESPD and SMR/VTMS can be indicative of poorer filler dispersion, as also seen from the comparison of low- and high-rate data especially for SMR/TESPD that forms large ND agglomerates.

Table 21. Hysteresis loss of SMR compounds filled with 1 phr NDs.

Sample	Hysteresis loss at low rate (%)		Hysteresis loss at high rate (%)	
	1st cycle	10th cycle	1st cycle	10th cycle
SMR/0	5.4 ± 0.8	1.6 ± 0.3	10.9 ± 0.4	3.2 ± 0.2
SMR/COOH	4.9 ± 0.8	1.1 ± 0.6	10.0 ± 0.7	3.2 ± 0.5
SMR/TESPD	5.2 ± 0.4	0.8 ± 0.2	12.5 ± 1.3	4.3 ± 0.8
SMR/VTMS	6.7 ± 1.7	1.9 ± 0.8	10.9 ± 0.3	2.7 ± 0.2
SMR/H	5.9 ± 1.2	0.8 ± 0.1	11.6 ± 0.1	2.9 ± 0.1

In PDMS samples, the addition of oil results in some increase in hysteresis, but the addition of even 0.1 phr of NDs is found to reduce hysteresis losses especially after 10th cycle (Table 22). Surface-modified NDs are more efficient in reducing the hysteresis of PDMS than ND-COOH, which is related to the polarity of the fillers and their ability to interact with the crosslinker.

Table 22. Hysteresis loss at low rate of silicone compounds.

Sample	Hysteresis loss at low rate (%)	
	1st cycle	10th cycle
PDMS/0	1.49 ± 0.17	0.63 ± 0.20
PDMA_oil10/0	2.21 ± 0.27	0.64 ± 0.15
PDMS_oil10/COOH_0.1	1.70 ± 0.25	0.64 ± 0.37
PDMS_oil10/VTMS_0.1	1.59 ± 0.66	0.46 ± 0.23
PDMS_oil10/ED_0.1	1.89 ± 0.71	0.30 ± 0.10
PDMS_oil10/GOPTMS_0.1	1.48 ± 0.37	0.37 ± 0.18

8 DISCUSSIONS

In this chapter, the presented results of the study are discussed. In section 8.1, the effect of different matrix compositions on the material losses is discussed and compared to the reference materials. Moreover, the applicability of the studied materials for DEGs is evaluated. In the section 8.2, the effectiveness of ND modification is assessed and in the section 8.3 the effect of NDs on material-related losses of elastomers is discussed.

8.1 Unfilled elastomers

When comparing three types of rubber most used in DEGs, one can notice the benefits of NR and PDMS over acrylic Ref.VHB, which exhibits dramatic mechanical losses. NR, especially SMR form, offers comparably low dielectric losses combined with high elasticity and strength. Moreover, the stress relaxation and hysteresis losses of SMR are considerably better compared to the NR latex compounds. However, PDMS compounds have even lower stress relaxation and hysteresis losses, but poor mechanical properties and a significant contribution of conductivity to otherwise low dielectric loses.

Although VHB tape is considered in literature to have high dielectric losses, its dielectric properties seemed to be well suited for DEG use, when frequencies below 10 Hz are considered, as it possesses a high dielectric permittivity as well. Moreover, from the dielectric losses and permittivity of the studied unfilled and reference compounds at room temperature at 1 Hz, the benefits of SMR and PDMS compounds are obvious. The initial comparison of the developed SMR recipe to the commercial reference materials revealed that high dielectric losses of Ref.NR were related to a very pronounced conductivity effect, some contribution from electrode polarization and some interfacial effect. The interfacial polarization contribution is most likely related to the presence of fillers, as was supported by the increase in dielectric permittivity at low frequency area. The presence of inorganic non-black filler in Ref.NR was suggested by the TGA, where the inorganic residual was considerably high (10.4%) indicating the presence of both small amount of mineral

filler and ZnO. Therefore, lower dielectric losses of the custom-made SMR/0 compound over the Ref.NR can be related to the lower content of stearic acid and zinc oxide in the recipe. Thus, among NR materials, dielectric properties of SMR/0 were confirmed to be more suitable for a DEG application especially as dielectric loss was lowered from 0.194 (Ref. NR) to 0.005, as seen from the comparison chart in Figure 39. As was mentioned previously, PDMS samples possesses the second lowest dielectric losses among the unfilled samples, which still contain a large conductivity contribution to it. The addition of plasticizing oil increased the losses a little. The effect can be related to the small reduction of the apparent crosslink density and possibly easier charge transport paths. Nevertheless, the overall loss properties of the PDMS compounds are well suitable for the DEGs.

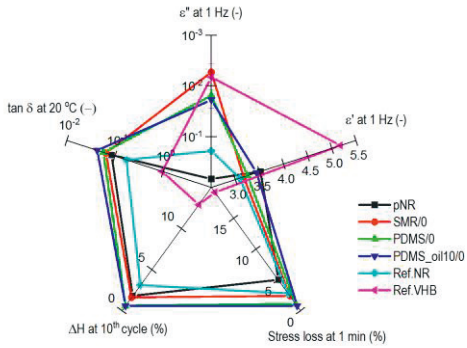

Figure 39. The comparison of the unfilled and reference materials based on their loss properties (properties improve from the center of the graph).

Generally, as the changes in dielectric loss with time in latex compounds were observed below 10^4-10^5 Hz, they are not related to the polymer network or chain dynamics, but rather to the reduction of conductivity contribution and interfacial polarization due to the migration of ions and small molecules to the surface of the sample, or a time-dependent decomposition of ZDBC accelerator, which is more pronounces for the dNR samples [36]. Moreover, among the latex-based compounds, dielectric losses of the deproteinized samples are clearly much lower than of normal rubber samples without a decrease in relative dielectric permittivity, even if the crosslink density of such compounds is lower than of a standard NR. The comparison chart of the latex compounds is shown in Figure 40. Furthermore, the losses of NR containing ammonium caseinate stabilizer are almost twice lower compared to the compound stabilized with KOH. However, when leaching is

applied to the NR_KOH samples, their losses are reduced almost to the same level as NR_a.c., which indicates that leaching procedure removes small ions and molecules like KOH much more readily than large protein molecules. This can be suggested when comparing the effect of leaching on dielectric losses of deproteinized dNR_KOH to dNR_a.c. Moreover, from the colorimetric measurements it was concluded that the added protein-based ammonium caseinate is most likely migrating to the sample surface already upon drying of the film. Therefore, leaching seems to have no effect on dNR_a.c. The same effect is not achieved with acetone treatment, which rather removed water-insoluble particles and broke down some proteins but did not affect the KOH content. Thus, acetone-treatment is not efficient for the deproteinized NR regardless of the stabilizer. Nevertheless, both post-treatment methods reduced the dielectric losses of pNR sample successfully mostly by lowering the conductivity contribution part of the losses.

a) b)

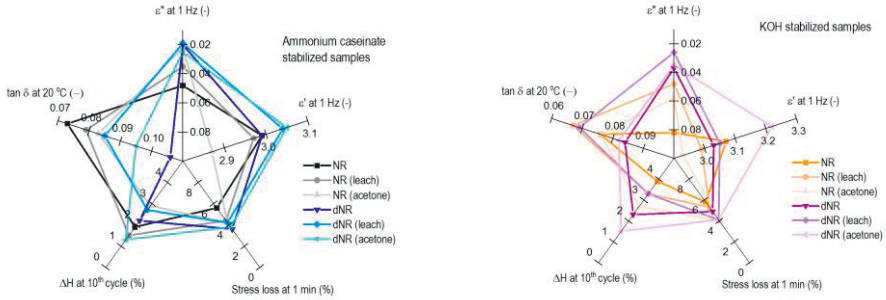

Figure 40. The comparison of the loss properties of the latex-based materials containing a) ammonium caseinate stabilized; and b) KOH stabilizer (properties improve from the center of the graph).

When the stress relaxation is concerned, molecules start rearranging and slipping along one another under stress, which results in the reduction of stress required to maintain this strain level. As the stress relaxation is a major drawback for some of the materials used in DEG, the effect of proteins, stabilizers and post-treatment needed to be evaluated. All the latex compounds showed pronounced stress relaxation compared to SMR/0 sample, and both leaching and acetone-treatment seemed to have little effect on the stress loss reduction of the deproteinized NR samples. Nevertheless, dNR had clearly the lowest stress relaxation. Stress loss of the dNR_KOH was a little higher than of dNR_a.c., which may be related to the

effect of KOH stabilizer on proteins, which reduces the rubber-protein bond strength and allows more stress to be lost during the stretch. Some positive effect of the post treatment on NR can be related to the removal of any "weak" interactions, such as uncrosslinked chains or terminal links that would otherwise contribute to the stress relaxation by slippage. However, the same reason may be responsible for the increase in tan δ at 20 °C pf the deproteinized and acetone-treated samples. In case of tan δ, dNR samples generally have higher energy dissipation than NR due to a bit lower crosslink density and less protein contribution to the network. Generally, deproteinized and leached latex samples have the combination of loss properties making them most suitable for DEG application among the latex samples. Among the stabilizers, ammonium caseinate can be preferable, but the final difference in properties is not that critical. However, when all the unfilled samples are considered, PDMS is another good candidate for the DEG use, as it has low dielectric losses combined with a very low hysteresis loss and stress relaxation that is not affected much by the addition of plasticizer, as can be seen from Figure 39. Furthermore, the tan δ of PDMS compounds is also one of the lowest.

8.2 Modified nanodiamonds

Nanodiamonds with carboxylated surface originally used in the study are much more polar than both PDMS and NR. For the composite materials such difference in polarity usually means poor filler-rubber interaction and the formation of filler aggregates. However, in case of wet compounding process (latexes), the polar surface of NDs makes the particles stably dispersed in water without use of surfactant, which would otherwise increase the dielectric losses of the system. At the same time, a polar layer is formed around the rubber latex particles owing to the presence of natural proteins and phospholipids, which also stabilize the system. Thus, carboxylated surface of NDs is expected to be beneficial for inducing some stronger physical interactions between NR latex particles and NDs. However, in case of dry rubber systems and other elastomers, like PDMS, the polar surface of ND can be undesirable. Therefore, NDs are modified in order to reduce the polarity of the surface and even attach the chemical groups able to induce chemical bonds to the elastomer during the vulcanization process. As a result, a stronger interface with less losses is expected. However, before the addition of the modified NDs into the recipe, the effectiveness of the surface modification needs to be assessed.

The aim of the silane modification of ND was to introduce vinyl groups (VTMS) and sulfur (TESPD) onto its surface through a reaction between carboxyl and silanol. However, the reaction in expected to happen more readily between two –OH groups in silanol rather than –COOH and –OH groups, which would result in a self-condensation of silane with less probability of chemical attachment to the ND surface. Even when acetic acid was added to prevent a condensation, the reaction between the carboxylic and silanol groups was found unlikely. It was clear from the FTIR spectra and TGA curves of NDs treated by silanes containing single silanol group. No presence of the silanes was seen in FTIR spectra, neither additional mass loss event occurred in TGA at 200 - 300 °C. This implies that during the modification process, a silanol group from one molecule reacted with a silanol from another molecule and was removed by washing and filtration. However, as in case on multifunctional silanes, their presence was clearly detected on the ND surface by FTIR, TGA and EDS analysis, which implies the formation of a silane shell around ND without any chemical bonding to its surface.

The shell formation around ND is not considered as a negative effect, as the resulting surfaces has lower polarity due to Si-O-Si groups, as well as the presence of some vinyl groups and sulfur, depending on the silane type, which are available for the curing process. However, uncontrolled and extensive silane shell formation leads to the agglomeration of particles that is very difficult to break down. Agglomerated particles cannot be evenly distributed through the composite during the mixing and cause fluctuation of properties in a sample. Moreover, concerning the DEG application, large agglomerates increase possibility for a short circuit during the operation. Therefore, the extensive shell formation needs to be prevented. One possibility of reducing the shell formation is lowering the silane-filler ratio, or selecting other silane types with less functional groups. Furthermore, due to the structural differences between two used silane types, namely doubled amount of alkoxy-groups in TESPD compared to VTMS and its steric effect, different route of modification may need to be developed.

When performing the reaction between carboxylated ND and an epoxy-group containing compound (ED), different reaction products can be expected depending on the ring-opening mechanism. For example, at high temperatures and acidic conditions, the attached ED can bond to ND through a reaction between a hydroxyl and carboxyl group, which also leads to the introduction of water to the system. Water hydrolyses the epoxy-group and can reduce the yield of the reaction between ND and ED. However, as was seen from the experiment with silanes, the probability of the reaction between –COOH and –OH is small, especially when the temperature

is kept 40 °C. Nevertheless, some possibility exists of the reaction between –OH groups of different modified NDs, which would bind the particles into a very strong aggregates and can cause similar agglomeration-related problems, as discussed previously. According to the relatively small mass loss at 200 - 300 °C detected with TGA, as well as visual analysis of the SEM images, no extensive agglomeration happened during the modification of NDs with ED.

Finally, as GOPTMS modification agent combines the chemical features of both silane- and epoxy-compounds, all the types of previously discussed reactions are possible during the ND modification procedure. However, it became clear from the FTIR and TGA analyses that despite the presence of multiple silanol groups, no extensive shell formation occurred. This conclusion can be drawn also from the low Si content and Si : O ratio obtained by the EDS analysis and the SEM images. The result can be related to the more bulky structure of the molecule, which reduces accessibility of the reaction sites of GOPTMS attached to the ND surface, and high probability of the reaction between –COOH and epoxy-group. Thus, the modification is considered as successful.

8.3 Composites

Elastomer composites were prepared aiming to improve the dielectric and mechanical behavior of the materials. As a result, addition of NDs helps reducing the conductivity contribution to the dielectric losses and leads to some reduction of stress relaxation and tan δ in NR samples. However, the most effective loss property improvements, including the reduction of hysteresis losses, are achieved for the PDMS composites. It can also be concluded that high amounts of NDs are not needed to achieve the best combination of properties.

8.3.1 Natural rubber

As discussed in Chapter 8.1, dielectric losses of prevulcanized latex pNR are the highest, which is most likely related to the presence of a surfactant causing some electrode polarization combined with the conductivity contribution. When small amounts of NDs are added to pNR, dielectric losses start decreasing, as does the relative dielectric permittivity. This effect can be explained by the reduction of electrode polarization at this frequency, as some mobile charges can be bonded to

the ND surface. However, after addition of 10 phr of NDs, dielectric losses start increasing again, and the dielectric permittivity becomes even higher than for the unfilled pNR. The effect of the addition of fillers to the selected rubbers is seen by comparing the loss property graphs (Figure 41). As suggested from the results, such change can be related to the effect of interfacial polarization. Interfacial polarization is also believed to be the reason for the increased losses in SMR upon the addition of 1 phr NDs with different surface treatments. Among the samples, SMR-VTMS and SMR-TESPD show less pronounced increase in both dielectric losses and permittivity, which indicates less discrepancy at the filler-rubber interface. Moreover, the changes may be related to the difference in the volume ratio of NDs to rubber. As seen from the SEM images of SMR/ND composites (Figure 42), the interface between filler and matrix looks uniform and good adhesion between the matrix and the filler can be suggested. This can be related to the stronger interactions between the silane shell on the filler surface and the NR chains. However, in all the samples some filler aggregates are present. These filler aggregates and poorer filler dispersion can be responsible for the high deviations in hysteresis loss data, especially for NR/ND-TESPD and NR/ND-VTMS, as also seen from the comparison of low- and high-rate data.

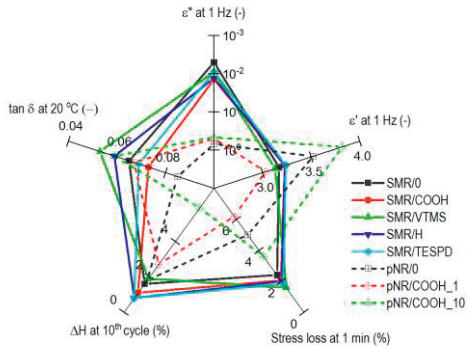

Figure 41. The comparison chart of the NR-ND composites (properties improve from the center of the graph).

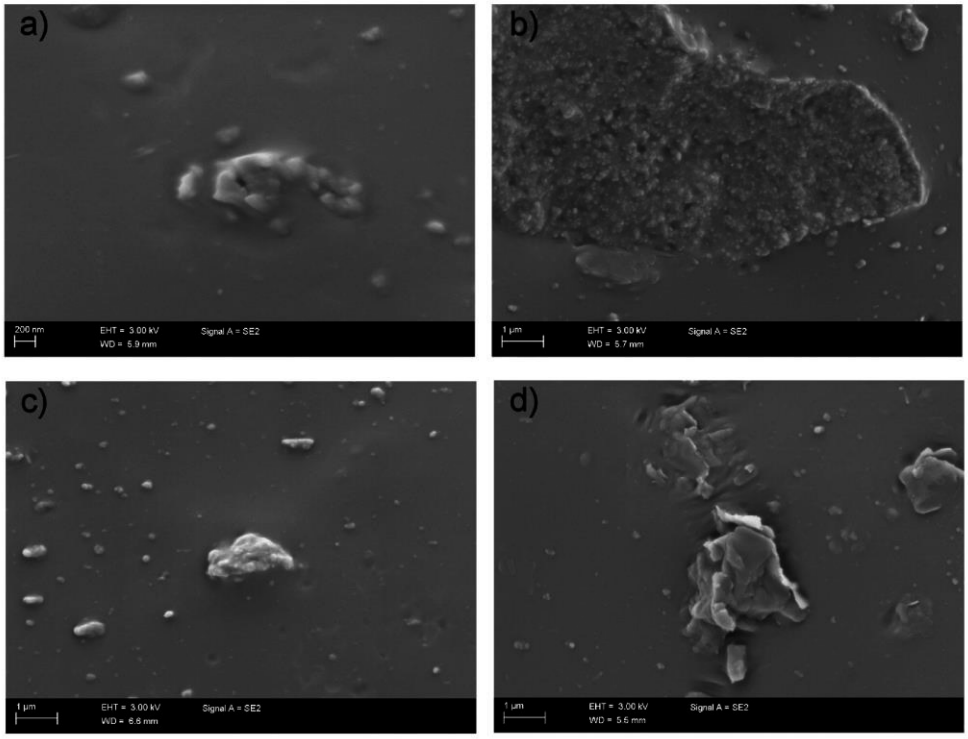

Figure 42. SEM images of SMR composites containing 1 phr NDs with a) –COOH, b) –H, c) –VTMS, and d) –TESPD surface treatments. *[Publication III]*

Generally, as seen in Figure 42, it can be concluded that SMR samples have sufficiently low losses that the addition of NDs is not improving their properties sufficiently. In terms of mechanical losses, no clear trend was seen in hysteresis loss upon the addition of NDs to SMR, but all composites showed some reduction is the stress loss compared to the unfilled SMR/0. Nevertheless, all the custom-made NR compounds showed significantly lower hysteresis and stress relaxation than any of the commercial reference materials. At the same time, addition of NDs to the prevulcanized latex was found not efficient to achieve a good balance of properties – at low loads the hysteresis loss and stress relaxation were comparably high, but at high loads the dielectric loss was increasing. Considering the overall losses including tan δ, SMR/ND-VTMS compound can be found most suitable for the energy harvesting.

8.3.2 Silicones

Even more improvement of the dielectric properties was seen upon addition of 0.1 phr of NDs to the PDMS compounds containing 10 phr plasticizing oil (Figure 43). The modified NDs know to contribute to the curing process (ND-VTMS and ND-ED) reduce the losses of the samples much significantly than the samples, which are expected just to improve compatibility between PDMS and ND (ND-GOPTMS) or trap the mobile charge carriers (ND-COOH). Thus, NDs with the modified surface containing the groups allowing chemical bonding between the elastomer and filler during the curing process are able to reduce the dielectric losses of PMDS compounds most efficiently even when only very small amounts are added.

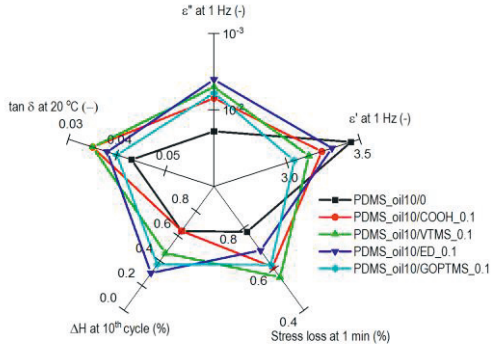

Figure 43. The comparison chart of the PDMS-ND composites (properties improve from the center of the graph).

Furthermore, low tan δ values were achieved by the addition of NDs (especially ND-COOH and ND-VTMS) to the plasticized PDMS (Figure 43). Such low losses are preferable for the dielectric energy harvesting application, and can be related to the reduced internal friction within the composites, as NDs are believed to behave as dry lubricants facilitating the orientation of macromolecules upon the applied stress [7, 45].

The effect of NDs on the arrangements of the rubber chains is known to be responsible for the dry lubrication action can be clearly seen from the DSC numerical results of PDMS samples (Table 17). In this case, NDs are expected to affect the orientation of the PDMS molecules by acting as crystallization centers and restricting the molecular mobility at the glass transition, as can be seen from the increased T_g temperatures. The higher T_g indicates stronger filler-matrix interactions. Significant T_g temperature increase of PDMS_oil10/VTMS and PDMS_oil10/ED samples

suggested the presence of chemical bonds between the filler and matrix while less pronounced increase in T_g of PDMS_oil10/COOH_0.1 and PDMS_oil10/GOPTMS_0.1 implies the physical nature of the induced filler-matrix interactions. The presence of chemical or physical filler-matrix bonds upon addition of NDs can be also suggested from the increased apparent crosslink densities of the materials. Moreover, the lowest degree of crystallinity of PDMS_oil10/GOPTMS_0.1 among the PDMS composites can be related to more branched and bulky structure of GOPTMS compared to the other ND modifications, which was also seen in the reduction of the apparent crosslink density. It can be suggested that the crosslinking process is most probably interfered by the presence of methoxysilane or –OH groups at the ND-GOPTMS filler surface.

Due to the combination of low moduli and sufficient crosslink density, lowered dielectric and hysteresis losses, as well as low stress relaxation, PDMS_oil10/VTMS_0.1 and PDMS_oil10/ED_0.1 can have the highest potential for energy harvesting applications compared to the other samples.

9 CONCLUDING REMARKS

This study was focusing on investigating the material-related losses of natural rubber (NR) and rubber-nanodiamond composites in order to compare them to the currently used materials and explore their perspectives for a dielectric elastomer generator (DEG) application. First, it was confirmed that despite of the wide use of acrylic VHB tape in DEGs and its suitable dielectric properties in the low frequency area, its mechanical losses and stress relaxation are so severe that the VHB tape cannot provide the needed efficiency in energy harvesting. The commercial NR, instead, possesses fair mechanical losses and stress relaxation, but experience high dielectric losses due to increased electrical conductivity. While the dielectric loss at 1 Hz of the commercial NR reference was 0.194, the custom-made unfilled NR had dielectric loss of only 0.005. The effect was most likely achieved by the specially designed rubber recipe containing low amounts of ZnO and stearic acid.

Although NR latex compounds do not require stearic acid for the vulcanization, other compounding ingredients and naturally occurring rubber constituents contribute to the dielectric losses. When a deproteinized NR latex containing 80% less proteins was used, it was found that such rubbers showed not only lower dielectric losses, but also hysteresis and stress relaxation were reduced without compromising the outstanding mechanical properties and elasticity. Therefore, deproteinized NR is a potentially good candidate for the preparation of DEG membranes.

Furthermore, a clear difference in dielectric losses of latex NR compounds was noticed depending on the type of a stabilizer used – KOH and ammonium caseinate, which are frequently used for compounding in latex industry. Mobile ions of KOH are believed to contribute to the dielectric losses by increasing the electrical conductivity effect, which is dominating at low frequency area. In case of ammonium caseinate, most of the stabilizer is believed to have migrated to the surface of the rubber film during the drying stage and the first days after cure resulting in lower dielectric losses of the films compared to KOH. However, the dielectric losses of KOH stabilized compounds were successfully lowered by the post-treatment of the samples by water-leaching. Generally, leaching helped to decrease the dielectric losses of all latex films more efficiently than the acetone-treatment, and the same

applied for the prevulcanized NR films as well. Furthermore, regardless of the stabilizer type, both leaching and acetone treatment resulted in reduction in mechanical losses of the samples. While leaching was most effective for reducing the hysteresis, acetone-treatment led to lower stress loss. As leaching is already utilized in latex industry and does not involve the use of strong chemicals, the method is preferred over the acetone-treatment for the reduction of material-related losses of NR films.

Additionally, it was found that dielectric losses were dependent on the time between the sample curing and testing, if the same temperature and humidity conditions were maintained. The losses reached equilibrium after 2-3 weeks after vulcanization depending on the sample. The change in dielectric properties with time is believed to depend on many factors with overlapping effects, but mostly on the migration of the stabilizers and water-soluble proteins to the surface of the sample. Among the latex samples, deproteinized films showed less time-dependency.

The further reduction of both dielectric and mechanical losses was attempted in the study by the addition of NDs, which were expected to bond the ions, impurities and mobile charge carries owing to their active and versatile surface and to work as dry lubricants between the rubber chains. Addition of the high amounts of NDs was found unnecessary due to the unbalanced effect on the properties – when the dielectric loss was reduced, the mechanical losses increased.

Finally, the effect of the surface chemistry of NDs was assessed for the ability of loss reduction, when up to 1 phr modified NDs were added to NR and PDMS matrix. In the study, carboxylated nanodiamonds were successfully modified with the agents containing silane or epoxy-groups. The reaction between carboxylic and epoxy-groups at 40 °C offered a relatively easy way to introduce groups that can improve the interaction between ND and silicone matrix to the ND surface. In the case of modification with 1,2-epoxy-9-decene containing a vinyl-group, NDs can participate in the crosslinking process of the PDMS matrix, thus creating strong chemical interactions. In case of epoxy-compound containing silane, an alkoxysilane group can improve the compatibility between the filler and PDMS matrix, or be used for further surface modification. A direct reaction between carboxyl and silanol groups, however, was shown to be improbable due to the dominating condensation of silanol groups. This condensation reaction resulted in a formation of a thick shell around the ND clusters thus increasing the aggregate size, but at the same time compatibilizing its surface. Therefore, more work on adjusting the silane functionalization procedure is needed in the future.

The present study indicated that although the modified NDs performed better than unmodified, no reduction in dielectric losses of NR was achieved. The reduction in stress relaxation and hysteresis loss at high deformation rate (up to 34% and almost 15%, respectively) was especially pronounced for the NR composites containing 1 phr of VTMS-modified NDs.

Nevertheless, the most improvement by the addition of NDs was achieved with silicone composites. The suitable surface functionalization of nanodiamonds allowed coupling of the NDs to the silicone rubber matrix and could efficiently reduce both dielectric and mechanical losses of the PDMS composites. All studied nanodiamonds were effective in the reducing the losses of PDMS. Remarkably, a very small amount of NDs was needed to reach such effect. For example, only 0.1 phr of NDs modified with 1,2-epoxy-9-decene was enough to reduce the dielectric loss of PDMS fivefold at 1 Hz and reduce the hysteresis losses at 10th cycle by half. Therefore, the application of small amounts of NDs, especially those containing the surface chemical groups able to participate in the curing reaction, can be considered beneficial in improving the efficiency of silicones applied in DEGs. However, as PDMS compounds also showed some dependency of dielectric losses on the time after curing, the positive effect of NDs on dielectric losses was reduced with time, which was related to the change in the loss properties of the matrix.

9.1 Initial hypotheses and research questions revisited

Initial hypotheses have been reassessed based on the outcomes of the study. As a result:

- *Natural proteins present in natural rubber* NR *increase the dielectric losses of the elastomer, and the removal of the large portion of those proteins by deproteinization helps to avoid this issue.* Indeed, the dielectric losses of deproteinized NR latex are lower than of a standard rubber, and the mechanical properties are not compromised. Therefore, deproteinized NR is recommended for the DEG application
- *Post-treatment of elastomer films by acetone and water leaching partly removes non-rubber constituents responsible for the higher dielectric loss.* This assumption is found to be partly correct, as leaching is especially efficient in reducing both dielectric and mechanical losses of a standard (not deproteinized) compounds. Acetone-treatment was found to reduce both dielectric and mechanical losses of NR latex, but not that successfully. Furthermore, the effect of the

acetone treatment on rubber is more complicated compared to the leaching, and less predictable, as it seems to affect also insoluble rubber proteins on the rubber surface.

- *Nanodiamonds (NDs) have an active surface that can interact with proteins and other impurities in rubber, thus decreasing the material-related losses at low frequency area. NDs are expected to be more effective for the complex systems and their effectiveness is suggested to decrease in a row: latex NR → dry NR → deproteinized NR and silicone.* This hypothesis was found to be partly correct, as the addition of NDs effectively reduced the contribution of electrical conductivity to the dielectric losses of the samples. However, as any other sample, it induced some interfacial polarization, which increased the losses. NDs are believed to be more effective for trapping the small ions and mobile carriers originating from the stabilizers, surfactants and catalysts rather than for large proteins. Therefore, the effectiveness of NDs is decreasing in the row: latex NR → PDMS → deproteinized NR and dry NR, meaning that NDs reduce dielectric losses of latex NR the most, but are the least effective for deproteinized and dry NR.
- *Surface modification of NDs improves the interaction between rubber and filler by creating chemical or physical bonding, and facilitates the loss reduction by reducing the interfacial effect.* The expected effect of ND surface modification was not very pronounced in NR composites, however, it was found very successful for the PDMS systems. Nevertheless, more adjustments need to be done on the mechanism of the modification, as well as on the selection of the modifying agents.

Based on the results of the study and their analysis presented in this thesis and the included four publications, the three research questions stated in Chapter 4 are revisited and answered:

RQ1. *How the presence of naturally occurring proteins in natural rubber films, and system complexity in general, affect material-related losses?* The presence of natural protein results in higher losses, especially dielectric, of the latex-based compounds. However, the presence of natural proteins resulted in lower dynamic loss tangent of the compounds, which also can be related to a little higher crosslink density of such compounds. The stabilizers used in latex compounding also can increase the losses of the materials, which are related to the increased ionic conductivity. The effect is valid mostly for freshly prepared sampled without any post-treatment. Moreover, some other compounding ingredients, such as ZnO and stearic acid, also have a

negative effect on dielectric losses due to the increased interfacial polarization contribution.

RQ2. *Can the material–related losses of natural rubber be lowered by the post-treatment methods (leaching with water and acetone)?* The post-treatment methods were found efficient in reduction of both mechanical and dielectric losses of latex-based compounds, but the effect was much less pronounced for the deproteinized samples. Such difference can be related to the initially lower protein content, which, as discussed in the answer for the RQ1, has much effect on the loss reduction. Among the post-treatment methods, leaching with water can be preferable over the acetone-treatments, as it provides the notable loss reduction but involves no strong chemicals. Moreover, leaching is already a part of industrial production of most latex goods.

RQ3. *Can the material-related losses be lowered by the incorporation of nanodiamond filler, and what is the effect of the nanodiamond surface treatment on its performance?* Addition of high amounts of NDs increases the overall materials losses of the composite. However, the positive effect of NDs can be seen in the reduction of the electrical conductivity contribution to the dielectric losses and lower dynamic loss tangent at room temperature of prevulcanized NR latex compounds. The effectiveness of the NDs on the reduction of mechanical losses is found dependent on the surface chemistry of the NDs and its compatibility with the elastomer. NDs decorated with the chemical groups able to participate in the crosslinking reactions showed a pronounced reduction of losses, especially mechanical ones, for the PDMS composites.

REFERENCES

[1] S. Solomon, G. Plattner, R. Knutti, P. Friedlingstein, Irreversible climate change due to carbon dioxide emissions, Proceedings of the National Academy of Sciences, Vol. 106, No. 6, 2009, pp. 1704-1709.

[2] J.G.J. Olivier, G. Janssens-Maenhout, M. Muntean, J.A.H.W. Peters, Trends in Global CO_2 Emissions: 2013 Report, 2013, .

[3] S. Chiba, R. Kornbluh, R. Pelrine, M. Waki, Novel Electric Generator Using Electroactive Polymer Artificial Muscle (EPAM), 18th World, pp. 22-30.

[4] G. Moretti, G.P.R. Papini, M. Righi, D. Forehand, D. Ingram, R. Vertechy, M. Fontana, Resonant wave energy harvester based on dielectric elastomer generator, Smart Materials and Structures, Vol. 27, No. 3, 2018, pp. 035015-1-14.

[5] R. Kaltseis, C. Keplinger, S.J. Adrian Koh, R. Baumgartner, Y.F. Goh, W.H. Ng, A. Kogler, A. Trols, C.C. Foo, Z. Suo, S. Bauer, Natural rubber for sustainable high-power electrical energy generation, RSC Advances, Vol. 4, No. 53, 2014, pp. 27905-27913.

[6] Review on Life Cycle Assessment of Greenhouse Gas Emission Profit of Solar Photovoltaic Systems, in: 8th International Conference on Applied Energy, ICAE2016, 8-11 October 2016, Beijing, China, Photovoltaic systemMulti-SiLife cycle assessmentGreenhouse gas emission., 2017, pp. 1289-1294.

[7] T. Hoffstadt, C. Graf, J. Maas, Optimization of the energy harvesting control for dielectric elastomer generators, Smart Materials and Structures, Vol. 22, No. 9, 2013, pp. 094028.

[8] S. Chiba, M. Waki, T. Wada, Y. Hirakawa, K. Masuda, T. Ikoma, Consistent ocean wave energy harvesting using electroactive polymer (dielectric elastomer) artificial muscle generators, Applied Energy, Vol. 104, No. 0, 2013, pp. 497-502.

[9] R. Kornbluh, R. Pelrine, H. Prahlad, A. Wong-Foy, B. McCoy, S. Kim, J. Eckerle, T. Low, From Boots to Buoys: Promises and Challenges of Dielectric Elastomer Energy Harvesting, in: L. Rasmussen (ed.), Springer US, 2012, pp. 67-93.

[10] K. Ahnert, M. Abel, M. Kollosche, P.J. Jorgensen, G. Kofod, Soft capacitors for wave energy harvesting, Journal of Materials Chemistry, Vol. 21, No. 38, 2011, pp. 14492-14497.

[11] C. Jean-Mistral, S. Basrour, Scavenging energy from human motion with tubular dielectric polymer, pp. 764209-764209-12.

[12] G. Kang, K. Kim, S. Kim, Note: Analysis of the efficiency of a dielectric elastomer generator for energy harvesting, Review of Scientific Instruments, Vol. 82, No. 4, 2011, pp. 046101.

[13] A. Tutcuoglu, C. Majidi, Energy harvesting with stacked dielectric elastomer transducers: Nonlinear theory, optimization, and linearized scaling law, Applied Physics Letters, Vol. 105, No. 24, 2014, pp. 241905.

[14] V. Goudar, M. Potkonjak, Dielectric Elastomer Generators for foot plantar pressure based energy scavenging, Sensors, 2012 IEEE, pp. 1-4.

[15] S. Astariz, G. Iglesias, The economics of wave energy: A review, Renewable and Sustainable Energy Reviews, Vol. 45, 2015, pp. 397-408.
[16] J. Lilliestam, R. Pitz-Paal, Concentrating solar power for less than USD 0.07 per kWh: finally the breakthrough? Renewable Energy Focus, Vol. 26, 2018, pp. 17-21.
[17] P. Binh, D. Nam, K. Ahn, Modeling and experimental investigation on dielectric electro-active polymer generator, International Journal of Precision Engineering and Manufacturing, Vol. 16, No. 5, 2015, pp. 945-955.
[18] P. Brochu, Q. Pei, Advances in Dielectric Elastomers for Actuators and Artificial Muscles, Macromolecular Rapid Communications, Vol. 31, No. 1, 2010, pp. 10-36.
[19] C. Jean-Mistral, T.V. Cong, A. Sylvestre, Advances for dielectric elastomer generators: Replacement of high voltage supply by electret, Applied Physics Letters, Vol. 101, No. 16, 2012, pp. 162901.
[20] P. Zanini, J. Rossiter, M. Homer, Self-stabilizing dielectric elastomer generators, Smart Materials and Structures, Vol. 26, No. 3, 2017, pp. 035037-1-5.
[21] T. McKay, B. O'Brien, E. Calius, I. Anderson, Self-priming dielectric elastomer generators, Smart Materials and Structures, Vol. 19, No. 5, 2010, pp. 055025-1-7.
[22] C. Chiang Foo, S. Jin Adrian Koh, C. Keplinger, R. Kaltseis, S. Bauer, Z. Suo, Performance of dissipative dielectric elastomer generators, Journal of Applied Physics, Vol. 111, No. 9, 2012, pp. 094107.
[23] G. Thomson, D. Yurchenko, D.V. Val, Dielectric Elastomers for Energy Harvesting, in: R. Manyala (ed.), Energy Harvesting, IntechOpen, 2018, pp. 41-61.
[24] G. Moretti, M. Fontana, R. Vertechy, Parallelogram-shaped dielectric elastomer generators: Analytical model and experimental validation, Journal of Intelligent Material Systems and Structures, Vol. 26, No. 6, 2015, pp. 740-751.
[25] D. Schapeler, C. Graf, J. Maas, Method for obtaining electrical energy from the kinetic energy of waves, 2015, .
[26] D. Peter, R. Pichler, S. Bauer, R. Schwödiauer, Electrostatic converter with an electret-like elastomer membrane for large scale energy harvesting of low density energy sources, Extreme Mechanics Letters, Vol. 4, 2015, pp. 38-44.
[27] J. Huang, S. Shian, Z. Suo, D.R. Clarke, Maximizing the Energy Density of Dielectric Elastomer Generators Using Equi-Biaxial Loading, Advanced Functional Materials, Vol. 23, No. 40, 2013, pp. 5056-5061.
[28] C. Chiang Foo, S. Cai, S. Jin Adrian Koh, S. Bauer, Z. Suo, Model of dissipative dielectric elastomers, Journal of Applied Physics, Vol. 111, No. 3, 2012, pp. 034102.
[29] T. Li, S. Qu, W. Yang, Energy harvesting of dielectric elastomer generators concerning inhomogeneous fields and viscoelastic deformation, Journal of Applied Physics, Vol. 112, No. 3, 2012, pp. 034119.
[30] C. Mistral, S. Basrour, J. Chaillout, A. Bonvilain, A complete study of electroactive polymers for energy scavenging: modelling and experiments, 25-27 April 2007, EDA Publishing Association, Grenoble, France, pp. 301-305.
[31] J. Plante, S. Dubowsky, On the performance mechanisms of Dielectric Elastomer Actuators, Sensors and Actuators A: Physical, Vol. 137, No. 1, 2007, pp. 96-109.
[32] J. Huang, T. Li, C. Chiang Foo, J. Zhu, D.R. Clarke, Z. Suo, Giant, voltage-actuated deformation of a dielectric elastomer under dead load, Applied Physics Letters, Vol. 100, No. 4, 2012, pp. 041911.
[33] S. Usha, M. Sreekumar, Elastic Behaviour of DEAP Film in the Development of Actuators, Procedia Engineering, Vol. 41, 2012, pp. 1154-1161.

[34] E. Bortot, M. Gei, G. deBotton, Optimal energy harvesting cycles for load-driven dielectric elastomer generators under equibiaxial deformation, Meccanica, Vol. 50, No. 11, 2015, pp. 2751-2766.
[35] G. Kofod, P. Sommer-Larsen, Silicone dielectric elastomer actuators: Finite-elasticity model of actuation, Sensors and Actuators A: Physical, Vol. 122, No. 2, 2005, pp. 273-283.
[36] M. Wissler, E. Mazza, Modeling of a pre-strained circular actuator made of dielectric elastomers, Sensors and Actuators A: Physical, Vol. 120, No. 1, 2005, pp. 184-192.
[37] Z. Ahmad, Polymer Dielectric Materials, in: Dr. M A Silaghi (ed.), Dielectric Material, InTech, 2012, pp. 3-26.
[38] G. Kofod, P. Sommer-Larsen, R. Kornbluh, R. Pelrine, Actuation Response of Polyacrylate Dielectric Elastomers, Journal of Intelligent Material Systems and Structures, Vol. 14, No. 12, 2003, pp. 787-793.
[39] M. Hernandez, M.A. Lopez-Manchado, A. Sanz, A. Nogales, T.A. Ezquerra, Effects of Strain-Induced Crystallization on the Segmental Dynamics of Vulcanized Natural Rubber, Macromolecules, Vol. 44, No. 16, 2011, pp. 6574-6580.
[40] S.J. Havriliak, S.J. Havriliak, Dielectric and mechanical relaxation in materials: analysis, interpretation, and application to polymers, Hanser Gardner Publications, Göttingen, 1997, 508 p.
[41] H. Stoyanov, Soft nanocomposites with enhanced electromechanical response for dielectric elastomer actuators, D.Sc. thesis, 2010, .
[42] ИИ Перепечко, Введение в физику полимеров, Химия, Москва, 1978, 312 p.
[43] A. Schönhals, F. Kremer, Analysis of Dielectric Spectra, in: F. Kremer, A. Schönhals (ed.), Broadband Dielectric Spectroscopy, Springer Berlin Heidelberg, Berlin, Heidelberg, 2003, pp. 59-98.
[44] G. Kofod, Dielectric Elastomer Actuators, Ph.D. thesis, 2001, .
[45] M. Hernandez, J. Carretero-Gonzalez, R. Verdejo, T.A. Ezquerra, M.A. Lopez-Manchado, Molecular Dynamics of Natural Rubber/Layered Silicate Nanocomposites As Studied by Dielectric Relaxation Spectroscopy, Macromolecules, Vol. 43, No. 2, 2010, pp. 643-651.
[46] Wagner, M. (ed.). 2013. Thermal analysis in practice. Collected applications. Switzerland, Mettler-Toledo AG.
[47] L.R.G. Treloar, The Physics of Rubber Elasticity, 3rd ed. Oxford University Press, New York, 2009, .
[48] P. Garnier, J.-. Le Cam, M. Grédiac, The influence of cyclic loading conditions on the viscoelastic properties of filled rubber, Mechanics of Materials, Vol. 56, 2013, pp. 84-94.
[49] S.S. Ahankari, K.K. Kar, Hysteresis measurements and dynamic mechanical characterization of functionally graded natural rubber–carbon black composites, Polymer Engineering & Science, Vol. 50, No. 5, 2010, pp. 871-877.
[50] W. Lai, A.F. Bastawros, Wei Hong, Soon-Jo Chung, Fabrication and analysis of planar dielectric elastomer actuators capable of complex 3-D deformation, Robotics and Automation (ICRA), 2012 IEEE International Conference on, pp. 4968-4973.
[51] D. Sahu, R.K. Sahu, K. Patra, Effects of uniaxial and biaxial strain on molecular structure of VHB 4910 dielectric elastomer, AIP Conference Proceedings, Vol. 2057, No. 1, 2019, pp. 020032.
[52] J. Sheng, H. Chen, B. Li, L. Chang, Temperature dependence of the dielectric constant of acrylic dielectric elastomer, Applied Physics A, Vol. 110, No. 2, 2013, pp. 511-515.

[53] G. Yin, Y. Yang, F. Song, C. Renard, Z. Dang, C. Shi, D. Wang, Dielectric Elastomer Generator with Improved Energy Density and Conversion Efficiency Based on Polyurethane Composites, ACS Applied Materials & Interfaces, Vol. 9, No. 6, 2017, pp. 5237-5243.
[54] C. Graf, J. Hitzbleck, T. Feller, K. Clauberg, J. Wagner, J. Krause, J. Maas, Dielectric elastomer–based energy harvesting: Material, generator design, and optimization, Journal of Intelligent Material Systems and Structures, Vol. 25, No. 8, 2014, pp. 951-966.
[55] A. Troels, A. Kogler, R. Baumgartner, R. Kaltseis, C. Keplinger, R. Schwoediauer, I. Graz, S. Bauer, Stretch dependence of the electrical breakdown strength and dielectric constant of dielectric elastomers, Smart Materials and Structures, Vol. 22, No. 10, 2013, pp. 104012-1-5.
[56] T. McKay G., E. Calius, I. Anderson A., The dielectric constant of 3M VHB: a parameter in dispute, 03/26, pp. 72870P-72870P.
[57] T. Vu-Cong, C. Jean-Mistral, A. Sylvestre, Impact of the nature of the compliant electrodes on the dielectric constant of acrylic and silicone electroactive polymers, Smart Materials and Structures, Vol. 21, No. 10, 2012, pp. 105036-1-10.
[58] R. Pelrine, R. Kornbluh, Q. Pei, J. Joseph, High-Speed Electrically Actuated Elastomers with Strain Greater Than 100%, Science, Vol. 287, No. 5454, 2000, pp. 836-839.
[59] F.B. Madsen, L. Yu, A.E. Daugaard, S. Hvilsted, A.L. Skov, Silicone elastomers with high dielectric permittivity and high dielectric breakdown strength based on dipolar copolymers, Polymer, Vol. 55, No. 24, 2014, pp. 6212-6219.
[60] R. Glowacki, Smart Materials, web page. Available (accessed 10/22): https://www.wacker.com/cms/en/wacker_group/innovations/innovations_2015/smart_fabrics/smart_fabrics1.jsp.
[61] S. Jin Adrian Koh, C. Keplinger, T. Li, S. Bauer, Z. Suo, Dielectric Elastomer Generators: How Much Energy Can Be Converted? Mechatronics, IEEE/ASME Transactions on, Vol. 16, No. 1, 2011, pp. 33-41.
[62] Zrunek Gummiwaren Gesellschaft M.B.H., Price Catalogue 2018, web page. Available (accessed 10/22): http://www.zrunek.at/uk/viton/zrunek/fkm-fpm-download.html.
[63] S.J.A. Koh, X. Zhao, Z. Suo, Maximal energy that can be converted by a dielectric elastomer generator, Applied Physics Letters, Vol. 94, No. 26, 2009, pp. 262902.
[64] Morton, M. (ed.). 1995. Rubber Technology. 3rd edition ed. London, Chapman&Hall. 638 p.
[65] E.C. Gregg, J.H. Macey, The Relationship of Properties of Synthetic Poly(Isoprene) and Natural Rubber in The Factory. The Effect of Non-Rubber Constituents of Natural Rubber, Rubber Chemistry and Technology, Vol. 46, No. 1, 1973, pp. 47-66.
[66] H.Y. Yeang, S.A.M. Arif, F. Yusof, E. Sunderasan, Allergenic proteins of natural rubber latex, Methods, Vol. 27, No. 1, 2002, pp. 32-45.
[67] G.L. Sussman, D.H. Beezhold, V.P. Kurup, Allergens and natural rubber proteins, Journal of Allergy and Clinical Immunology, Vol. 110, No. 2, Supplement, 2002, pp. S33-S39.
[68] Y. Tanaka, L. Tarachiwin, Recent Advances in Structural Characterization of Natural Rubber, Rubber Chemistry and Technology, Vol. 82, No. 3, 2009, pp. 283-314.
[69] L. Tarachiwin, J. Sakdapipanich, K. Ute, T. Kitayama, T. Bamba, E. Fukusaki, A. Kobayashi, Y. Tanaka, Structural Characterization of Alpha-Terminal Group of

Natural Rubber. 1. Decomposition of Branch-Points by Lipase and Phosphatase Treatments, Biomacromolecules, Vol. 6, No. 4, 2005, pp. 1851-1857.
[70] H. Yeang, E. Sunderasan, Latex allergy studies: extraction of natural rubber latex proteins with reference to film thickness, latex DRC and protein migration behaviour, Journal of Natural Rubber Research, Vol. 10, 1995, pp. 46-46.
[71] C.C. Ho, M.C. Khew, Surface Morphology of Prevulcanized Natural Rubber Latex Films by Atomic Force Microscopy: New Insight into the Prevulcanization Mechanism, Langmuir, Vol. 15, No. 19, 1999, pp. 6208-6219.
[72] F.W. Perrella, A.A. Gaspari, Natural rubber latex protein reduction with an emphasis on enzyme treatment, Methods, Vol. 27, No. 1, 2002, pp. 77-86.
[73] K. Berthelot, S. Lecomte, Y. Estevez, V. Zhendre, S. Henry, J. Thévenot, E.J. Dufourc, I.D. Alves, F. Peruch, Rubber particle proteins, HbREF and HbSRPP, show different interactions with model membranes, Biochimica et Biophysica Acta (BBA) - Biomembranes, Vol. 1838, No. 1, Part B, 2014, pp. 287-299.
[74] K. Nawamawat, J.T. Sakdapipanich, C.C. Ho, Effect of Deproteinized Methods on the Proteins and Properties of Natural Rubber Latex during Storage, Macromolecular Symposia, Vol. 288, No. 1, 2010, pp. 95-103.
[75] D.M. Simpson, R.J. Beynon, Acetone Precipitation of Proteins and the Modification of Peptides, Journal of Proteome Research, Vol. 9, No. 1, 2010, pp. 444-450.
[76] S. Amnuaypornsri, J. Sakdapipanich, Y. Tanaka, Green strength of natural rubber: The origin of the stress–strain behavior of natural rubber, Journal of Applied Polymer Science, Vol. 111, No. 4, 2009, pp. 2127-2133.
[77] J. Liu, S. Wu, Z. Tang, T. Lin, B. Guo, G. Huang, New evidence disclosed for networking in natural rubber by dielectric relaxation spectroscopy, Soft Matter, Vol. 11, No. 11, 2015, pp. 2290-2299.
[78] K.T. Cheang, A.R. Rais, K.B. Basir, Depronteinised Natural Rubber (DPNR), Malaysian Rubber Board Monograph No. 10, C&D Trading, Kuala Lumpur, 2003, .
[79] S. Amnuaypornsri, J. Sakdapipanich, Y. Tanaka, Highly purified natural rubber by saponificaion of latex: Analysis of green and cured properties, Journal of Applied Polymer Science, Vol. 118, No. 6, 2010, pp. 3524-3531.
[80] M. Hernandez, T.A. Ezquerra, R. Verdejo, M.A. Lopez-Manchado, Role of Vulcanizing Additives on the Segmental Dynamics of Natural Rubber, Macromolecules, Vol. 45, No. 2, 2012, pp. 1070-1075.
[81] J. Carretero-Gonzalez, T.A. Ezquerra, S. Amnuaypornsri, S. Toki, R. Verdejo, A. Sanz, J. Sakdapipanich, B.S. Hsiao, M. Lopez-Manchado, Molecular dynamics of natural rubber as revealed by dielectric spectroscopy: The role of natural cross-linking, Soft Matter, Vol. 6, No. 15, 2010, pp. 3636-3642.
[82] Y. Oka, N. Koizumi, Effects of Impurity Ions on Electrical Properties of Poly(vinylidene fluoride), Polymer Journal, Vol. 14, No. 11, 1982, pp. 869-876.
[83] O. Chaikumpollert, Y. Yamamoto, K. Suchiva, S. Kawahara, Protein-free natural rubber, Colloid and Polymer Science, Vol. 290, No. 4, 2012, pp. 331-338.
[84] J.T. Sakdapipanich, P. Rojruthai, Molecular Structure of Natural Rubber and Its Characteristics Based on Recent Evidence, in: Prof. Reda Sammour (ed.), Biotechnology - Molecular Studies and Novel Applications for Improved Quality of Human Life, InTech, 2012, pp. 213-238.
[85] P. Ortiz-Serna, R. Diaz-Calleja, M.J. Sanchis, G. Floudas, R.C. Nunes, A.F. Martins, L.L. Visconte, Dynamics of Natural Rubber as a Function of Frequency, Temperature,

and Pressure. A Dielectric Spectroscopy Investigation, Macromolecules, Vol. 43, No. 11, 2010, pp. 5094-5102.
[86] D. Boese, F. Kremer, Molecular dynamics in bulk cis-polyisoprene as studied by dielectric spectroscopy, Macromolecules, Vol. 23, No. 3, 1990, pp. 829-835.
[87] K. Adachi, H. Hirano, Slow Dielectric Relaxation of cis-Polyisoprene near the Glass Transition Temperature, Macromolecules, Vol. 31, No. 12, 1998, pp. 3958-3962.
[88] P.G. Santangelo, C.M. Roland, Temperature Dependence of Mechanical and Dielectric Relaxation in cis-1,4-Polyisoprene, Macromolecules, Vol. 31, No. 11, 1998, pp. 3715-3719.
[89] Franta, I. (ed.). 1989. Elastomers and Rubber Compounding Materials. Manufacture, Properties and Applications. Elsevier. 608 p.
[90] F.B. Madsen, A.E. Daugaard, S. Hvilsted, M.Y. Benslimane, A.L. Skov, Dipolar cross-linkers for PDMS networks with enhanced dielectric permittivity and low dielectric loss, Smart Materials and Structures, Vol. 22, No. 10, 2013, pp. 104002.
[91] K. Goswami, A.E. Daugaard, A.L. Skov, Dielectric properties of ultraviolet cured poly(dimethyl siloxane) sub-percolative composites containing percolative amounts of multi-walled carbon nanotubes, RSC Advances, Vol. 5, No. 17, 2015, pp. 12792-12799.
[92] S. Michel, X.Q. Zhang, M. Wissler, C. Löwe, G. Kovacs, A comparison between silicone and acrylic elastomers as dielectric materials in electroactive polymer actuators, Polymer International, Vol. 59, No. 3, 2010, pp. 391-399.
[93] P.J. Madsen, L. Yu, S. Boucher, A.L. Skov, Enhancing the electro-mechanical properties of polydimethylsiloxane elastomers through blending with poly(dimethylsiloxane-co-methylphenylsiloxane) copolymers, RSC Advances, Vol. 8, No. 41, 2018, pp. 23077-23088.
[94] S. Zakaria, L. Yu, G. Kofod, A.L. Skov, The influence of static pre-stretching on the mechanical ageing of filled silicone rubbers for dielectric elastomer applications, Materials Today Communications, Vol. 4, 2015, pp. 204-213.
[95] A. Iannarelli, M. Ghaffarian Niasar, Mechanical stretch influence on lifetime of dielectric elastomer films, /4/17, .
[96] F.B. Madsen, A.E. Daugaard, S. Hvilsted, A.L. Skov, The Current State of Silicone-Based Dielectric Elastomer Transducers, Macromolecular Rapid Communications, Vol. 37, No. 5, 2016, pp. 378-413.
[97] F.B. Madsen, S. Zakaria, L. Yu, A.L. Skov, Mechanical and Electrical Ageing Effects on the Long-Term Stretching of Silicone Dielectric Elastomers with Soft Fillers , Advanced Engineering Materials, Vol. 18, No. 7, 2016, pp. 1154-1165.
[98] F. Galantini, F. Carpi, G. Gallone, Effects of plasticization of a soft silicone for dielectric elastomer actuation, Smart Materials and Structures, Vol. 22, No. 10, 2013, pp. 104020.
[99] G. Gallone, F. Galantini, F. Carpi, Perspectives for new dielectric elastomers with improved electromechanical actuation performance: composites versus blends, Polymer International, Vol. 59, No. 3, 2010, pp. 400-406.
[100] V. Dolmatov, Polymer-diamond composites based on detonation nanodiamonds. Part 2, Journal of Superhard Materials, Vol. 29, No. 2, 2007, pp. 65-75.
[101] A. Bele, G. Stiubianu, C. Varganici, M. Ignat, M. Cazacu, Silicone dielectric elastomers based on radical crosslinked high molecular weight polydimethylsiloxane co-filled

with silica and barium titanate, Journal of Materials Science, Vol. 50, No. 20, 2015, pp. 6822-6832.
[102] H. Böse, D. Uhl, K. Flittner, H. Schlaak, Dielectric elastomer actuators with enhanced permittivity and strain, March 24, pp. 79762J-79762J.
[103] Z. Zhang, L. Liu, J. Fan, K. Yu, Y. Liu, L. Shi, J. Leng, New silicone dielectric elastomers with a high dielectric constant, pp. 692610-18.
[104] L. Yu, A.L. Skov, Silicone rubbers for dielectric elastomers with improved dielectric and mechanical properties as a result of substituting silica with titanium dioxide, International Journal of Smart and Nano Materials, Vol. 6, No. 4, 2015, pp. 268-289.
[105] D.N. Mc Carthy, S. Risse, P. Katekomol, G. Kofod, The effect of dispersion on the increased relative permittivity of TiO2 /SEBS composites, Journal of Physics D: Applied Physics, Vol. 42, No. 14, 2009, pp. 145406.
[106] D. Yang, M. Tian, Y. Dong, H. Kang, D. Gong, L. Zhang, A high-performance dielectric elastomer consisting of bio-based polyester elastomer and titanium dioxide powder, Journal of Applied Physics, Vol. 114, No. 15, 2013, .
[107] N.H. Chuc, V.T. Doan, J.K. Park, J.C. Koo, Y.K. Lee, J. Nam, R.C. Hyouk, The effects of additives on the actuating performances of a dielectric elastomer actuator, Smart Materials and Structures, Vol. 18, No. 1, 2009, pp. 015006.
[108] Z. Jia, S. Chen, J. Zhang, RTV Silicone Rubber Filled with Surface Modified Montmorillonite, Journal of Macromolecular Science, Part B, Vol. 51, No. 12, 2012, pp. 2449-2461.
[109] A.L. Skov, B. Anca, J. Bogelund, B. Mohamed, A.D. Egede, Influence of micro- and nanofillers on electro-mechanical performance of silicone EAPs, Proc.SPIE, Vol. 8340, 2012, pp. 83400M-1.
[110] S.K. Yadav, I.J. Kim, H.J. Kim, J. Kim, S.M. Hong, C.M. Koo, PDMS/MWCNT nanocomposite actuators using silicone functionalized multiwalled carbon nanotubes via nitrene chemistry, Journal of Materials Chemistry C, Vol. 1, No. 35, 2013, pp. 5463-5470.
[111] S.K. Yadav, S.S. Mahapatra, J.W. Cho, Tailored dielectric and mechanical properties of noncovalently functionalized carbon nanotube/poly(styrene-b-(ethylene-co-butylene)-b-styrene) nanocomposites, Journal of Applied Polymer Science, Vol. 129, No. 4, 2013, pp. 2305-2312.
[112] Z. Dang, B. Xia, S. Yao, M. Jiang, H. Song, L. Zhang, D. Xie, High-dielectric-permittivity high-elasticity three-component nanocomposites with low percolation threshold and low dielectric loss, Applied Physics Letters, Vol. 94, No. 4, 2009, .
[113] D. Yang, M. Tian, W. Wang, D. Li, R. Li, H. Liu, L. Zhang, Controllable dielectric and electrical performance of polymer composites with novel core/shell-structured conductive particles through biomimetic method, Electrochimica Acta, Vol. 87, 2013, pp. 9-17.
[114] J.E.Q. Quinsaat, F.A. Nueesch, H. Hofmann, D.M. Opris, Dielectric properties of silver nanoparticles coated with silica shells of different thicknesses, RSC Advances, Vol. 3, No. 19, 2013, pp. 6964-6971.
[115] J.E.Q. Quinsaat, M. Alexandru, F.A. NÃ¼esch, H. Hofmann, A. Borgschulte, D.M. Opris, Highly stretchable dielectric elastomer composites containing high volume fractions of silver nanoparticles, Journal of Materials Chemistry A, Vol. 3, No. 28, 2015, pp. 14675-14685.
[116] I. Neitzel, V. Mochalin, Y. Gogotsi, Chapter 13. Advances in surface chemistry of nanodiamond and nanodiamond-polymer composites, in: O.A. Shenderova, D.M.

Gruen (ed.), Ultrananocrystalline diamond: synthesis, properties and applications, 2 ed., William Andrew, 2012, pp. 421-457.
[117] T. Kondo, I. Neitzel, V.N. Mochalin, J. Urai, M. Yuasa, Y. Gogotsi, Electrical conductivity of thermally hydrogenated nanodiamond powders, Journal of Applied Physics, Vol. 113, No. 21, 2013, pp. 214307.
[118] V.N. Mochalin, Y. Gogotsi, Nanodiamond–polymer composites, Diamond and Related Materials, Vol. 58, 2015, pp. 161-171.
[119] Y. Zhang, K.Y. Rhee, D. Hui, S. Park, A critical review of nanodiamond based nanocomposites: Synthesis, properties and applications, Composites Part B: Engineering, Vol. 143, 2018, pp. 19-27.
[120] A. Shakun, J. Vuorinen, M. Hoikkanen, M. Poikelispää, A. Das, Hard nanodiamonds in soft rubbers: Past, present and future – A review, Composites Part A: Applied Science and Manufacturing, Vol. 64, 2014, pp. 49-69.
[121] V.Y. Dolmatov, T. Fujimura, Physical and Chemical Problems of Modification of Detonation Nanodiamond Surface Properties, in: D. Gruen, O. Shenderova, A. Vul' (ed.), Synthesis, Properties and Applications of Ultrananocrystalline Diamond, Springer Netherlands, 2005, pp. 217-230.
[122] A. Krueger, The structure and reactivity of nanoscale diamond, Journal of Materials Chemistry, No. 18, 2008, pp. 1485-1492.
[123] M. Baidakova, A. Vul, New prospects and frontiers of nanodiamond clusters, Journal of Physics D: Applied Physics, Vol. 40, No. 20, 2007, pp. 6300.
[124] A. Neverovskaya, A. Voznyakovskii, V. Dolmatov, Structure of the dispersive medium and sedimentation resistance of suspensions of detonation nanodiamonds, Physics of the Solid State, Vol. 46, No. 4, 2004, pp. 662-664.
[125] O. Shenderova, C. Jones, V. Borjanovic, S. Hens, G. Cunningham, S. Moseenkov, V. Kuznetsov, G. McGuire, Detonation nanodiamond and onion-like carbon: applications in composites, Physica status solidi (a), Vol. 205, No. 9, 2008, pp. 2245-2251.
[126] A.P. Voznyakovski, M.F. Kudoyarov, O.F. Pozdnyakov, Self-organization and sedimentation stability of detonation nanodiamond suspensions, Technical Physics Letters, Vol. 33, No. 20, 2007, pp. 29-36.
[127] S.M. Kong, M. Mariatti, J.J.C. Busfield, Effects of types of fillers and filler loading on the properties of silicone rubber composites, Journal of Reinforced Plastics and Composites, Vol. 30, No. 13, 2011, pp. 1087-1096.
[128] A. Krueger, The chemistry of nanodiamond, RSC Nanoscience and Nanotechnology, Vol. 2014-January, No. 31, 2014, pp. 49-88.
[129] S. Osswald, G. Yushin, V. Mochalin, S.O. Kucheyev, Y. Gogotsi, Control of sp2/sp3 Carbon Ratio and Surface Chemistry of Nanodiamond Powders by Selective Oxidation in Air, Journal of the American Chemical Society, Vol. 128, No. 35, 2006, pp. 11635-11642.
[130] C. Bradac, T. Gaebel, C.I. Pakes, J.M. Say, A.V. Zvyagin, J.R. Rabeau, Effect of the Nanodiamond Host on a Nitrogen-Vacancy Color-Centre Emission State, Small, Vol. 9, No. 1, 2013, pp. 132-139.
[131] V.P. Efremov, E.I. Zakatilova, I.V. Maklashova, N.V. Shevchenko, Thermal stability of detonation-produced micro and nanodiamonds, Journal of Physics: Conference Series, Vol. 946, No. 1, 2018, pp. 012107.

[132] A. Kruger, Y. Liang, G. Jarre, J. Stegk, Surface functionalisation of detonation diamond suitable for biological applications, Journal of Materials Chemistry, Vol. 16, No. 24, 2006, pp. 2322-2328.
[133] R. Edgington, K.M. Spillane, G. Papageorgiou, W. Wray, H. Ishiwata, M. Labarca, S. Leal-Ortiz, G. Reid, M. Webb, J. Foord, N. Melosh, A.T. Schaefer, Functionalisation of Detonation Nanodiamond for Monodispersed, Soluble DNA-Nanodiamond Conjugates Using Mixed Silane Bead-Assisted Sonication Disintegration, Scientific Reports, Vol. 8, No. 1, 2018, pp. 728-1-11.
[134] K. Turcheniuk, V.N. Mochalin, Biomedical applications of nanodiamond (Review), Nanotechnology, Vol. 28, No. 25, 2017, pp. 252001-27.
[135] A. Krueger, D. Lang, Functionality is Key: Recent Progress in the Surface Modification of Nanodiamond, Advanced Functional Materials, Vol. 22, No. 5, 2012, pp. 890-906.
[136] V. Castano, Silanization of Carbon Nanotubes: Surface Modification and Polymer Nanocomposites, in: C. Velasco-Santos, S. Yellampalli (ed.), Carbon Nanotubes, InTech, Rijeka, 2011, pp. Ch. 13.
[137] A.M. Schrand, S.A.C. Hens, O.A. Shenderova, Nanodiamond Particles: Properties and Perspectives for Bioapplications, Critical Reviews in Solid State and Materials Sciences, Vol. 34, No. 1-2, 2009, pp. 18-74.
[138] A. Krueger, Chapter 8 - Current issues and challenges in surface chemistry of nanodiamonds, in: J. Arnault (ed.), Nanodiamonds, Elsevier, 2017, pp. 183-242.
[139] M. Brochier Salon, P. Bayle, M. Abdelmouleh, S. Boufi, M.N. Belgacem, Kinetics of hydrolysis and self condensation reactions of silanes by NMR spectroscopy, Colloids and Surfaces A: Physicochemical and Engineering Aspects, Vol. 312, No. 2, 2008, pp. 83-91.
[140] S. Altmann, J. Pfeiffer, The Hydrolysis/Condensation Behaviour of Methacryloyloxyalkylfunctional Alkoxysilanes: Structure-Reactivity Relations, Monatshefte fur Chemie / Chemical Monthly, Vol. 134, No. 8, 2003, pp. 1081-1092.
[141] Y. Zhang, S. Park, In-situ modification of nanodiamonds by mercapto-terminated silane agent for enhancing the mechanical interfacial properties of nitrile butadiene rubber nanocomposites, Polymer Composites, Vol. 39, No. 10, 2018, pp. 3472-3481.
[142] F. Hajiali, A. Shojaei, Silane functionalization of nanodiamond for polymer nanocomposites-effect of degree of silanization, Colloids and Surfaces A: Physicochemical and Engineering Aspects, Vol. 506, 2016, pp. 254-263.
[143] J. Neburkova, J. Vavra, P. Cigler, Coating nanodiamonds with biocompatible shells for applications in biology and medicine, Current Opinion in Solid State and Materials Science, Vol. 21, No. 1, 2017, pp. 43-53.
[144] Z. Li, T. Tatsuya, I. Masaaki, K. Naoko, K. Takahide, K. Naoki, Chromatographic Separation of Highly Soluble Diamond Nanoparticles Prepared by Polyglycerol Grafting, Angewandte Chemie International Edition, Vol. 50, No. 6, 2011, pp. 1388-1392.
[145] Z. Huang, H. Ji, J.W. Mays, M.D. Dadmun, Understanding the Grafting of Telechelic Polymers on a Solid Substrate to Form Loops, Macromolecules, Vol. 41, No. 3, 2008, pp. 1009-1018.
[146] W.J. Blank, Z.A. He, M. Picci, Catalysis of the epoxy-carboxyl reaction, Journal of Coatings Technology, Vol. 74, No. 926, 2002, pp. 33-41.
[147] W. Kaewsakul, K. Sahakaro, W.K. Dierkes, J.W.M. Noordermeer, Mechanistic aspects of silane coupling agents with different functionalities on reinforcement of silica-filled

natural rubber compounds, Polymer Engineering & Science, Vol. 55, No. 4, 2015, pp. 836-842.
[148] J. Schönherr, R.J. Buchheim, P. Scholz, P. Adelhelm, Boehm Titration Revisited (Part I): Practical Aspects for Achieving a High Precision in Quantifying Oxygen-Containing Surface Groups on Carbon Materials, C, Vol. 4, No. 2, 2018, pp. 1-13.
[149] M. Tiwari, R.N. Datta, A.G. Talma, J.W.M. Noordermeer, W.K. Dierkes, W.J. van Ooij, Comparative Study of Plasma-Thiophene and -Acetylene Coated Silica in SBR and EPDM Reinforcement, Rubber Chem. Technol., Vol. 82, No. 5, 2009, pp. 473-491.
[150] S. Stehlik, T. Glatzel, V. Pichot, R. Pawlak, E. Meyer, D. Spitzer, B. Rezek, Water interaction with hydrogenated and oxidized detonation nanodiamonds — Microscopic and spectroscopic analyses, Diamond and Related Materials, Vol. 63, 2016, pp. 97-102.
[151] R. Al-Oweini, H. El-Rassy, Synthesis and characterization by FTIR spectroscopy of silica aerogels prepared using several Si(OR)4 and R"Si(OR')3 precursors, Journal of Molecular Structure, Vol. 919, No. 1, 2009, pp. 140-145.
[152] I.M. El-Nahhal, J.K. Salem, S. Kuhn, T. Hammad, R. Hempelmann, S. Al Bhaisi, Synthesis & characterization of silica coated and functionalized silica coated zinc oxide nanomaterials, Powder Technology, Vol. 287, 2016, pp. 439-446.
[153] P. Post, L. Wurlitzer, W. Maus-Friedrichs, P.A. Weber, Characterization and Applications of Nanoparticles Modified in-Flight with Silica or Silica-Organic Coatings, Nanomaterials, Vol. 8, No. 7, 2018, pp. 530-1-19.
[154] S.A. Haddadi, A.R. S.A., M. Amini, A. Kheradmand, In-situ preparation and characterization of ultra-high molecular weight polyethylene/diamond nanocomposites using Bi-supported Ziegler-Natta catalyst: Effect of nanodiamond silanization, Materials Today Communications, Vol. 14, 2018, pp. 53-64.
[155] J. Coates, Interpretation of Infrared Spectra, A Practical Approach, in: Encyclopedia of Analytical Chemistry, John Wiley & Sons, Ltd, 2006, .
[156] P. Wang, Y. Chen, H. Qian, Vulcanization kinetics of low-protein natural rubber with use of a vulcameter, Journal of Applied Polymer Science, Vol. 105, No. 6, 2007, pp. 3255-3259.
[157] S. Rabiei, A. Shojaei, Vulcanization kinetics and reversion behavior of natural rubber/styrene-butadiene rubber blend filled with nanodiamond – the role of sulfur curing system, European Polymer Journal, Vol. 81, 2016, pp. 98-113.
[158] M. Poikelispää, A. Das, W. Dierkes, J. Vuorinen, The effect of coupling agents on silicate-based nanofillers/carbon black dual filler systems on the properties of a natural rubber/butadiene rubber compound, Journal of Elastomers & Plastics, Vol. 47, No. 8, 2015, pp. 738-752.
[159] A.R.S. Bahri, S. Hamzah, H.M. Ghazaly, Latex allergy studies: Location of soluble proteins in latex examination gloves, Journal of Natural Rubber Research, Vol. 8, No. 4, 1993, pp. 299-307.
[160] J. Yunyongwattanakorn, Y. Tanaka, S. Kawahara, W. Klinklai, J. Sakdapipanich, Effect of Non-Rubber Components on Storage Hardening and Gel Formation of Natural Rubber During Accelerated Storage under Various Conditions, Rubber Chemistry and Technology, Vol. 76, No. 5, 2003, pp. 1228-1240.
[161] A.M.Y. Hashim, M.S. Fauzi, Effect of Leaching on the Physical Characteristics of Cast NR Latex Films, Journal of Rubber Research, Vol. 5, No. 2, 2002, pp. 84-93.

[162] L.J. Yu, C.W.Y. Chi, V. Tangavaloo, K.W. Lim, M. A Tarawneh, Protein reduction of natural rubber films through leaching solvent, MATEC Web Conf., Vol. 268, No. 01011, 2019, pp. 1-5.
[163] F. Carpi, I. Anderson, S. Bauer, G. Frediani, G. Gallone, M. Gei, C. Graaf, C. Jean-Mistral, W. Kaal, G. Kofod, M. Kollosche, R. Kornbluh, B. Lassen, M. Matysek, S. Michel, S. Nowak, B. O'Brien, Q. Pei, R. Pelrine, B. Rechenbach, S. Rosset, H. Shea, Standards for dielectric elastomer transducers, Smart Materials and Structures, Vol. 24, No. 10, 2015, pp. 105025.
[164] D. Wititsuwaannakul, A. Rattanapittayaporn, T. Koyama, R. Wititsuwaannakul, Involvement of Hevea Latex Organelle Membrane Proteins in the Rubber Biosynthesis Activity and Regulatory Function, Macromolecular Bioscience, Vol. 4, No. 3, 2004, pp. 314-323.
[165] A. Maus, K. Saalwächter, Crystallization Kinetics of Poly(dimethylsiloxane) Molecular-Weight Blends—Correlation with Local Chain Order in the Melt? Macromolecular Chemistry and Physics, Vol. 208, No. 19, 2007, pp. 2066-2075.

PUBLICATIONS

PUBLICATION I

Energy dissipation in natural rubber latex films: the effect of stabilizers, leaching and acetone-treatment

A. Shakun, E. Sarlin, J. Vuorinen

Unpublished manuscript

PUBLICATION II

Natural rubber - nanodiamond films for the minimisation of losses in dielectric energy harvesters

A. Shakun, E. Sarlin, J. Vuorinen

International Journal of Exergy (2018) Vol.26, No. 1/2, pp. 170-185
https://doi.org/10.1504/IJEX.2018.092512

Natural rubber - nanodiamond films for the minimisation of losses in dielectric energy harvesters

Alexandra Shakun*, Essi Sarlin and Jyrki Vuorinen

Laboratory of Materials Science,
Tampere University of Technology,
P.O. Box 589, Tampere, FI-33101, Finland
E-mail: alexandra.shakun@tut.fi
E-mail: essi.sarlin@tut.fi
E-mail: jyrki.vuorinen@tut.fi
* Corresponding author

Abstract: Dielectric elastomer generators (DEGs) belong to the new and promising class of devices harvesting energy from ambient sources, e.g. ocean waves. However, the efficiency and energy output of the existing DEG prototypes are often limited, for example, by high material-related losses of the utilized dielectric elastomers. Therefore, despite of the recent advances in the DEG research, minimisation of losses of elastomeric material for DEG application is still in demand. The present study focuses on the material-related losses of natural rubber (NR) and shows the possibility to decrease the low frequency losses by the addition of nanodiamonds. The post-treatment of the films, namely leaching and acetone extraction, allows reducing the losses even more – by almost 25% for NR. Moreover, acetone treatment results in a positive effect on the mechanical properties of the samples, as well as reduced viscous losses and improved stress relaxation behaviour.

Keywords: wave energy harvesting, natural rubber latex, nanodiamonds, dielectric spectroscopy

Biographical notes: Alexandra Shakun is a Ph.D. student at the Laboratory of Materials Science, Tampere University of Technology, developing latex-based elastomer nanocomposites for dielectric energy harvesters. Her research interests include rubber technology and elastomer nanocomposites, nanodiamonds, dielectric elastomer transducers and energy harvesting.

Assistant Professor (Tenure Track) Essi Sarlin (D.Sc.) has worked in the Laboratory of Materials Science at Tampere University of Technology since 2006. Her research focus at moment is the ageing of composite and hybrid materials and the characterization methods of ageing phenomena. Her teaching responsibilities cover the areas of polymer physics and electron microscopy.

Professor Jyrki Vuorinen is currently the Dean of Faculty of Natural Sciences in Tampere University of Technology. Since 2004, he has worked as a professor of elastomer and composite materials in Laboratory of Materials Science.

1 Introduction

Energy harvesting is a comparably new and rapidly developing way of obtaining sustainable energy from ambient sources. Mechanical energy of an ambient source can be directly transformed into electricity by dielectric elastomer generators (DEGs), which belong to the newly emerged promising class of energy harvesters. Such transducers have most potential in harvesting energy from low frequency sources, such as waves (Ahnert et al. 2011; Kornbluh et al. 2012; Hoffstadt et al. 2013; Chiba et al. 2013; Kaltseis et al. 2014), or human motion (Jean-Mistral and Basrour 2010; Kang et al. 2011). Due to their simple working principle and versatile design possibilities, interest towards DEGs continues to increase.

The operating principle of DEGs is based on mechanically changing capacitance of soft elastomer membranes placed between compliant electrodes. As these elastomers show no piezoelectric properties, electrodes of a harvester must be charged from an external source to enable operation of a DEG. A harvesting cycle (Figure 1) starts when a dielectric membrane is stretched upon an action of an ambient

source. Then an electric charge is supplied to the electrodes. When the dielectric membrane is released, and it retracts to its original dimensions, simultaneous reduction of the electrode area and increase in the distance between the electrodes takes place. This results in increased potential difference that can be pumped into the battery, and the harvesting cycle is repeated. The cycle can be operated at constant charge, constant voltage or constant field conditions.

Most DEGs require a high voltage source supplying 2-3 kV to the electrodes. Although some researchers show that lower voltage source, can be successfully utilized (Jean-Mistral et al. 2012; Moretti et al. 2015), the study of Wang et al. (2012) indicated that the efficiency of DEG is strongly dependent on the cycle parameters, especially bias voltage. For bias voltage below 500 V, efficiency dropped about ten-fold. Many other factors affect the conversion efficiency and the energy output of a dielectric generator, such as the material properties of dielectric elastomer including its dielectric and viscous losses, the design of a generator, type, stability and compliancy of electrodes, strain levels, cycle length and others.

At the current stage, DEGs are not cost-effective when compared to the traditional energy sources and, therefore, require much development and modifications. Ahnert et al. (2011) have estimated the possible specific energy density for the wave harvester based on silicone material with silver electrodes to be 5 mJ/g at 0.1 Hz working frequency with charging voltage about 650 V. Moreover, the authors made an assumption that return on solely material investment in such conditions would be about 10 years. According to Chiba et al. (2010), the cost of energy obtained from waves by dielectric generator could be approximately 0.2 USD per kWh, but Kaltseis et al. (2014) estimated it to be 0.05-0.11 USD per kWh if the high-performance materials are applied. Further design and material modification should reduce the energy cost to the one of a traditional energy sources (Koh et al. 2009; Chiba et al. 2010).

As a general rule, dielectric material utilized for an energy harvesting application should have good mechanical properties and elasticity, as well as high electrical resistivity and minimal energy dissipation. However, most of the existing DEG prototypes utilize commercially available elastomers, which are not designed for such application. Therefore, they may not have all the required properties to make DEGs economically viable (Graf et al. 2014). As an example, an adhesive acrylic tape produced by 3M is the most widely used dielectric membrane for energy harvesting (McKay et al. 2011; Lai et al. 2012; Jean-Mistral et al. 2014; Kaltseis et al. 2014; Vertechy et al. 2014) despite of its many drawbacks. Such acrylic tape has comparably high viscous and dielectric losses – 19.3% and 0.025 respectively, as mentioned by Kaltseis et al. (2014) for VHB tape type. However, the main drawback of this acrylic material is pronounced stress relaxation after cyclic loading (Huang et al. 2013; Kaltseis et al. 2014). Other rubber types used in DEG prototypes include silicones (Chiba et al. 2010; T G McKay et al. 2015), polyurethanes (Cottinet et al. 2010; Graf et al. 2014) and natural rubber (NR) films (Kaltseis et al. 2014; Moretti et al. 2015) and its synthetic version (Vertechy and Fontana 2015). However, although it is crucial for the improvement of DEG performance, very little research has been conducted on material modification for the minimisation of its losses.

As a natural latex-based rubber band showed good energy harvesting performance in the research conducted by (Kaltseis et al. 2014; Vertechy and Fontana 2015), it was decided to focus the present research on natural rubber and its composites. Apart from low dielectric permittivity, like most rubbers, NR has low dielectric losses, which makes it a good candidate for DEG applications. Moreover, natural rubber has excellent mechanical properties and high elasticity – properties required for a dielectric membrane. At the same time, nanodiamonds (NDs), which have not been previously applied for DEG membranes, can reduce dielectric losses of a rubber compound in a wide frequency range (Shakun et al. 2017). Such effect is probably related to the active interaction of surface-treated NDs with the polymer chain, which reduces the chain mobility under the applied electric field. Moreover, addition of small loads of NDs may result in lower hysteresis losses in rubbers (Dolmatov 2007b) due to the structural activity of the filler.

The aim of the present study is to minimise the dielectric and viscous losses that should lead to the increased efficiency of DEGs. The research is focusing on the material properties of dielectric elastomer, and it investigates the effect of added filler and different treatment methods on the material-related losses that contribute to the efficiency of DEGs. In the present research, films prepared from commercial

prevulcanised natural latex are tested for energy dissipation. This study is focusing solely on the dielectric NR-based material, its material-related losses and mechanical properties. As no actual energy harvesting ability is tested at this stage, a commercial physiotherapeutic band with moderate stiffness is used as the reference to compare the properties of the fabricated films.

2 Experimental

2.1 Materials and sample preparation

In the present study, commercial prevulcanised natural rubber latex (Revultex MR, supplied by Algol Chemicals Oy) with medium modulus is used along with a nanodiamond powder with carboxylated surface (uDiamond Molto Vox, Carbodeon Oy). The prevulcanised latex is water-based and it contains an antioxidant. No additional compounding is required to obtain NR samples. The reference physiotherapeutic natural rubber band with medium stiffness (Duke Fitness) is used as received. The thickness of the reference rubber band is 0.35 mm.

First, nanodiamond powder is dispersed in distilled water to form a 5 wt.% suspension, which is then sonication for 30 minutes in FinnSonic m03 ultrasonicating bath. After sonication, suspensions are continuously stirred by magnetic stirrer to prevent ND sedimentation prior to compounding. Mixtures containing 0 to 10 phr (parts per hundred parts of rubber) of NDs are prepared as ND suspension is added to the latex slowly (1 drop/s) upon continuous stirring. The obtained solutions are poured into the moulds to obtain about 0.5 mm thick sheets and degassed in vacuum. The samples are left in ambient conditions for 24 hours for drying.

Post-treatment methods include leaching (washing) the dry films in distilled water for 20 minutes at 35 °C and swelling in acetone for 30 minutes at room temperature. Post-treatment is conducted at a constant stirring. After each type of post-treatment, samples are rinsed with deionized water and left on the flat surface to dry for 48 hours. Leaching is a process often employed in industry as a part of fabrication of rubber goods from latex. The main purpose of leaching is to remove water-soluble ingredients, e.g. natural proteins and salts, as well as excess curatives from the rubber film in order to provide better long-term stability. Other impurities that are not soluble by water, for example, fatty acids, can be extracted from the NR by acetone.

Sample designation: ND-x, where x is the amount of nanodiamond in phr. Leached and acetone-extracted samples are defined as ND-x L and ND-x A respectively. The physiotherapeutic band is designated as Ref.

2.2 Testing methods

A universal tester Messphysik Midi 10-20 is used for tensile testing (200 mm/min) of dumb-bell specimens with 10 mm test length. The thickness and width of the samples are measured precisely before testing. The average value of three specimens is reported for each sample.

Dielectric properties of the materials are measured with a Novocontrol Alpha-A dielectric analyser at room temperature in a frequency range from 0.05 Hz to 1 MHz. Temperature-dependent dielectric response is measured at the same frequency range from -80 to 30 °C with 10 °C step. The thickness of the samples is measured before each test. The sample is sandwiched between rigid gold-plated electrodes (2 mm thick by 20 mm in diameter). The average value of three specimens is reported for each sample.

Dynamic mechanical analysis (DMA) is conducted in shear at 1 Hz with 2 μm displacement amplitude and 5 N force from -80 to +25 °C heated at 3 °C/min rate on DMA/SDTA861e (Mettler Toledo). Stress relaxation and low speed cyclic loading of the samples is performed on Pyris Diamond DMA (Perkin Elmer). Samples are stretched to 10 % and kept at room temperature for an hour, while the change in force is recorded. The cyclic loading is conducted on the same equipment at ambient conditions, when samples of 10 mm test length are stretched to 45±1 % at 0.1 mm/s rate. The hysteresis loss is calculated by subtracting integrated loading and unloading curves and dividing the value by the area under the corresponding loading curves.

Fourier transform infrared spectra (FTIR) is obtained with Bruker Tensor 27 in attenuated total reflectance (ATR) mode in the range from 400 to 4000 cm^{-1} with diamond crystal background and 4 cm^{-1} resolution.

3 Results and discussions

3.1 Comparison of NR and the reference material

Industry provides a variety of latex formulations for different applications, fabrication processes and desired mechanical properties of the finished product. An elastomer membrane for a DEG is expected to have moderate tensile strength, high elongation and low to moderate elastic modulus. From the Table 1, it is seen that both rubbers have the needed properties, despite of the lower tensile strength of the fabricated film. Its lower tensile strength is compensated by higher maximum elongation, as well as reduced stress at 100% and 200% elongation (M_{100} and M_{200} respectively). Such differences can be explained by higher crosslink density and possible presence of filler in the reference sample.

The FTIR-ATR spectra (Figure 2) reveal very similar chemical structure of the fabricated unfilled rubber and the reference physiotherapy band. The main characteristic peaks of the materials are the same, and the only differences are the broadened peak at 1661 cm^{-1} that is related to C=C unsaturation, as well as increased absorption in 3200-3500 cm^{-1} area, indicating the presence of hydrogen bonds. Peaks below 800 cm^{-1} can be related to the presence of sulphur bonds and C-H bending (Coates 2006). These small differences in FTIR-ATR spectra may occur due to the presence of mineral fillers and pigments in the rubber band and reflect the differences in crosslink densities.

The dielectric properties of the elastomer membrane, namely dielectric permittivity (ε') and loss (ε''), are compared to evaluate their ability to improve the material-based performance of a DEG. Relative dielectric permittivity of ND-0 and Ref. materials is shown in Figure 3a. Above 10 Hz permittivities of both materials are virtually same with no frequency dependence. However, at lower frequencies, ND-0 show more pronounced increase in ε' than Ref., that can be related to interfacial polarization. In the case of natural rubber, the possible reason for interfacial polarization is the presence of natural impurities with higher electrical conductivity than the polymer itself, which leads to charge accumulation at the polymer-particle interface.

The shape of the loss factor ($\tan \delta = \varepsilon''/\varepsilon'$) curve is also different between ND-0 and Ref., as a broad partly masked peak appears in Ref. curve between 5 and 100 Hz (Figure 3b). Such peak is usually an indication of an additional relaxation process related either to the presence of fillers or chain motion of the polymer (Hernandez et al. 2010). The increase in the dielectric loss factor in the low frequency region can also be related to the interfacial polarization. Moreover, loss factor increases as the result of ionic conductivity due to the presence of naturally occurring mobile ions in NR. This is supported by the change of the slope of the real part of electrical conductivity (Figure 3c). However, the great increase in dielectric losses below 1 kHz shown by the tested materials can be additionally related to the parasitic effect of interfacial polarization between the electrode and the sample. In case of such electrode polarization, some effects in the lower frequency area may be masked and material losses also negatively affected. (Schönhals and Kremer 2003)

In order to detect a possible parasitic effect, the imaginary part of electrical conductivity (Figure 3d) must be considered. As the slopes of both curves are linearly dependent on the frequency, it is concluded that an electrode polarization effect is not affecting the measurements. Generally, the dielectric loss of ND-0 is lower than Ref. only at higher frequencies, which means that ND-0 still needs to be optimized for the DEG application, as it suggests low frequencies of operation. The minimisation of dielectric losses is achieved further by addition of nanodiamond powder and by two different types of the post-treatment of the composites.

3.2 The effect of nanodiamond filler on dielectric properties of NR

The effect of filler addition can be observed from temperature-dependent dielectric losses of ND-0 and ND-10 at different frequencies (Figure 4). No distinct relaxation peaks are seen from the loss factor

frequency scan at room temperature, but a low temperature frequency-dependent relaxation peak corresponding to the glass transition of NR appears around -60 °C for 1 Hz (Figure 4a). With increase in frequency, the peak is broadening and shifting to the higher temperatures, as expected. For lower frequency curves, a high temperature event is observed. This event is related to the contribution of chain dynamics and increased ionic conductivity, similarly as isothermal low frequency events, resulting in the increased dielectric losses (Schönhals and Kremer 2003). At the same time, the mentioned relaxations are much less pronounced for the ND-10 sample (Figure 4b). Moreover, it shows little dependence on the temperature, especially at low frequencies. This may suggest that presence of NDs restricts the mobility of rubber chains. The observed overall increase in dielectric loss for NR-ND composite is explained by reduced homogeneity of the system, as another component is introduced into it. In terms of DEG application, however, largely reduced dependence of dielectric loss on temperature can be viewed as a positive feature meaning more stable dielectric parameters of the membrane in the whole range of operating temperature of a DEG.

At room temperature, dielectric loss factor is notably reduced at frequencies below 0.1 Hz for ND-5 and ND-10 compounds (Figure 5a). This can be related to the lowered ionic conductivity generally affecting the losses at low frequencies. However, the filler-related effect discussed previously contributes to the increased losses at higher frequencies meaning that ND-5 and ND-10 show dielectric loss factor higher than Ref. Same effect of the filler addition is observed in electrical conductivity data shown in Figure 5b. Here, the addition of NDs results in decreased conductivity compared to the ND-0 sample, but only at 1 Hz and below. At higher frequencies, addition of filler leads to some increase in electrical conductivity, but at the same eliminates the slope change of the curve. This finding supports the assumption that higher loads of NDs help to reduce the ionic conductivity in the NR sample. As a DEG usually works at low frequencies, it can be concluded that the addition of up to 10 phr NDs is favourable in terms of reducing the dielectric losses of NR films.

The relative dielectric permittivity of the ND-containing compounds varies to some extend from ND-0 (Figure 5c), but stays below 3 in the upper part of the frequency range. It can be generally noted that the addition of NDs results in less significant increase in the relative permittivity below 1 Hz. Moreover, the effect of the filler addition is observed in shifting the onset of the permittivity growth to higher frequencies, meaning higher interfacial polarization in this case. Although for a higher capacitance the higher dielectric permittivity is preferable, for a DEG application a less rapid change in ε' values would be beneficial, as it would result in less frequency dependent performance.

3.3 The effect of sample post-treatment on dielectric properties of NR composites

The aim of the post-treatment is to reduce the dielectric losses of the materials by extracting naturally occurring impurities from NR either by deionized water, or by acetone. In this study, leaching is employed to improve the dielectric properties of the material by reducing the amount of water-soluble ingredients, especially salts, in the system. As seen from Figure 6a, leaching of the samples significantly reduces the dielectric losses of the films in the whole frequency range. Thus, the extraction of water-soluble components from NR not only reduces the ionic conductivity, but also lowers the disorder in the system by enhancing its purity. After leaching, even ND-0 compound reaches the loss level of Ref. at the low frequency area and decreases the losses remarkably at higher frequencies thus making the fabricated compounds favourable for the DEG application in terms of loss minimisation. The leaching treatment also improves electrical resistivity of all compounds (Figure 6b), which is advantageous for a dielectric application, but has no effect on the shapes of the conductivity curves.

Similarly to water leaching, sample post-treatment by swelling in acetone is applied in this study to reduce the dielectric losses of the materials by removing non-rubber impurities that are not soluble in water. Dielectric loss measured after acetone treatment (Figure 7a) shows a notable decrease when compared to the untreated samples. As non-rubber ingredients, including, for instance, organic acids, are known to increase dielectric losses of the material, the reduction of dielectric losses can be related to the extraction of such impurities by the acetone treatment. While at low frequency area the decrease is comparable to the effect of water leaching, for acetone-treated samples, some decrease in the loss factor is observed also

in the higher frequencies. The effect is mostly pronounced for ND-0 A. Therefore, the acetone treatment may be more preferable for dielectric loss reduction compared to the water leaching. However, as acetone is more aggressive solvent for NR than water, some rubber can be extracted from the sample during the treatment. Therefore, the effect of acetone treatment on mechanical properties of the samples should be considered.

Although in terms of minimisation of the dielectric losses, both post-treatment types seem to be almost equally effective, but they show different results in case of relative dielectric permittivity. For the leached samples, the dielectric permittivity stays below 3 for all the materials above 100 Hz, and is otherwise similar to Ref, as can be seen from Figure 8a. At low frequencies, the polarization-related increase in the dielectric permittivity is not as pronounced as for the untreated samples. The acetone-treated samples show more remarkable increase in permittivity at low frequency than the leached samples. However, acetone treatment increases the overall dielectric permittivity of all compounds except for ND-0.5 A, when compared to Ref. As a DEG is basically a capacitor, higher dielectric permittivity is a positive improvement. Therefore, acetone treatment can be employed as a more useful method to improve dielectric properties of prevulcanised NR films.

3.4 The effect of nanodiamonds on mechanical properties and viscous losses of NR.

Good mechanical properties are important for a demanding DEG application. The effect of NDs on the mechanical properties of NR is shown in Table 2. Addition of ND filler rarely results in the reinforcement of rubbers (Shakun et al. 2014). Nevertheless, addition of up to 2 phr NDs leads to some improvement in the mechanical properties of NR. Tensile strength and modulus at 100 and 200% elongation of NR (M_{100} and M_{200} respectively) are increased without a pronounced effect on maximum elongation. In practice, increase in modulus results in more force required to stretch the material. Compared to ND-0, ND-5 and ND-10 composites both show reduced stress and elongation at break. The changes can be explained by the filler agglomeration and an inefficient load transfer between matrix and filler. At the same time, M_{100} and M_{200} of ND-5 are comparable to Ref, and the increase in M_{100} and M_{200} can generally be explained by the hydrodynamic effect.

The effect of acetone post-treatment on the mechanical properties of the composites is very pronounced, as seen from Table 2. Such treatment increased the elongation at break for all the materials. The tensile strength and moduli of all the composites except for ND-10 A is increased to some extent. This can be related to the increase in total elastomer content in the system after removal of non-rubber impurities. The drawback of such a treatment is difficulty do get uniform properties between the specimen, as can be seen from the increased deviations of the results. Nevertheless, the mechanical properties of NR-ND composites generally remain suitable for the DEG application.

As severe stress relaxation is the main drawback of the popular acrylic adhesive often utilized in DEGs, the stress relaxation properties of the fabricated materials are evaluated and compared to the reference rubber band. Table 3 presents the stress loss percentage of the samples stretched uniaxially to 10% after 1, 5 and 60 minutes of the test. The effect of post-treatment with acetone is also included into evaluation. It is seen that ND composites containing 2 and more phr of nanodiamonds show less stress relaxation than the unfilled material. However, only ND-5 and ND-10 have smaller relaxation than Ref. after one hour test. After one minute of the test, the stress loss of the most materials is less than Ref., which can be related to the differences in the slope of the relaxation curve. This means faster and almost instantaneous loss of stress for the Ref. compared to the other samples. When compared to Ref., acetone treatment decreases the stress loss of ND-0 after 1 and 5 minute significantly from 6.6 % to 4.5 % and from 10.9 % to 9.5 % respectively. Thus, the fabricated samples can be considered more suitable for the DEG application in terms of the stress relaxation meaning that such samples would suffer less the loss of tension during the service.

The effect of filler on the energy damping properties of the composites can be estimated by the dynamic loss tangent ($\tan \delta$), which is the ratio of energy lost to energy stored in a cycle. The loss tangent measured by DMA may be a representation of a hysteresis loss at strains below 1% (Ahankari and Kar 2010). All

the studied materials show the maximum loss tangent close to -49 °C indicating the glass transition temperature (T_g) of the materials (Figure 9). The addition of up to 2 phr of NDs leads to both a small decrease of T_g and an increase in the tan δ peak, while the addition of higher amounts of filler results in the opposite effect. Dry lubricating phenomenon of NDs at low concentrations may be responsible for the effect (Dolmatov 2007a). An increase in T_g at higher filler loads with the decrease of loss tangent is probably due to the domination of decreased free volume.

The insert in Figure 9 presents tan δ of the studied compounds at the temperature range of interest. All the fabricated composites show lower viscous losses than Ref. up to 20 °C, but above 20 °C the loss tangent of ND-0 starts to grow. Samples with low ND content (ND-0.5, ND-1 and ND-2) show the lowest viscous losses indicated by the dynamic loss tangent. This can be possibly explained by good rubber-filler interaction, as an improvement of tensile properties is also observed for the same compounds. Even ND-10 shows low viscous losses that are comparable to ND-0, but without an increase at elevated temperature. The presented results would suggest that viscous losses of the fabricated composites are low, and such materials can be recommended for the DEG application, and they may over perform the reference rubber band.

The losses related to the viscoelastic nature can be further studied by calculating the hysteresis loss of the material, as certain portion of energy is always lost during the dynamic cycle. Here, the materials are also tested for hysteresis loss at 45% tensile strain and a very low frequency (about 0.01 Hz) to evaluate the performance of the material close to the real energy harvesting conditions. The obtained hysteresis loss is presented in Table 4. The results indicate that the addition of a filler results in increased hysteresis losses, especially after the first cycle. Both break-up and reassembly of filler agglomerates at high strains and slippage of the polymer chains along the filler surface can be responsible for the increased hysteresis. This is the stress softening of rubber also known as Mullins effect. Such hysteresis behaviour suggests that the membrane material should be preconditioned for several cycles before the actual operation in a DEG in order to achieve stable harvesting cycles. Somewhat higher hysteresis loss of the reference material compared to ND-0 can possibly be explained by the presence of small amounts of filler in Ref. Treatment with acetone reduces the hysteresis losses for all materials after the first cycle, but does not show that significant effect after the tenth cycle, except for the acetone-treated MR-10 A. This materials shows more than a threefold and eightfold decrease of hysteresis losses after first and tenth cycle respectively. Although no trend in these changes is observed, acetone treatment seems to be more successful for MR-0.5 A and MR-10 A in terms of reducing the hysteresis losses.

4 Conclusions

The research investigated the material-related losses of natural rubber and rubber-nanodiamond composites in order to explore the perspectives of such materials to be used in DEGs and probability to improve their efficiency. Generally, NR has the required properties to be successfully used for the energy harvesting. However, its dielectric and viscous losses were reduced even more by the addition of NDs. Moreover, other successful methods of minimising the losses, namely sample post-treatment by leaching or acetone-extraction, were discussed in the study. Such treatment is capable to reduce the low frequency dielectric losses of NR by almost 25%. The study of the viscous losses at low strains indicated that below 20 °C all the fabricated materials had less mechanical energy dissipation (up to 35% for NR-ND composites containing 2 phr of filler) compared to the reference physiotherapy band that has showed advantageous energy harvesting results in the number of studies. However, despite of the expectations, the addition of fillers, except for 10 phr of NDs, failed to reduce hysteresis losses of the materials at higher strain.

Nevertheless, the addition of 5 phr of NDs resulted in an optimum combination of dielectric, viscous and stress relaxation properties, as well as fair mechanical properties. The further minimisation of material-related losses at low frequencies was achieved by the acetone treatment. Such treatment was especially useful for the reduction of the low frequency dielectric losses far below the reference rubber band, as well as for the improving the elasticity and the dynamic performance of the samples. Moreover, treatment with acetone increased the relative dielectric permittivity of NR-ND composites thus improving their

capacitance. Therefore, an acetone treated NR containing 5 phr of NDs can be recommended for the further study of the actual energy harvesting performance.

References

Ahankari, S.S. and Kar, K.K. (2010), 'Hysteresis measurements and dynamic mechanical characterization of functionally graded natural rubber–carbon black composites', *Polymer Engineering & Science,* Vol. 50, No. 5, pp. 871-877.

Ahnert, K., Abel, M., Kollosche, M., Jorgensen, P.J. and Kofod, G. (2011), 'Soft capacitors for wave energy harvesting', *Journal of Materials Chemistry,* Vol. 21, No. 38, pp. 14492-14497.

Chiba, S., Kornbluh, R., Pelrine, R. and Waki, M. (2010), 'Novel Electric Generator Using Electroactive Polymer Artificial Muscle (EPAM)' in Proceedings of the WHEC, Essen, pp. 22-30.

Chiba, S., Waki, M., Wada, T., Hirakawa, Y., Masuda, K. and Ikoma, T. (2013), 'Consistent ocean wave energy harvesting using electroactive polymer (dielectric elastomer) artificial muscle generators', *Applied Energy,* Vol. 104, pp. 497-502.

Coates, J. (2006) 'Interpretation of infrared spectra, a practical approach', in *Encyclopedia of Analytical Chemistry,* John Wiley & Sons, Ltd.

Cottinet, P.-., Guyomar, D., Guiffard, B., Putson, C. and Lebrun, L. (2010), 'Modeling and experimentation on an electrostrictive polymer composite for energy harvesting', *IEEE Transactions On Ultrasonics, Ferroelectrics and Frequency Control,* Vol. 57, No. 4, pp. 774-784.

Dolmatov, V. (2007a), 'Polymer-diamond composites based on detonation nanodiamonds. Part 2', *Journal of Superhard Materials,* Vol. 29, No. 2, pp. 65-75.

Dolmatov, V. (2007b), 'Polymer—diamond composites based on detonation nanodiamonds. Part 3', *Journal of Superhard Materials,* Vol. 29, No. 4, pp. 199-205.

Graf, C., Hitzbleck, J., Feller, T., Clauberg, K., Wagner, J., Krause, J. and Maas, J. (2014), 'Dielectric elastomer–based energy harvesting: Material, generator design, and optimization', *Journal of Intelligent Material Systems and Structures,* Vol. 25, No. 8, pp. 951-966.

Hernandez, M., Carretero-Gonzalez, J., Verdejo, R., Ezquerra, T.A. and Lopez-Manchado, M.A. (2010), 'Molecular dynamics of natural rubber/layered silicate nanocomposites as studied by dielectric relaxation spectroscopy', *Macromolecules,* Vol. 43, No. 2, pp. 643-651.

Hoffstadt, T., Graf, C. and Maas, J. (2013), 'Optimization of the energy harvesting control for dielectric elastomer generators', *Smart Materials and Structures,* Vol. 22, No. 9, pp. 094028-1-7.

Huang, J., Shian, S., Suo, Z. and Clarke, D.R. (2013), 'Maximizing the energy density of dielectric elastomer generators using equi-biaxial loading', *Advanced Functional Materials,* Vol. 23, No. 40, pp. 5056-5061.

Jean-Mistral, C. and Basrour, S. (2010), 'Scavenging energy from human motion with tubular dielectric polymer' in *SPIE Proceedings 7642, Electroactive Polymer Actuators and Devices (EAPAD),*Vol. 7642, pp. 764209-764209-12.

Jean-Mistral, C., Beaune, M., Vu-Cong, T. and Sylvestre, A. (2014), 'Energy scavenging strain absorber: application to kinetic dielectric elastomer generator' in *SPIE Proceedings 7642, Electroactive Polymer Actuators and Devices (EAPAD),*Vol.9056, pp. 90561H-90561H-8.

Jean-Mistral, C., Cong, T.V. and Sylvestre, A. (2012), 'Advances for dielectric elastomer generators: Replacement of high voltage supply by electret', *Applied Physics Letters,* Vol. 101, No. 16, pp. 162901-162901-5.

Kaltseis, R., Keplinger, C., Adrian Koh, S.J., Baumgartner, R., Goh, Y.F., Ng, W.H., Kogler, A., Trols, A., Foo, C.C., Suo, Z. and Bauer, S. (2014), 'Natural rubber for sustainable high-power electrical energy generation', *RSC Advances,* Vol. 4, No. 53, pp. 27905-27913.

Kang, G., Kim, K. and Kim, S. (2011), 'Note: Analysis of the efficiency of a dielectric elastomer generator for energy harvesting', *Review of Scientific Instruments*, Vol. 82, No. 4, pp. 046101-046101-3.

Koh, S.J.A., Zhao, X. and Suo, Z. (2009), 'Maximal energy that can be converted by a dielectric elastomer generator', *Applied Physics Letters*, Vol. 94, No. 26, pp. 262902-1-3.

Kornbluh, R., Pelrine, R., Prahlad, H., Wong-Foy, A., McCoy, B., Kim, S., Eckerle, J.and Low, T. (2012) 'From boots to buoys: Promises and challenges of dielectric elastomer energy harvesting', in Rasmussen, L. (Eds.) *Electroactivity in Polymeric Materials*, Springer US, Boston, pp. 67-93.

Lai, W., Bastawros, A.F., Wei Hong and Soon-Jo Chung (2012), 'Fabrication and analysis of planar dielectric elastomer actuators capable of complex 3-D deformation' in *IEEE International Conference on Robotics and Automation (ICRA)*, pp. 4968-4973.

McKay, T.G., O'Brien, B.M., Calius, E.P. and Anderson, I.A. (2011), 'Soft generators using dielectric elastomers', *Applied Physics Letters*, Vol. 98, No. 14, pp. 142903-142903-3.

Moretti, G., Fontana, M. and Vertechy, R. (2015), 'Parallelogram-shaped dielectric elastomer generators: Analytical model and experimental validation', *Journal of Intelligent Material Systems and Structures*, Vol. 26, No. 6, pp. 740-751.

Schönhals, A. and Kremer, F. (2003) 'Analysis of dielectric spectra', in Kremer, F. and Schönhals, A. (Eds.), *Broadband Dielectric Spectroscopy*, Springer Berlin, Heidelberg, pp. 59-98.

Shakun, A., Poikelispää, M., Das, A. and Vuorinen, J. (2017), 'Improved electromechanical response in acrylic rubber by different carbon-based fillers', *Polymer Engineering & Science*,[online] http://dx.doi.org/10.1002/pen.24586 (Accessed 8.12.2017).

Shakun, A., Vuorinen, J., Hoikkanen, M., Poikelispää, M. and Das, A. (2014), 'Hard nanodiamonds in soft rubbers: Past, present and future – A review', *Composites Part A: Applied Science and Manufacturing*, Vol. 64, pp. 49-69.

McKay, T.G., Rosset, S., Anderson, I.A. and Shea, H. (2015), 'Dielectric elastomer generators that stack up', *Smart Materials and Structures*, Vol. 24, No. 1, pp. 015014-1-8.

Vertechy, R. and Fontana, M. (2015), 'Electromechanical characterization of a new synthetic rubber membrane for dielectric elastomer transducers' in pp. 94300K-94300K-7.

Vertechy, R., Fontana, M., Rosati Papini, G.P. and Forehand, D. (2014), 'In-tank tests of a dielectric elastomer generator for wave energy harvesting' in *Electroactive Polymer Actuators and Devices (EAPAD)*, pp. 90561G-90561G-11.

Wang, H., Zhu, Y., Wang, L. and Zhao, J. (2012), 'Experimental investigation on energy conversion for dielectric electroactive polymer generator', *Journal of Intelligent Material Systems and Structures*, Vol. 23, No. 8, pp. 885-895.

Nomenclature

ε'	Relative dielectric permittivity
ε''	Dielectric loss
M_{100}	Modulus at 100% elongation
M_{200}	Modulus at 200% elongation
$\tan\delta$	Loss factor
T_g	Glass transition temperature
ATR	Attenuated total reflectance
DEG	Dielectric elastomer generator
DMA	Dynamic mechanical analysis
FTIR	Fourier transform infrared spectra
ND	Nanodiamond
NR	Natural rubber
phr	Parts per hundred rubber

Tables

Table 1 Mechanical properties of the fabricated and reference samples

Sample	*Tensile strength, MPa*	*Elongation at break, %*	*M_{100}, MPa*	*M_{200}, MPa*
ND-0	22.18 ± 0.09	797.24 ± 14.87	0.66 ± 0.03	0.92 ± 0.04
Ref.	29.42 ± 1.56	715.8 ± 12.95	0.88 ± 0.04	1.42 ± 0.04

Table 2 The mechanical properties of untreated vs. acetone treated NR–nanodiamond composites

Property	*Acetone post-treatment*	*Amount of NDs, phr*					
		0	*0.5*	*1*	*2*	*5*	*10*
Tensile strength, MPa	-	22.18 ± 0.09	24.47 ± 2.05	24.87 ± 0.49	23.61 ± 1.23	18.57 ± 1.81	19.48 ± 0.83
	+	23.43 ± 0.98	24.63 ± 2.17	26.32 ± 1.26	23.31 ± 1.43	21.17 ± 1.24	15.00 ± 1.39
Elongation at break, %	-	797.24± 14.87	797.84 ± 23.28	807.03± 10.65	762.44 ± 5.18	641.11 ± 10.10	578.28 ± 5.93
	+	829.64 ± 14.42	850.82 ± 22.03	840.62 ± 16.59	781.63 ± 14.91	713.03 ± 8.97	589.53 ± 34.58
M_{100}, MPa	-	0.66 ± 0.03	0.66 ± 0.01	0.67 ± 0.01	0.71 ± 0.03	0.89 ± 0.00	1.33 ± 0.02
	+	0.68 ± 0.02	0.66 ± 0.01	0.69 ± 0.02	0.74 ± 0.02	0.93 ± 0.02	1.32 ± 0.09
M_{200}, MPa	-	0.92 ± 0.04	0.94 ± 0.02	0.95 ± 0.01	1.02 ± 0.01	1.43 ± 0.02	2.21 ± 0.05
	+	0.98 ± 0.02	0.96 ± 0.00	1.00 ± 0.02	1.08 ± 0.01	1.44 ± 0.03	2.11 ± 0.11

Table 3 Stress relaxation of NR-ND composites with the effect of acetone post-treatment

Sample	*Stress loss, %*					
	after 1 min		*after 5 min*		*after 1 hour*	
	non-treated	*acetone-treated*	*non-treated*	*acetone-treated*	*non-treated*	*acetone-treated*
MR-0	5.0	4.5	10.2	9.5	20.1	19.0
MR-0.5	7.9	4.5	14.9	9.7	25.2	19.2
MR-1	6.2	4.7	12.0	10.0	20.2	19.4
MR-2	6.1	3.6	11.4	8.0	18.1	16.9
MR-5	4.9	2.9	9.6	5.7	17.8	11.8
MR-10	3.6	3.9	6.7	5.8	12.1	9.6
Ref	6.6		10.9		17.6	

Table 4 The hysteresis loss of non-treated and acetone-treated materials after 1 and 10 cycles

Sample	*Hysteresis loss, J/mm^3*			
	after 1st cycle		*after 10th cycle*	
	non-treated	*treated*	*non-treated*	*treated*
MR-0	0.039	0.041	0.007	0.007
MR-0.5	0.041	0.037	0.010	0.005
MR-1	0.061	0.048	0.005	0.009
MR-2	0.053	0.040	0.007	0.008

MR-5	0.045	0.042	0.008	0.006
MR-10	0.137	0.045	0.017	0.002
Ref.	0.043		0.005	

Figures

Figure1 Schematic work cycle of a DEG

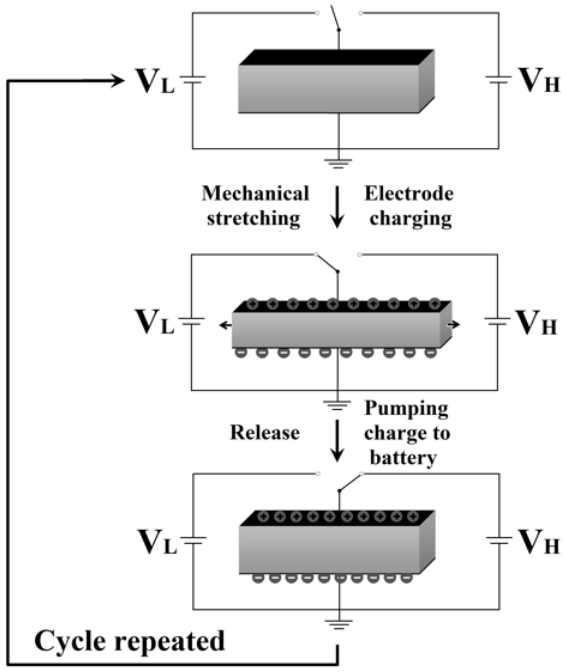

Figure 2 The FTIR-ATR spectra of the reference rubber band and unfilled NR latex film

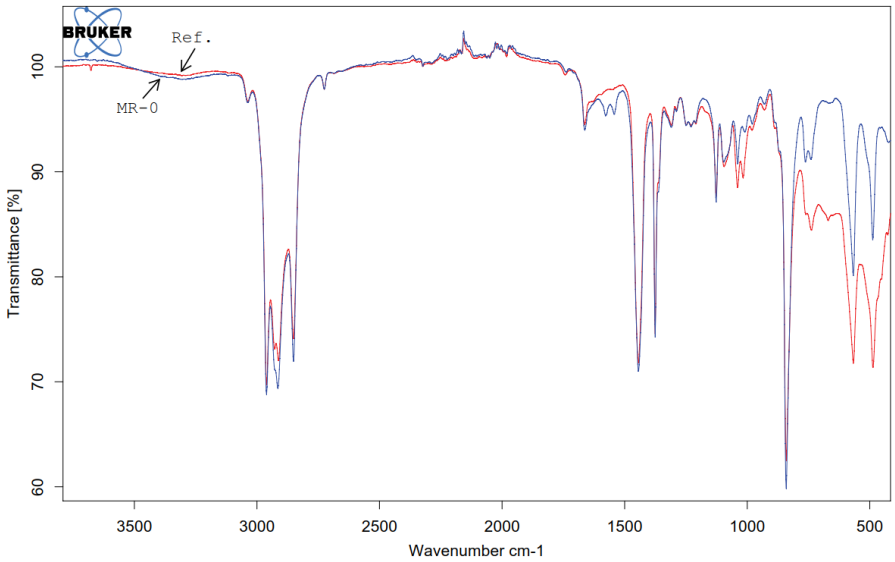

Figure 3 The frequency dependence of a) dielectric permittivity; b) loss factor; c) real and d) imaginary part of electrical conductivity of ND-0 and Ref.

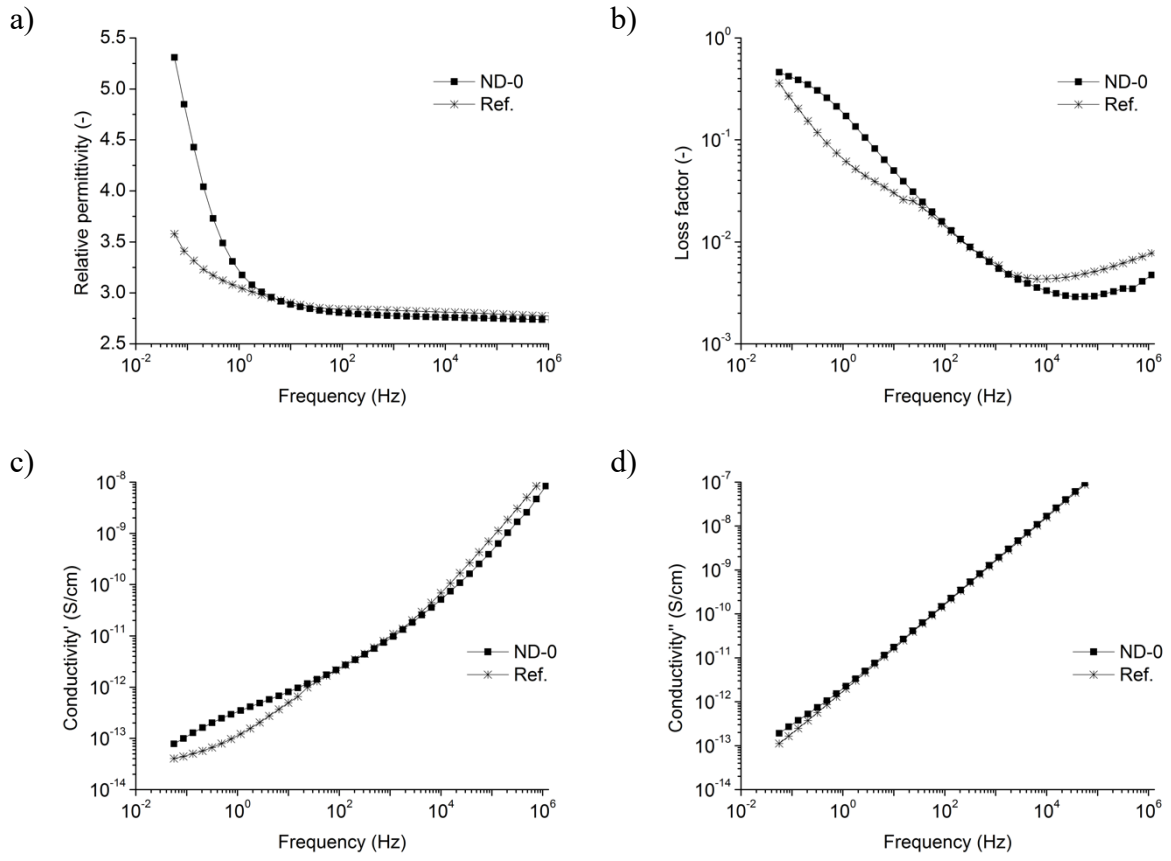

Figure 4 Temperature dependence of dielectric loss at different frequencies for a) ND-0 and b) ND-10

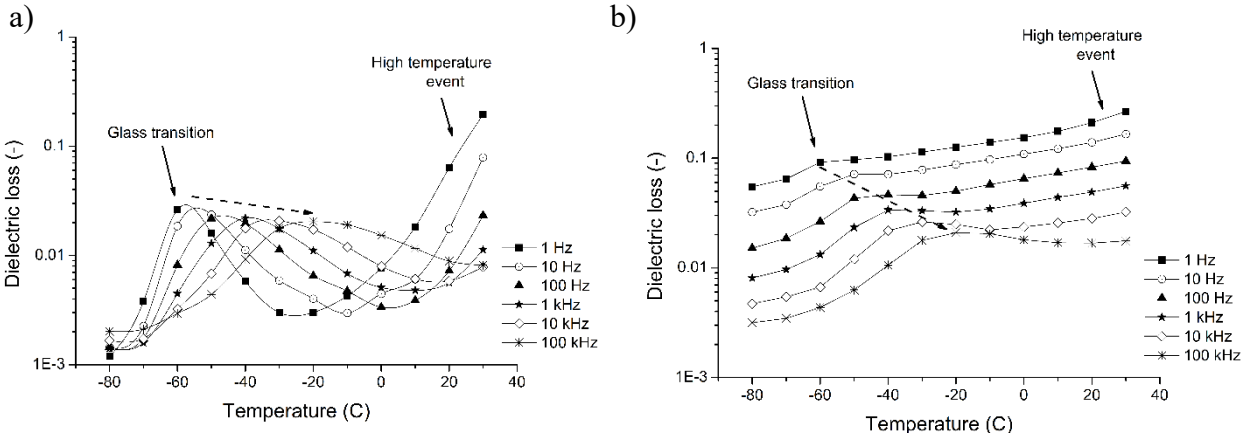

Figure 5 The frequency dependence of a) loss factor; b) electrical conductivity and c) relative dielectric permittivity of NR-ND composites

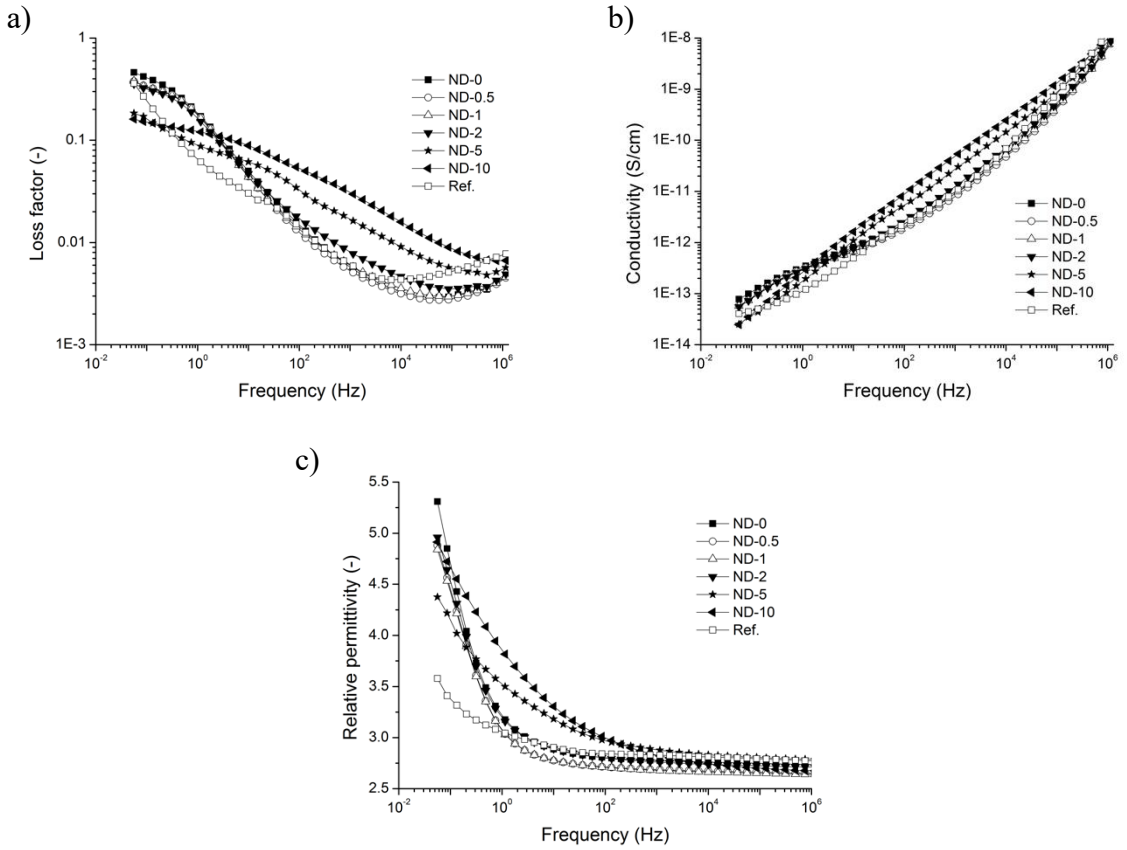

Figure 6 Frequency dependence of a) loss factor and b) electrical conductivity of leached NR-ND composites

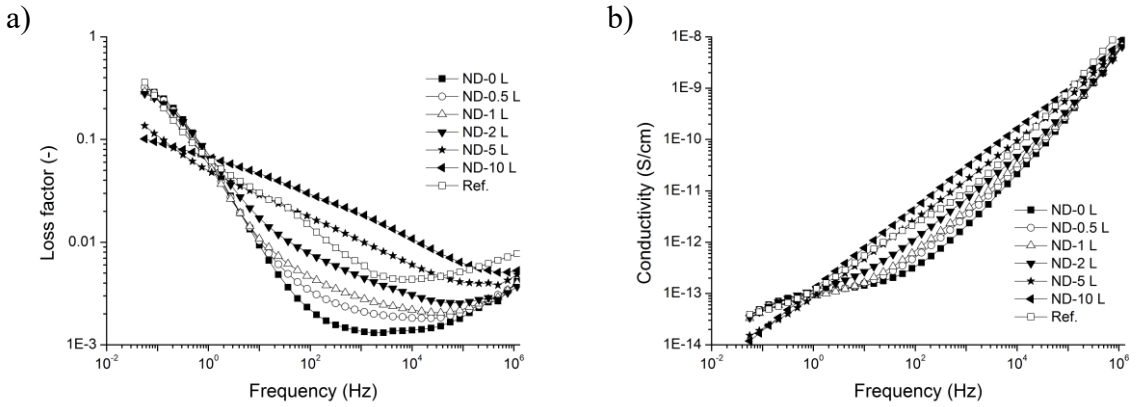

Figure 7 Frequency dependence of a) loss factor and b) electrical conductivity of acetone treated NR-ND composites

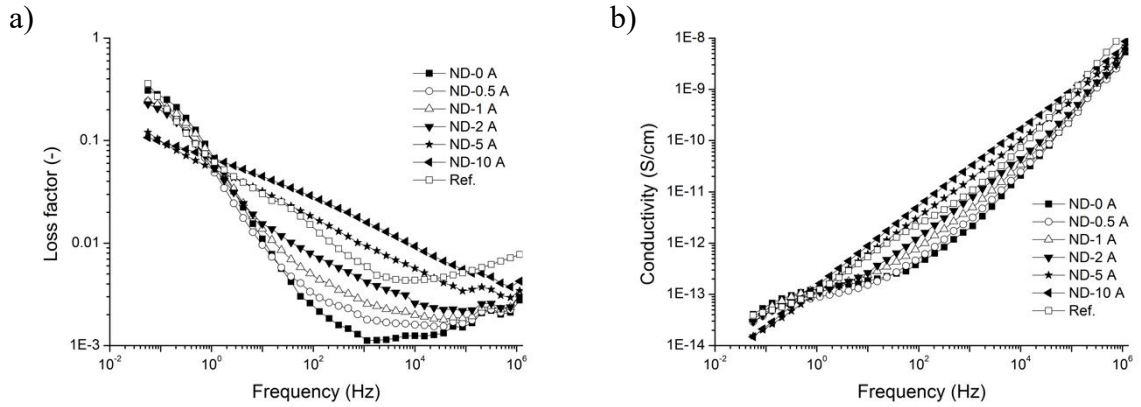

Figure 8 Relative dielectric permittivity of a) leached and b) acetone-treated NR-ND compounds

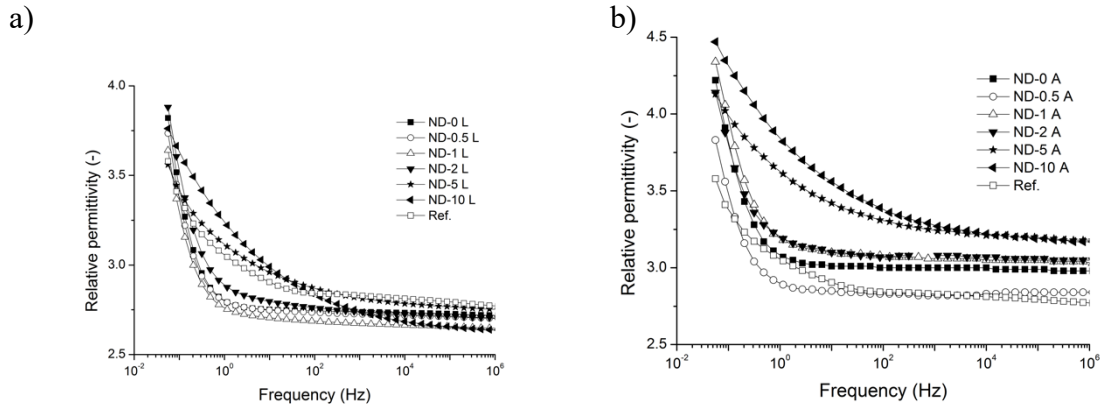

Figure 9 The loss tangent of the studied materials

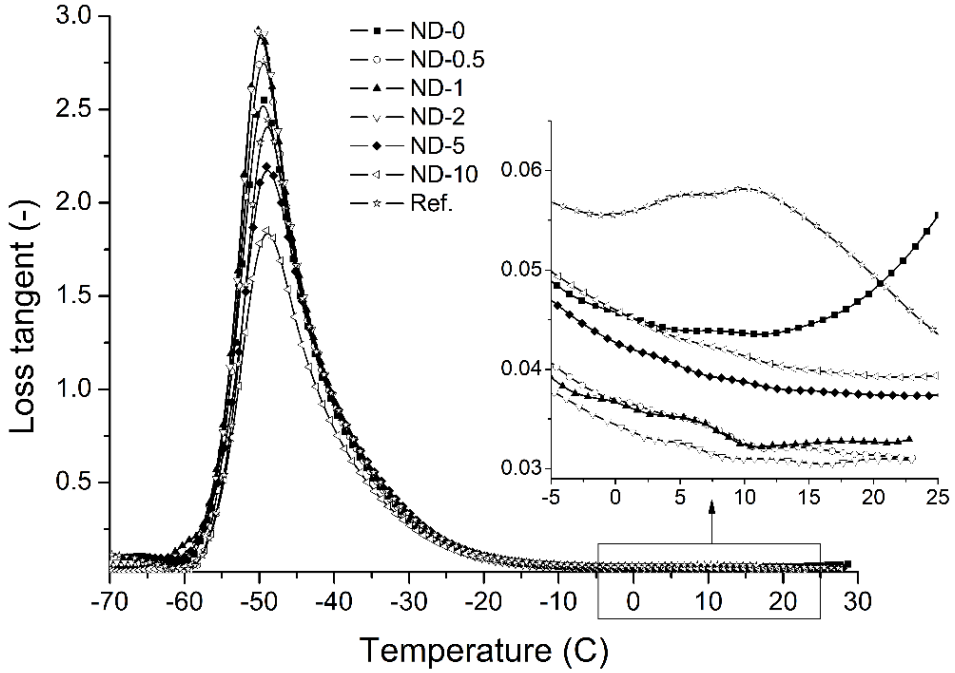

PUBLICATION III

Material-related losses of natural rubber composites with surface-modified nanodiamonds

A. Shakun, E. Sarlin, J. Vuorinen

Journal of Applied Polymer Science (2019) Vol.137, 48629
https://doi.org/10.1002/app.48629
Supplementary information available online

JOURNAL OF Applied Polymer SCIENCE

Material-related losses of natural rubber composites with surface-modified nanodiamonds

Alexandra Shakun, Essi Sarlin, Jyrki Vuorinen
Materials Science and Environmental Engineering, Tampere University, P.O. Box 589, FI-33014 Tampere, Finland
Correspondence to: A. Shakun (E-mail: alexandra.shakun@tuni.fi)

ABSTRACT: Dielectric elastomer generators (DEGs) offer a solution for the growing sustainable energy needs. Despite the active research on DEGs, currently used materials do not possess the required properties to achieve the full potential performance of such generators, thus, limiting an economical attractiveness of DEGs. Therefore, tailor-made materials for DEGs are in demand. Customizing the natural rubber recipe allows both dielectric and mechanical loss reduction, while the addition of nanodiamonds lowers the stress relaxation and hysteresis loss even further. The effect is most pronounced after chemical modification of nanodiamonds with silane coupling agents. Moreover, such modified nanodiamonds show less dielectric losses compared to unmodified nanodiamonds and allow reducing the dynamic loss tangent of the compound. © 2019 Wiley Periodicals, Inc. J. Appl. Polym. Sci. **2019**, *137*, 48629.

Received 12 April 2019; accepted 7 October 2019
DOI: 10.1002/app.48629

INTRODUCTION

Growing population and developing industry set a request on sustainable energy sources. Newly emerged energy technologies, such as dielectric energy harvesting, set a demand for materials with a combination of specific properties. In the past decades, much attention has been attracted to energy harvesting possibilities offered by dielectric elastomers, and different harvester prototypes have been introduced.

Dielectric elastomer generators (DEGs) are designed to work at low frequencies (below about 10–100 Hz) and are especially suitable for wave energy harvesting.[1–5] The working principle of a DEG is simple and based on changing capacitance (Figure 1). Elastomeric film sandwiched between the compliant electrodes works as a stretchable capacitor and needs to be electrically charged from an external source during the stretching (step 1). When the membrane returns to the original dimensions, distance between the electrodes increases leading to the increased potential difference that can be collected (step 2). Then, the cycle is repeated (step 3). Due to the described working principle, common unwanted energy dissipation routes in DEGs are through the dielectric losses and mechanical hysteresis. Therefore, the demanded material properties of the rubber film include low dielectric and viscous losses especially at low frequencies, low stress relaxation, and high elasticity.

Most often used elastomeric membranes for DEGs are made of commercial acrylic adhesives (such as VHB tape by 3 M), silicones, and natural rubber (NR). Each of these materials has their own benefits and drawbacks, but none of them has been specifically tailored for energy harvesting purposes. As much research has been focused on dielectric actuators, little attention has been paid to the improving materials for dielectric energy harvesting, and current DEG prototypes often utilize VHB adhesive as elastomeric membrane. VHB is very well-studied material, and its behavior in DEGs is easily predictable,[4,6–9] which makes it a good reference material. However, VHB tape shows high viscous losses and suffers from severe stress relaxation. Silicone rubber is known as a good candidate for energy harvesting applications,[2,5,10] and the potential of filled silicones[11] and silicone copolymers[12,13] has already been discussed in the literature. However, belonging to a specialty rubber type, silicones are more expensive than general rubber types. Moreover, silicones have low dielectric constant, and their mechanical properties may need improvements. Similarly to the VHB tape, dielectric behavior of NR is well studied, including the effect of compounding ingredients,[14] pressure,[15] and strain.[16,17] NR films are known to outperform the widely used VHB adhesive tape.[4] However, an improvement can be made to the comparably high dielectric losses of such films. At this stage, lack of tailor-made elastomeric materials is one of the reasons why wave energy harvesting is far behind its full potential. Further design and material modification is crucial to make DEGs economically viable and reduce the energy cost to one of the traditional energy sources.[18,19]

Some research has been done on filled NR, showing the effect of filler modification on dielectric behavior, which usually increased

Additional Supporting Information may be found in the online version of this article.

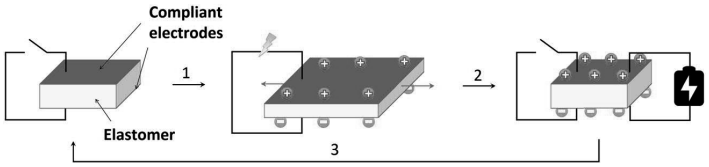

Figure 1. The simplified working principle of DEGs. [Color figure can be viewed at wileyonlinelibrary.com]

losses.[20,21] Indeed, the addition of filler particles into elastomeric matrix is known to increase dielectric losses at lower frequencies due to the interfacial polarization or the Maxwell–Wagner effect. The effect arises due to the differences in dielectric permittivity and electrical conductivity at the filler-matrix interface because of virtual charge accumulation.[22] Small amounts of nanodiamond powders (NDs) have shown the ability to reduce dielectric and viscous losses of some rubber types, which is believed to be related to the high structural activity of NDs and its active surface.[23,24] Although NR–ND composites have been discussed in the literature, dielectric properties of such composites have not been extensively studied. As for mechanical losses, addition of NDs can have potential in elastomer composite applications due to the reduced hysteresis of ND-filled rubbers, which is has been found to be much lower than for other carbon-based fillers.[25] Therefore, NDs can have potential in elastomer composites applied for energy harvesting.

Due to the active surface of NDs containing different chemical groups, it can be adjusted to become compatible with the polymer matrix. Silane coupling agents are often used in rubber industry to compatibilize silica and other fillers. The application of a coupling agent makes the filler surface more hydrophobic and compatible with the elastomer. Some successful methods of silanizing NDs have also been undertaken. Conventionally, silanization of NDs is performed in several stages involving surface reduction, which requires strong chemicals and leaves residues difficult to remove.[26,27] Direct functionalization of carboxylated NDs (ND-COOH) with vinyl-silane has been reported in a study discussing the possibility of the reaction between carboxylic group on the filler surface and silanol group of hydrolyzed coupling agent.[28] However, this approach has not been applied with NDs and the other silane coupling agents widely used in rubber technology.

Here, NDs were added to NR and the resulting composite properties were compared to the commercial materials previously successfully used in DEG prototypes—to an acrylic adhesive tape VHB4910 by 3 M, which is the most studied DEG membrane, and to a commercial NR physiotherapy band. The present study explored the behavior of NR–ND composites in terms of material-related losses and evaluated the effect of surface modification on them. The aim of using silanes in this work was to improve the interaction between the filler and polymer, possibly creating chemical bonds during crosslinking and reduce energy loss trough rubber-filler interface. The effect of ND surface modification by silane coupling agents was evaluated in terms of dielectric and mechanical losses. Both types of losses were reduced upon ND surface modification as compared to unmodified NR–ND composites, but failed to decrease dielectric losses below the level of unfilled NR. Nevertheless, all the studied materials showed significant loss-reduction compared to the commercial reference membranes. The most significant loss reduction was achieved in hysteresis losses and stress relaxation when applying silane-modified NDs in NR.

Table I. The Recipe of NR Compounds

Ingredient	Amount (phr)
Standard Malaysian Rubber (SMR10)	100
Zink oxide	3
Stearic acid	1
Sulfur	1.75
2-mercaptobenzothiazole	1
ND powders	0/1

EXPERIMENTAL

The polymer and the ingredients were compounded in a laboratory scale mixer (Brabender W 50 driven by Brabender Plasti-Corder) with the rotor speed 60 rpm and the starting temperature 50 °C according to the recipe shown in Table I. All compounding ingredients were commercial grade. The recipe was developed to minimize the negative effect of the compounding ingredients on dielectric losses without compromising elastic properties. ND powders with carboxylated surface (Molto Vox P, Carbodeon Oy, Finland) and hydrogenated surface (Molto Nuevo, Carbodeon Oy, Finland) were used as received. Moreover, ND-COOH were chemically modified with vinyltrimethoxysilane (VTMS, Sigma Aldrich, Finland) and triethoxysilylpropyldisulfide (TESPD, Sigma Aldrich) for NR compounds. Both surface-treated NDs were prepared prior to compounding according to the procedure described elsewhere,[28] and 1:5 ND:silane mass ratio was used. The materials were cured at 150 °C in hot press to form 1 mm sheets. The samples are designated as NR/0 for the unfilled NR, and NR/ND-x for the rubber filled with 1 phr (parts per hundred rubber) of ND, where x is the surface group of the ND. Commercial acrylic adhesive tape (VHB4910, 3 M) designated as VHB and 0.35 mm thick physiotherapeutic NR band with medium stiffness (Duke Fitness), designated as reference NR, were used as reference.

Dielectric properties of the samples were obtained with a Novocontrol Alpha-A dielectric analyzer at room temperature in a frequency (f) range $5{\cdot}10^{-2}$–10^{6} Hz with the rigid gold-plated electrodes (20 mm in diameter). The dielectric response of the

samples was obtained as complex permittivity $\varepsilon^*(\omega) = \varepsilon'(\omega) - j\varepsilon''(\omega)$, where $\omega = 2\pi f$ is the angular frequency. The real part of the complex dielectric permittivity (ε'), the imaginary part - dielectric loss (ε''), and electrical conductivity (σ) were reported for the measurements. Dielectric loss data in the same frequency range were also measured in −80–70 °C range with 10 °C steps. The average value of minimum three specimens was reported for each sample.

Dynamic mechanical analysis (DMA), stress relaxation, and low rate cyclic loading of the samples was performed with Pyris Diamond DMA (Perkin Elmer). DMA was measured in tension mode at 1 Hz with 20 μm displacement amplitude and 3 °C min^{-1} heating rate. For the stress relaxation measurement, samples were stretched to 10% and the change in force was recorded for an hour. The stress change values were calculated by dividing the force by the sample cross-sectional area. The cyclic loading tests used for the determination of hysteresis loss were conducted at ambient conditions, when samples with 10 mm test length were stretched to 45 ± 1% at 6 mm min^{-1} rate. High rate cycling loading of the samples at 500 mm min^{-1} rate and 100% maximum elongation and determination of moduli was performed on Z1.0 tensile testing machine (Zwick/Roell). The test length was 35 mm. Prestress up to 0.1 N was applied to avoid buckling of the samples. From the cyclic loading test, the hysteresis loss was calculated by integrating loading and unloading curves, subtracting the values and dividing the resulting value by the area under the corresponding loading curves. More details can be found in Figure S1a, showing the example of the high rate cycling loading of a reference NR sample, and in Figure S1b explaining the performed calculations of the hysteresis loss with the example of the first loading-unloading cycle of reference NR.

Fourier transform infrared (FTIR) spectra was obtained with Bruker Tensor 27 in attenuated total reflectance (ATR) mode in the range from 400 to 4000 cm^{-1} with diamond crystal background and 4 cm^{-1} resolution. The cryofracture surfaces of ND filled rubbers were studied with a scanning electron microscope (SEM, Zeiss ULTRAplus). The composite samples were coated with thin carbon layer to prevent charging during SEM analysis. Thermogravimetry (TGA) was performed with TG 209 F3 Tarsus (Netzsch) in nitrogen flow. Samples were heated to 125 °C with 20 K min^{-1} rate, kept at 125 °C for 10 min to remove humidity, and then heated to 850 °C with 20 K min^{-1} rate. The full raw TGA data of the test without an empty crucible correction are presented in Figure S2. Curing behavior was studied with Advanced Polymer Analyzer APA 2000 (Alpha Industries) for 20 min at 150 °C.

Apparent crosslink density (Q) was calculated for the 1 × 1 cm samples immersed in toluene for 72 h based on the equation[29]:

$$Q = 1/\left(\frac{m_s - m_d}{m_0}\right)\frac{F}{100} \quad (1)$$

where m_s and m_d are the weights of the swollen and dried specimen, respectively, m_o is the initial weight of the specimen, and F is the formula weight, phr.

RESULTS AND DISCUSSION

NDs have an active surface, which can be utilized to adjust the interaction with polymer matrix. Silane coupling agents were applied in order to modify the surface of the ND powders and reduce its hydrophilicity. Due to nonpolar nature of NR, NDs with hydrogenated surface (ND-H) are expected to have better affinity to matrix than ND-COOH. However, ND-COOH offers the possibility to incorporate a coupling agent onto its surface, which is expected to improve rubber-filler interactions and reduce the losses originating from rubber-filler interface.

First, the successful ND surface modification was confirmed with FTIR analysis. In Figure 2(a), the FTIR spectra of both VTMS-modified NDs (ND-VTMS) and TESPD-modified NDs (ND-TESPD) is compared to the reference ND-COOH. The reference ND-COOH shows characteristic carbonyl weak peaks around 1780 cm^{-1} and number of broad peaks at 1300–900 cm^{-1} as a combination of overlapping C—O stretch peaks from multiple oxygen-containing groups, for example, lactones and phenoles.[30] Both modified and reference fillers have an indication of —CH_2 groups due to peaks at 2860–2930 cm^{-1} and 1408/1453 cm^{-1}. The presence of the —OH group can be specified at 3100–3600 cm^{-1} (stretching) and 1625 cm^{-1} (bending).[31] Upon both modifications, a characteristic broad peak around 1020 cm^{-1} corresponding to Si—O—Si bond appeared due to the condensation of hydrolyzed alkoxy groups, and

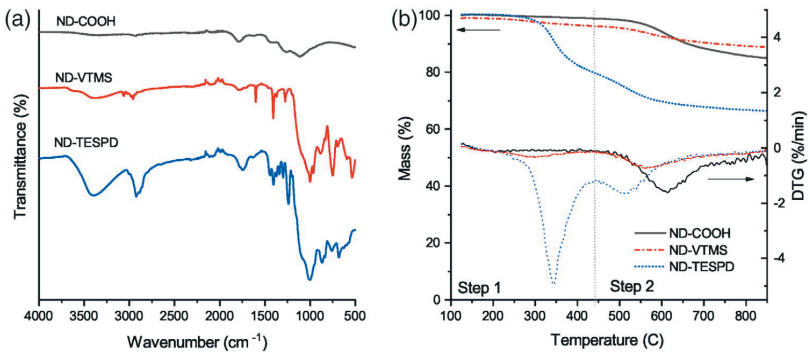

Figure 2. (a) FTIR-ATR spectra for ND-COOH and silane-modified NDs. Curves are shifted vertically for clarity. (b) TGA mass loss and mass loss rate curves for ND-COOH and silane-modified NDs. [Color figure can be viewed at wileyonlinelibrary.com]

the notable shoulder around 1100–1150 cm^{-1}, which are characteristics for silica.[32,33] Moreover, it is known as an indication of overlapping with Si—O—Si and Si—C peaks originating from the silane with the contribution from C—O bond.[34] The intensity of the peaks suggests an extensive shell formation around ND clusters especially for ND-TESPD powder. Peaks at 1275 cm^{-1} correspond to a Si—C stretching.[31,35,36] Modification with ND-VTMS is further confirmed by the appearance of peaks at 3062, 1601—, and 985 cm^{-1} due to the C=C bond, and 749 cm^{-1} due to C—H bend of the vinyl group.[34] ND-TESPD spectra showed multiple peaks for —CH_3 and —CH_2— groups in the range 1340–1412 cm^{-1} and more pronounced presence of —OH and COOH— groups.

Modification of NDs was also confirmed by TGA. The observed changes shown in Figure 2(b) indicated that the first mass loss step corresponds to the removal of strongly bound water and grafted organic molecules from the ND surface. The second mass loss step appeared from the removal of lactonic and other oxygen-containing surface groups, as when heated above 600 °C in inert atmosphere, ND surface usually loses its oxygen-containing groups and then undergoes graphitization and sintering above 800 °C resulting in a mass loss up to 10–20%.[37] The numerical results of TGA shown in Table II imply that TESPD formed a thick shell around ND clusters, as ND-TESPD lost about one-fifth of its mass during the first step. In comparison, ND-VTMS lost only 2.9% mass during the first degradation step. Temperature shift of the second step indicated reduced thermal stability of the modified NDs. Virtually same mass loss of ND-COOH and ND-TESPD samples during the second step may indicate that chemical interaction between ND surface and TESPD was improbable. Higher residual mass of ND-VTMS than ND-COOH was related to the significant amount of Si in the sample, and 0.9% mass loss during the isothermal step could be related to the presence of water or solvent residues. Due to the structural differences between two used silane types, namely, doubled amount of alkoxy groups in TESPD compared to VTMS and its steric effect, different route of modification may need to be developed for ND-TESPD, and the filler-silane ratio could be reduced.

According to the curing behavior shown in Figure 3 and summarized in Table III, addition of NDs to the compound resulted in minor reduction of curing times. Moreover, addition of ND-COOH and ND-VTMS increased maximum torque values and reduced the scorch times. This effect may be related to the high thermal conductivity of NDs, effective crosslinking reactions and presence of carboxylic groups on the surface.[38] TESPD modification of NDs led to an opposite effect on curing, and showed no reversion. TESPD-modified sample had the lowest torque and

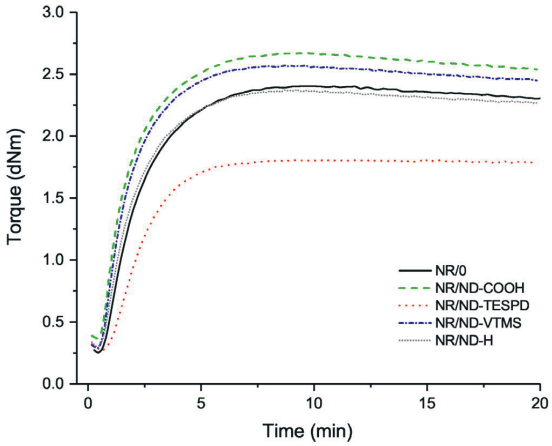

Figure 3. Curing curves of NR/ND compounds at 150 °C. [Color figure can be viewed at wileyonlinelibrary.com]

increased scorch time. This effect may be explained by less efficient crosslinking reaction and deactivation of curatives due to the presence of some silanol groups on the modified filler, as these groups are known to interact with accelerator.[39] Moreover, unwanted bubble formation may be responsible for the effect. Finally, hydrolysis of the alkoxy groups of silanes and self-condensation creates a shell around ND particles,[40] which may affected its surface properties and thermal conductivity.

The SEM images of the obtained filled composites are shown in Figure 4. The interface between filler and matrix looked uniform and showed good adhesion between the matrix and the filler. However, in all the samples, filler aggregates were present. Among the samples, NR/ND-H contained the largest clusters of NDs. Moreover, increase in aggregate size was noticed also for surface-modified NDs when compared to ND-COOH. As seen from Figure 4(d), ND-TESPD cluster seems more irregular in shape and no separate ND particles forming the cluster were visible. In other samples, the aggregates clearly consisted of the smaller particles. This could be an indication of an excessive shell formation over the ND aggregate.

The effect of NDs on moduli (stress at certain elongation) of NR was evaluated at 10, 50, and 100% strain, as it falls into the working strains of the DEG. The successful DEG membrane is expected to have low modulus. As can be seen from Table IV, the reference VHB tape had significantly lower moduli, and reference NR band had the highest moduli. At 10% elongation the

Table II. Thermogravimetric Data for ND Powders

		Temperature at DTG_{max} (°C)		Mass loss (%)		
Sample	Mass loss at isothermal step (%)	First step	Second step	First step	Second step	Residual mass (%)
ND-COOH	-	-	614.0	1.2	13.9	85.0
ND-VTMS	0.9	302.2	557.6	2.9	7.4	88.9
ND-TESPD	-	343.3	512.9	20.7	13.1	66.5

Table III. Curing Characteristics of NR-Based Materials

	Delta torque (dNm)	Scorch time (min)	Curing time (min)
NR/0	2.17	1.75	4.9
NR/ND-COOH	2.39	1.27	4.4
NR/ND-TESPD	1.55	2.68	4.5
NR/ND-VTMS	2.33	1.36	4.1
NR/ND-H	2.11	1.63	4.5

custom made NR–ND composite showed marginally same modulus values, and only NR/ND-TESPD resulted in decreased moduli compared to the unfilled material, which may be related to the imperfections within the material. This finding along with the curing curve would be consistent for a material with lower rubber network. However, NR/ND-TESPD had the highest apparent crosslink density Q among all materials (see Table IV). The increase in apparent crosslink density of NR/ND-TESPD implied that interaction between the silane shell and NR may be present, and the effect was more pronounced than for NR/ND-VTMS compound. However, due to the low torque and moduli, the bonds between NR and silane shell seemed not to be contributing to the efficient rubber network. Moreover, the low moduli and low delta torque of NR/ND-TESPD could be related to a dry lubricating effect NDs may show at low filler loads.[41]

The initial comparison of the developed NR recipe to the commercial reference materials, which are often used in DEGs, revealed their different dielectric nature, as seen in Figure 5. VHB tape is considered in the literature to have high dielectric losses,[42] as many sources report dielectric permittivity and loss only at 1 kHz. According to Figure 5(a), VHB shows a broad relaxation peak at this frequency and above, which is associated to the molecular mobility of this lightly crosslinked adhesive. However, when only frequencies below 10 Hz are considered, the dielectric properties are well suitable for DEG use due to low dielectric losses and comparably high dielectric permittivity, which is always beneficial for a capacitor. Moreover, the study of Vu-Cong *et al.*[43] has shown that the dielectric losses of VHB below 10 Hz are lower than most of the silicones, which are successfully applied in DEGs. The unusually high deviations of VHB tape especially at low frequencies can be related to the softness and high adhesiveness of the material and difficulty to eliminate air between sample and electrode without compressing and disturbing the sample. Due to this reason, VHB is known for the discrepancy of the dielectric permittivity (4.2–6) and loss values reported in the literature.[42,44]

The measured dielectric losses of VHB started to increase below 1 Hz due to the conductivity contribution effect, as seen from Figure 5(a). The conductivity contribution is detected at low frequencies as a linear portion of a dielectric loss curve increasing as frequency decreases.[22] Nevertheless, dielectric loss was the highest for the reference NR due to the most pronounced conductivity effect and additional relaxation peak around 10 Hz, which can be associated with interfacial Maxwell–Wagner polarization.[45,46] The relaxation peak was related to the presence of fillers (confirmed by the TGA in our previous publication[47]), as was supported by the increase in dielectric permittivity and the change of slope of the conductivity graph at low frequency area [Figure 5(b,c), respectively]. The increase in dielectric loss above 10^4 Hz was associated with the segmental dynamics of the sample

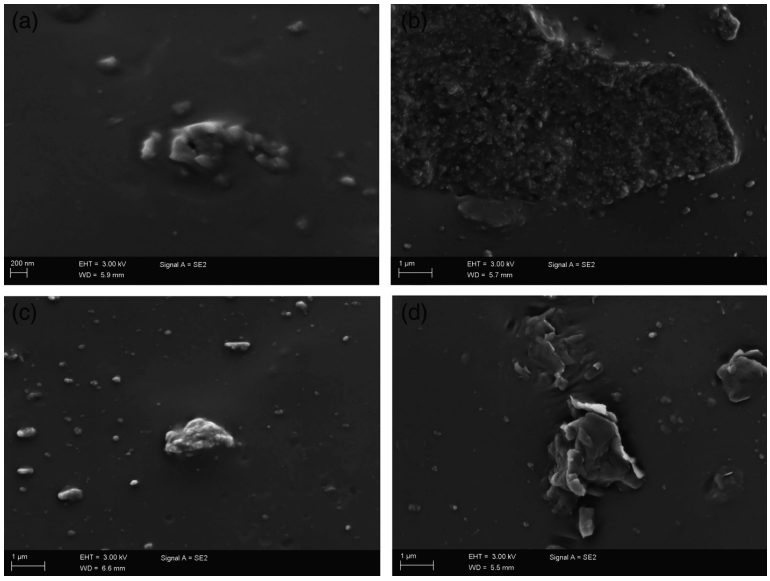

Figure 4. SEM images of (a) NR/ND-COOH, (b) NR/ND-H, (c) NR/ND-VTMS, and (d) NR/ND-TESPD samples. [Color figure can be viewed at wileyonlinelibrary.com]

Table IV. Moduli and Apparent Crosslink Densities of NR–ND and Reference Materials

	Modulus (MPa)			
Sample	10%	50%	100%	Q (–)
NR/0	0.121 ± 0.001	0.425 ± 0.004	0.634 ± 0.009	0.241 ± 0.002
NR/ND-COOH	0.123 ± 0.004	0.425 ± 0.026	0.632 ± 0.041	0.238 ± 0.001
NR/ND-TESPD	0.114 ± 0.007	0.389 ± 0.029	0.566 ± 0.045	0.262 ± 0.001
NR/ND-VTMS	0.136 ± 0.005	0.461 ± 0.005	0.690 ± 0.006	0.248 ± 0.001
NR/ND-H	0.129 ± 0.005	0.453 ± 0.005	0.672 ± 0.006	0.244 ± 0.001
Reference NR	0.171 ± 0.002	0.510 ± 0.002	0.723 ± 0.002	0.220 ± 0.002
VHB	0.051 ± 0.005	0.107 ± 0.009	0.128 ± 0.009	0.172 ± 0.001

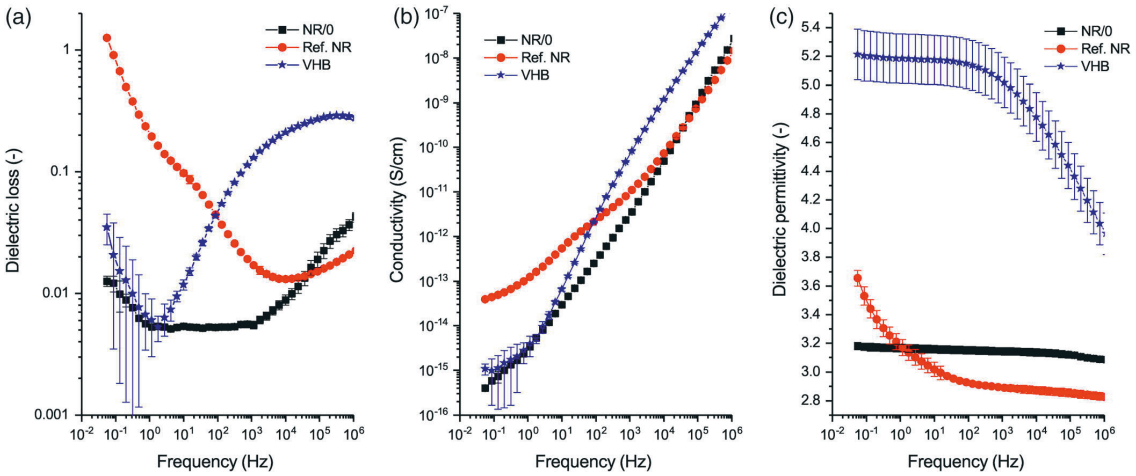

Figure 5. (a) Dielectric loss, (b) electrical conductivity, and (c) dielectric permittivity of unfilled NR/0 in comparison with commercial reference materials. [Color figure can be viewed at wileyonlinelibrary.com]

(α-relaxation), which is known to shift to higher frequency with increase in temperature,[20] as can be observed in Figure S2 showing the dependence of dielectric losses on both temperature and frequency. Lower dielectric loss of the custom-made NR/0 over the reference NR could be explained by the reduction of stearic acid and zinc oxide content in the recipe, which are known to

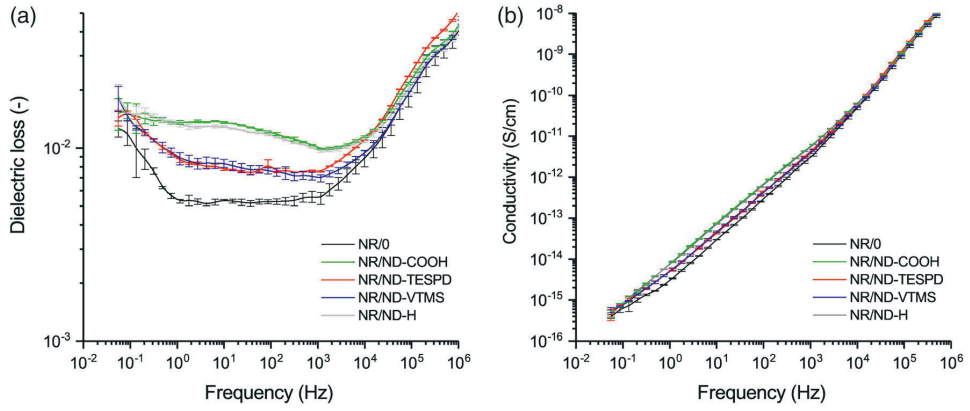

Figure 6. (a) Dielectric loss factor and (b) electrical conductivity of NR compounds. [Color figure can be viewed at wileyonlinelibrary.com]

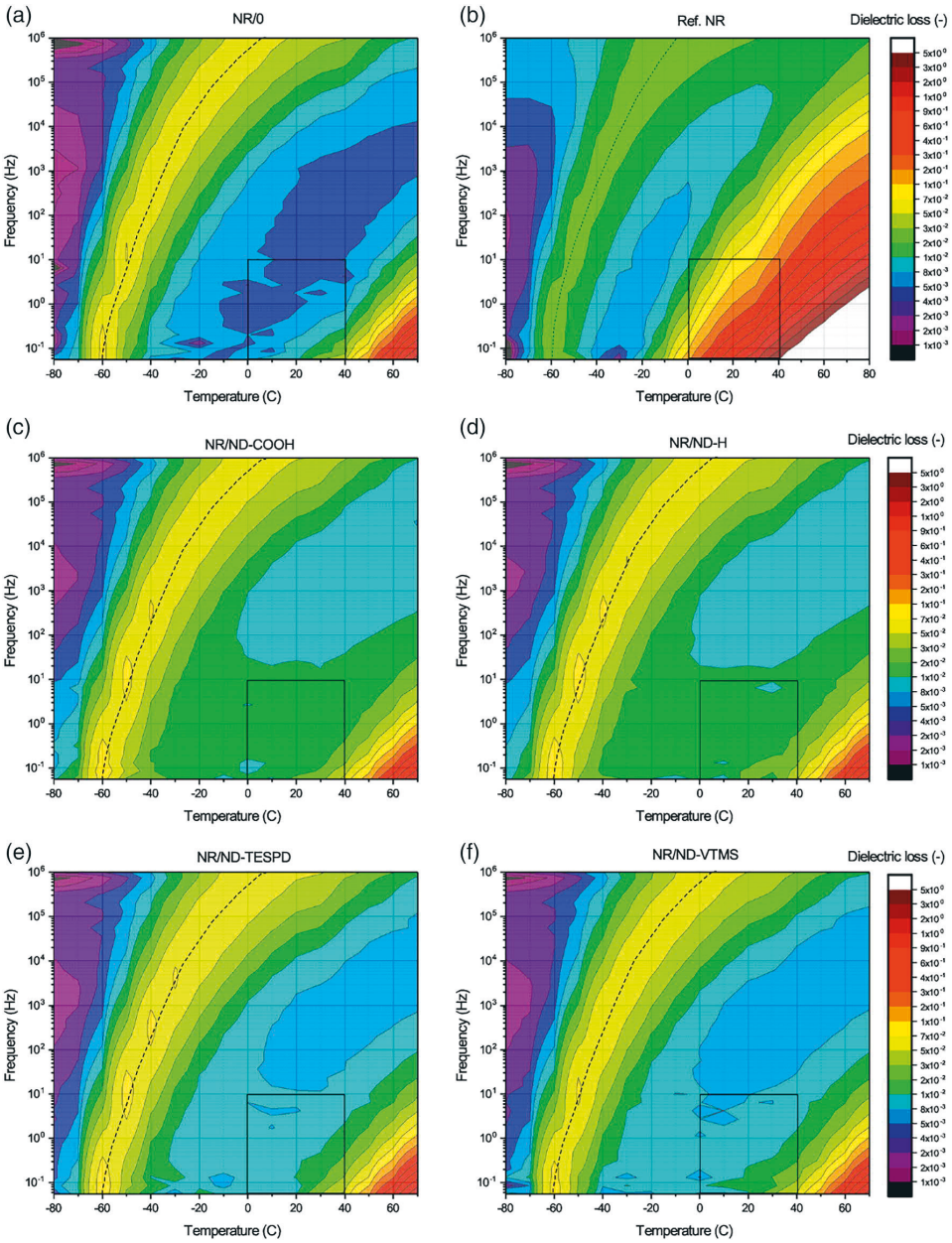

Figure 7. Temperature and frequency dependences of dielectric losses of (a) NR/0, (b) reference NR, (c) NR/ND-COOH, (d) NR/ND-H, (e) NR/ND-TESPD, and (f) NR/ND-VTMS compounds. The frames highlight the area of focus for DEG application, dashed lines corresponds to the maximum of the low temperature relaxation - T_g. [Color figure can be viewed at wileyonlinelibrary.com]

facilitate the dielectric losses through the increase of conductivity contribution,[14] and by the absence of fillers. Among unfilled NR materials, the custom-made NR/0 was confirmed more suitable for a DEG application especially as dielectric loss was lowered from 0.194 (reference NR) to 0.005 at 1 Hz.

When comparing the effect of NDs on dielectric losses of NR [-Figure 6(a)], one could notice the increase in the loss factor in the whole low frequency area. The reason could be in the filler-matrix interface that causes additional relaxation at low frequencies, which can be related to interfacial polarization effect.

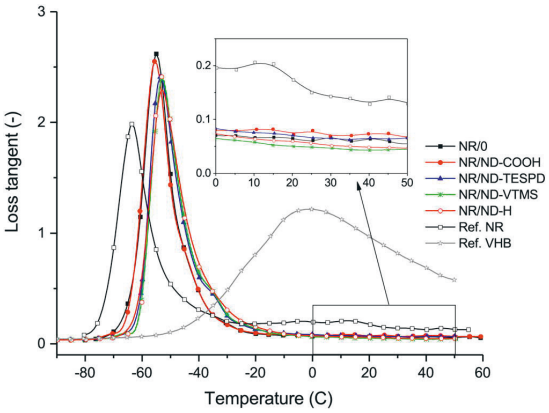

Figure 8. Temperature dependence of mechanical loss tangent (tan δ) of NR/ND composites and reference materials. [Color figure can be viewed at wileyonlinelibrary.com]

Modification of the filler surface resulting in improved interactions at the filler-matrix interface can reduce the dielectric difference between matrix and filler thus decreasing the interfacial effect.[21] For silane modified NDs losses stayed at lower level than for unmodified ND, which was probably due to better interaction between the filler and the polymer, as well as the difference in the volume ratio of fillers. The conductivity contribution overlapping with the interfacial polarization effect at low frequencies was the lowest for NR compounds containing unmodified NDs. The conductivity effect contributing to the dielectric loss is seen from the dielectric loss slope below 1 Hz and from the increased electrical conductivity shown in Figure 6(b). The changes in the conductivity contribution could be explained by the active surface of unmodified NDs and their ability to interfere with ions, which often cause conduction. After the surface modification with silanes, NDs mostly lost this ability. In case of all NR compounds, electrode polarization was not seen in the measured dielectric spectra, as it usually causes high simultaneous increase in losses and permittivity combined with frequency independence of electrical conductivity graph. Electrical AC conductivity of the compound changed only marginally with addition of fillers, as can be seen from Figure 6(b). Finally, the addition of NDs and their functionalization had no significant effect on relative permittivity, and it stayed within 3.2 ± 0.1 range independently of the frequency. The reason for that is a dielectric nature of NDs, as well as small filler amount added to the matrix. Compared to the VHB tape, NR/ND composites showed a little higher dielectric losses at frequencies below 1 Hz, and lower dielectric permittivity.

As no significant changes in the segmental relaxation area above 1 kHz was noticed in the dielectric curves at room temperature, addition of 1 phr of NDs was assumed to have a little effect on the chain mobility of NR. However, in order to have a broader view on the nature of ND effect on dielectric loss, temperature- and frequency-dependent dielectric loss was measured. The mentioned loss properties are presented in Figure 7(a–f), and their representation is based on the projection of 3D plots (Figures S3 to Figure S8). Glass transition temperature (T_g) can be used to study the possible effect of NDs on the chain mobility of NR. T_g determined at the low temperature relaxation peak, also known as α-relaxation, seemed to be same for all custom-made compounds, but the addition of fillers made the relaxation peaks broader. This indicated some molecular motion restriction induced by the filler-matrix interaction. Therefore, the effect on NDs on dielectric loss was not only related to the interaction with the mobile charges but also to the existing interactions between NDs and NR. For reference NR, as seen in Figure 7(b), dielectric losses near T_g peak were lower than for other materials. However, dielectric losses of reference NR increased drastically with increase in temperature and decrease in frequency, which was attributed to the stronger increase in electrical conductivity and interfacial polarization effect, as discussed previously. The increase in losses due to the contribution of the filler interface electrical conductivity was much lower for NR/0 than for reference NR, and even a little less pronounced for the ND-containing compounds. The effect of NDs was seen in generally higher losses, but steadier plateau between −30 and 30 °C at the frequency range of interest (about 0.1–10 Hz). As the plateau covered the large part of the DEG operation range, it could contribute to the stable performance of DEGs. The plateau was located at the lower dielectric loss range for surface modified ND compounds, and showed a little difference between NR/ND-VTMS and NR/ND-TESPD. Therefore, NR/ND-TESPD compound would be the second best choice for a DEG after NR/0 from the dielectric loss point of view.

Next, the mechanical energy dissipation was studied. DMA analysis allows to assess the mechanical damping properties of

Table V. Hysteresis Loss and Stress Relaxation of NR Compounds

	Hysteresis loss at low rate (%)		Hysteresis loss at high rate (%)		Stress loss (%)		
Sample	First cycle	10th cycle	First cycle	10th cycle	After 1 min	After 5 min	After 1 h
NR/0	5.36 ± 0.77	1.57 ± 0.27	10.85 ± 0.44	3.18 ± 0.19	2.40 ± 0.08	3.67 ± 0.02	6.20 ± 0.61
NR/ND-COOH	4.92 ± 0.76	1.12 ± 0.56	9.95 ± 0.67	3.18 ± 0.49	2.05 ± 0.26	3.27 ± 0.26	4.22 ± 0.72
NR/ND-TESPD	5.21 ± 0.40	0.83 ± 0.15	12.46 ± 1.33	4.34 ± 0.77	1.83 ± 0.38	2.98 ± 0.67	4.90 ± 1.56
NR/ND-VTMS	6.67 ± 1.67	1.87 ± 0.76	10.93 ± 0.25	2.71 ± 0.18	1.58 ± 0.40	2.72 ± 0.66	4.11 ± 1.11
NR/ND-H	5.89 ± 1.24	0.76 ± 0.14	11.57 ± 0.12	2.89 ± 0.10	2.00 ± 0.10	3.35 ± 0.23	4.63 ± 0.37
Reference NR	8.07 ± 0.09	3.06 ± 0.19	16.19 ± 0.64	6.73 ± 0.08	2.84 ± 0.16	4.51 ± 0.37	6.99 ± 0.68
VHB	19.54 ± 2.93	12.90 ± 1.34	N/A	N/A	19.23 ± 1.60	28.62 ± 2.89	37.05 ± 4.77

rubbers. Similarly to the dielectric analysis, the DMA loss tangent (tan δ) expresses the ratio of energy lost to energy stored in the cycle and describes energy dissipation. DMA can also be used to assess the effect of NDs to the NR chain dynamics similar to the dielectric analysis. Both techniques confirm marginal changes induced to the molecular motion of NR by the addition of NDs. This small effect of NDs on filler matrix interaction observed in Figure 7 can be seen from Figure 8 as well. There, the addition of ND-COOH shifted the glass transition at the maximum tan δ of NR towards lower temperatures and increased maximum tan δ, while the modified NDs had an opposite effect. Such effect of unmodified NDs has been observed previously and can be explained by a little lower crosslink density and the ability of nanodiamonds to facilitate the rearrangement of elastomer chains under mechanical loading,[41] which was not detected by dielectric analysis due to the absence of mechanical disturbance. This, as well as marginally increased loss tangent at room temperature, implied that no strong interaction was introduced between NR and ND-COOH. Some positive effect of VTMS-modified and hydrogenated NDs on the loss tangent could mean better affinity between the filler and NR. As the tan δ values of all NR compounds were much lower compared to both references NR band and VHB tape, custom-made compounds could perform better in DEGs. In case of VHB, the high loss tangent is expected, as VHB is a very lightly crosslinked material showing a high portion of a viscous flow.[48] Moreover, the glass transition of VHB is much higher than of NR and exhibits a broad tan δ peak spreading up to 50 °C.

The mechanical energy dissipation was studied further by addressing the losses during the stretch-release cycles and the stress relaxation. Due to their viscoelastic nature, rubbers experience hysteresis loss upon cyclic loading. The first several cycles always show higher hysteresis loss due to the Mullins effect related to the slipping and rearrangement of the rubber chains along each other and the filler particles.[25] As shown in Table V, VHB showed the highest hysteresis loss, which can be related to the lack of crosslinking points which could prevent the irreversible flow and rearrangement of the polymer chains upon cyclic loading. In NR samples, differences in the hysteresis loss during the first slow cycles upon addition of NDs were not very pronounced in both low- and high-rate cycles. Small decrease of the hysteresis at first cycle of ND-COOH containing compound was probably related to the induced polymer chain rearrangement, which is consistent with the DMA results at the T_g. Due to the severe stress loss, testing of VHB at higher cyclic rate was not performed. High deviations in hysteresis loss data, especially for NR/ND-TESPD and NR/ND-VTMS, could be indicative of poorer filler dispersion, as also seen from the comparison of low- and high-rate data. No clear trend was seen in hysteresis loss data concerning the addition of NDs. Nevertheless, all the custom-made NR compounds showed significantly lower hysteresis losses than either of the commercial reference materials. In terms of stress relaxation, all compounds filled with NDs showed small reduction is the stress loss, and the effect was especially pronounced for the compounds containing modified NDs. Therefore, custom-made NR compounds containing NDs expected to have high possibility in over-performing VHB and reference NR in energy harvesting performance. NR/ND-VTMS compound showed especially low hysteresis at high rate and stress loss compared to NR/0. The same compound was found most suitable for the energy harvesting, according to its low dielectric losses and tan delta.

CONCLUSIONS

Despite the wide use of 3 M tape in DEGs and its suitable dielectric properties in the low frequency area, its mechanical losses and stress relaxation are so severe that the 3 M tape cannot provide the needed efficiency in energy harvesting. The commercial NR, instead, possesses fair mechanical losses and stress relaxation, but experience high dielectric losses due to increased electrical conductivity. Therefore, custom-made NR composites containing NDs offered a compromise when combining the best features of the abovementioned materials. The custom-made NR materials showed significantly reduced dielectric and mechanical loss properties compared to the commercial materials widely used for energy harvesting. At 1 Hz, custom-made unfilled NR had dielectric loss of only 0.005 compared to the dielectric loss of 0.194 for the reference NR. Silane-modified NDs enabled dielectric loss reduction only up to 0.009 at 1 Hz. Among silane-modified NDs, ND-VTMS filler showed somewhat better properties, as ND-TESPD modification process may need some adjustments due to the thick shell formation. The reduction in stress relaxation and hysteresis loss at high deformation rate was especially pronounced for the custom-made NR containing ND-VTMS – up to 34% and almost 15%, respectively, when compared to the unfilled NR. Such modified NDs also have big potential in reducing the dynamic loss tangent at temperatures above 0 °C, which can be beneficial not only for the energy harvesting, but for other industries.

ACKNOWLEDGMENTS

The study was financially supported by the Tampere University Graduate School. This work made use of Tampere Microscopy Center facilities at Tampere University. The authors are thankful to the Department of Elastomer Technology and Engineering of the University of Twente, Netherlands, for allowing using the tensile testing machine.

REFERENCES

1. Hoffstadt, T.; Graf, C.; Maas, J. *Smart. Mater. Struct.* **2013**, *22*, 094028.
2. Chiba, S.; Waki, M.; Wada, T.; Hirakawa, Y.; Masuda, K.; Ikoma, T. *Appl. Energy*. **2013**, *104*, 497.
3. Kornbluh, R.; Pelrine, R.; Prahlad, H.; Wong-Foy, A.; McCoy, B.; Kim, S.; Eckerle, J.; Low, T. In Electroactivity in Polymeric Materials, Rasmussen, L., Eds.; Springer: US, **2012**; pp. 67–93.
4. Kaltseis, R.; Keplinger, C.; Adrian Koh, S. J.; Baumgartner, R.; Goh, Y. F.; Ng, W. H.; Kogler, A.; Trols, A.; Foo, C. C.; Suo, Z.; Bauer, S. *RSC Adv.* **2014**, *4*, 27905.
5. Ahnert, K.; Abel, M.; Kollosche, M.; Jorgensen, P. J.; Kofod, G. *J. Mater. Chem.* **2011**, *21*, 14492.

6. Jean-Mistral, C.; Beaune, M.; Vu-Cong, T.; Sylvestre, A. *Proc. SPIE 9056*. **2014**, 90561H-1.
7. McKay, T. G.; O'Brien, B. M.; Calius, E. P.; Anderson, I. A. *Appl. Phys. Lett.* **2011**, *98*, 1.
8. Lai, W.; Bastawros, A. F.; Wei Hong; Soon-Jo Chung. Robotics and Automation (ICRA), 2012 IEEE International Conference: Saint Paul, MN, USA, **2012**, 4968–4973.
9. Vertechy, R.; Fontana, M.; Rosati Papini, G.P.; Forehand, D. *Proc. of SPIE*, **2014**, *9056*, 90561G-1.
10. Madsen, F. B.; Daugaard, A. E.; Hvilsted, S.; Skov, A. L. *Macromol. Rapid Commun.* **2016**, *37*, 378.
11. Yu, L.; Skov, A. L. *Int. J. Smart Nano Mater.* **2015**, *6*, 268.
12. Madsen, F. B.; Yu, L.; Daugaard, A. E.; Hvilsted, S.; Skov, A. L. *Polymer*. **2014**, *55*, 6212.
13. Madsen, P. J.; Yu, L.; Boucher, S.; Skov, A. L. *RSC Adv.* **2018**, *8*, 23077.
14. Hernandez, M.; Ezquerra, T. A.; Verdejo, R.; Lopez-Manchado, M. A. *Macromolecules*. **2012**, *45*, 1070.
15. Ortiz-Serna, P.; Diaz-Calleja, R.; Sanchis, M. J.; Floudas, G.; Nunes, R. C.; Martins, A. F.; Visconte, L. L. *Macromolecules*. **2010**, *43*, 5094.
16. Huang, Y.; Schadler, L. S. *Compos. Sci. Technol.* **2017**, *142*, 91.
17. Hernandez, M.; Lopez-Manchado, M. A.; Sanz, A.; Nogales, A.; Ezquerra, T. A. *Macromolecules*. **2011**, *44*, 6574.
18. Koh, S. J. A.; Zhao, X.; Suo, Z. *Appl. Phys. Lett.* **2009**, *94*, 1.
19. Chiba, S.; Kornbluh, R.; Pelrine, R.; Waki, M. In 18th World Hydrogen Energy Conference 2010, Proceedings of the WHEC, 2010, Essen, **2010**, 22–30.
20. Hernandez, M.; Carretero-Gonzalez, J.; Verdejo, R.; Ezquerra, T. A.; Lopez-Manchado, M. A. *Macromolecules*. **2010**, *43*, 643.
21. Romasanta, L. J.; Hernandez, M.; Lopez-Manchado, M. A.; Verdejo, R. *Nanoscale Res. Lett.* **2011**, *6*, 1.
22. Schönhals, A.; Kremer, F. Analysis of dielectric spectra. In Broadband Dielectric Spectroscopy; Kremer, F.; Schönhals, A., Eds., Springer: Berlin, Heidelberg, **2003**. p. 59.
23. Dolmatov, V. *J Superhard Mater.* **2007**, *29*, 199.
24. Shakun, A.; Poikelispää, M.; Das, A.; Vuorinen, J. *Polym. Eng. Sci.* **2018**, *58*, 395.
25. Mokhireva, K. A.; Svistkov, A. L.; Solod'ko, V. N.; Komar, L. A.; Stöckelhuber, K. W. *Polym. Test.* **2017**, *59*, 46.
26. Krueger, A.; Ozawa, M.; Jarre, G.; Liang, Y.; Stegk, J.; Lu, L. *Phys. Status Solidi A*. **2007**, *204*, 2881.
27. Duffy, E.; Mitev, D. P.; Thickett, S. C.; Townsend, A. T.; Paull, B.; Nesterenko, P. N. *Appl. Surf. Sci.* **2015**, *357*, 397.
28. Hajiali, F.; Shojaei, A. *Colloids Surf. A Physicochem. Eng. Asp.* **2016**, *506*, 254.
29. Tiwari, M.; Datta, R. N.; Talma, A. G.; Noordermeer, J. W. M.; Dierkes, W. K.; van Ooij, W. J. *Rubber Chem. Technol.* **2009**, *82*, 473.
30. Stehlik, S.; Glatzel, T.; Pichot, V.; Pawlak, R.; Meyer, E.; Spitzer, D.; Rezek, B. *Diamond Relat. Mater.* **2016**, *63*, 97.
31. Al-Oweini, R.; El-Rassy, H. *J. Mol. Struct.* **2009**, *919*, 140.
32. El-Nahhal, I. M.; Salem, J. K.; Kuhn, S.; Hammad, T.; Hempelmann, R.; Al Bhaisi, S. *Powder Technol.* **2016**, *287*, 439.
33. Post, P.; Wurlitzer, L.; Maus-Friedrichs, W.; Weber, P. A. *Nanomaterials* **2018**, 8, 530–1-19.
34. Coates, J. In Encyclopedia of Analytical Chemistry; Meyers, R., Ed., John Wiley & Sons Ltd: New York, **2006**.
35. Zhang, Y.; Park, S. *Polym. Compos.* **2018**, *39*, 3472.
36. Haddadi, S. A.; S.A., A. R.; Amini, M.; Kheradmand, A. *Mater. Today Commun.* **2018**, *14*, 53.
37. Efremov, V. P.; Zakatilova, E. I.; Maklashova, I. V.; Shevchenko, N. V. *J. Phys.: Conf. Ser.* **2018**, *946*, 012107–1–8.
38. Rabiei, S.; Shojaei, A. *Eur. Polym. J.* **2016**, *81*, 98.
39. Poikelispää, M.; Das, A.; Dierkes, W.; Vuorinen, J. *J. Elastomers Plast.* **2015**, *47*, 738.
40. Castano, V. In Carbon Nanotubes; Velasco-Santos, C.; Yellampalli, S., Eds., InTech: Rijeka, **2011**.
41. Dolmatov, V. *J. Superhard Mater.* **2007**, *29*, 65.
42. Brochu, P.; Pei, Q. *Macromol. Rapid Commun.* **2010**, *31*, 10.
43. Vu-Cong, T.; Jean-Mistral, C.; Sylvestre, A. *Smart Mater Struct* **2012**, *21*, 105036–1-10.
44. McKay, T.,. G.; Calius, E.; Anderson, I.,. A. *Proc. SPIE*. **2009**, *7287*, 72870P.
45. Samet, M.; Levchenko, V.; Boiteux, G.; Seytre, G.; Kallel, A.; Serghei, A. *J. Chem. Phys.* **2015**, *142*, 1.
46. Arruti, P.; Kortaberria, G.; Jimeno, A.; Tercjak, A.; Blanco, M.; Mondragon, I. In Biopolymers and Nanocomposites as Studied by Dielectric Spectroscopy; Kortaberria, G., Ed., Transworld Research Network: Trivandrum, **2009**. p. 97.
47. Shakun, A.; Sarlin, E.; Vuorinen, J. *Int. J. Exergy*. **2018**, *26*, 170.
48. Pelrine, R.; Kornbluh, R.; Pei, Q.; Joseph, J. *Science*. **2000**, *287*, 836.

PUBLICATION IV

Influence of Surface Modified Nanodiamonds on Dielectric and Mechanical Properties of Silicone Composites

A. Shakun, R. Anyszka, E. Sarlin, A. Blume, J. Vuorinen

Polymers (2019) Vol. 11, No. 7, pp. 1104-1118
https://doi.org/10.3390/polym11071104
Supplementary information available online

polymers

MDPI

Article

Influence of Surface Modified Nanodiamonds on Dielectric and Mechanical Properties of Silicone Composites

Alexandra Shakun [1,*], Rafal Anyszka [2,3], Essi Sarlin [1], Anke Blume [2] and Jyrki Vuorinen [1]

[1] Materials Science and Environmental Engineering, Tampere University, P.O. Box 589, FI-33014 Tampere, Finland
[2] Elastomer Technology and Engineering, University of Twente, P.O. Box 217, 7500 AE Enschede, The Netherlands
[3] Institute of Polymer and Dye Technology, Lodz University of Technology, Stefanowskiego 12/16, 90-924 Lodz, Poland
* Correspondence: alexandra.shakun@tuni.fi

Received: 11 June 2019; Accepted: 27 June 2019; Published: 29 June 2019

Abstract: Detonation nanodiamonds, also known as ultradispersed diamonds, possess versatile chemically active surfaces, which can be adjusted to improve their interaction with elastomers. Such improvements can result in decreased dielectric and viscous losses of the composites without compromising other in-rubber properties, thus making the composites suitable for new demanding applications, such as energy harvesting. However, in most cases, surface modification of nanodiamonds requires the use of strong chemicals and high temperatures. The present study offers a less time-consuming functionalization method at 40 °C via reaction between the epoxy-rings of the modifier and carboxylic groups at the nanodiamond surface. This allows decorating the nanodiamond surface with chemical groups that are able to participate in the crosslinking reaction, thus creating strong interaction between filler and elastomer. Addition of 0.1 phr (parts per hundred rubber) of modified nanodiamonds into the silicone matrix results in about fivefold decreased electric losses at 1 Hz due to a reduced conductivity. Moreover, the mechanical hysteresis loss is reduced more than 50% and dynamic loss tangent at ambient temperature is lowered. Therefore, such materials are recommended for the dielectric energy harvesting application, and they are expected to increase its efficiency.

Keywords: nanodiamonds; surface modification; silicone; dielectric spectroscopy

1. Introduction

Detonation-produced nanodiamonds (NDs), also named ultradispersed diamonds (UDDs), are known for their superior mechanical properties, low electrical conductivity, high thermal conductivity and a highly reactive surface. Single ND particles are about 5 nm in diameter consisting of a sp^3-carbon core, less than 1 nm thick sp^2–carbon transitional layer and an active surface [1]. The surface of a pristine ND is hydrophilic and mostly contains carboxyls, hydroxyls, lactones, ketones and ethers, but it can be modified and homogenized through a large number of methods [2]. However, due to the presence of carboxyl- and hydroxyl- groups, NDs form strong aggregates and agglomerates, which are difficult to break down, thus affecting the dispersability of NDs. Further surface modification allows introducing complex moieties onto the ND surface and could decrease interactions between the ND particles.

NDs are mostly applied for biomedical, electronic, and tribology applications and in different polymer-based composites [3–5]. Moreover, NDs have shown an ability to reduce dielectric losses in

some elastomeric matrices [6,7], which can be used for the dielectric energy harvesting. Dielectric energy harvesters can provide sustainable energy from the ambient sources, such as ocean waves [8–12] and human motion [13,14], but their efficiency and economic profitability is dependent, among others, on the material-related losses of the elastomeric membrane. Silicone rubber is often used for dielectric energy harvesting, as it possesses low dielectric losses, low mechanical hysteresis, dynamic damping and stress relaxation [15,16]. However, a modification of the material is needed in order to increase the economic profitability of elastomer-based energy harvesters [17]. A modification of the silicone matrix by covalent attachment of various molecules can not only improve mechanical properties of the material, but also result in lower dielectric losses and better electrical breakdown resistance in dielectric elastomer transducers [16]. Therefore, it is expected that the introduction of NDs into a silicone matrix improves the physical and chemical interactions within the matrix. Furthermore, the introduction of surface modified ND particles is expected to reduce the dielectric and mechanical losses of the composite further and increase its potential in energy harvesting.

Similar to other nanomaterials, the fabrication of ND-elastomer composites is associated with some challenges. They can be related to the poor ND-elastomer interactions and the strong agglomeration of NDs, resulting in poor dispersion and reduced composite strength. Due to the high surface energy of NDs, breaking up ND aggregates into primary particles cannot be achieved by direct ultrasound processing [18]. Moreover, a direct mixing of the ND powder into the polymer results in filler agglomeration and inadequate dispersion [19–21]. The situation can be improved by surface functionalization of NDs. A treatment with silanes creates a hydrophobic ND surface and, therefore, improves the dispersion of NDs in nonpolar organic media. If a vinyl-containing silane is used, it is reported that the dispersion is improved both in nonpolar and polar organic media [22]. However, an increase in the agglomerate size can be observed after silanization due to the condensation reaction between treated particles [23] or a self-condensation of the silane [24]. Owing to the self-condensation reaction, a siloxane shell is formed around the ND particle, which can further bond particles into very large aggregates. Basic conditions and elevated temperature facilitate the condensation of silanol groups [25]. A minimum condensation rate for tri-, di- and monosilanols can be achieved at pH 4, pH 6 and pH 6.5–7, respectively, which allows minimizing the siloxane shell formation [26].

Although NDs are considered easily reactive compared to other carbon materials, their surface modification often requires several steps, strong chemicals and/or high temperatures [27]. For example, the traditional route of ND functionalization often includes a reduction of a pristine ND surface to hydroxyl-groups followed by introduction of amine groups, e.g., by silanization, which is followed by further modifications [28,29]. Thus, more simple and low temperature surface modification methods designed for improved interaction with hydrophobic polymeric matrices are in demand.

A direct functionalization of carboxylated NDs with a vinyl-containing silane has been reported in the work of Hajiali et al. [30], and a possibility of such reaction was mentioned in the latest review of Zhang et al. [3]. However, no strong evidence has been provided for the existence of ND-silane bonds as the result of such modification. The goal of the modification was to create polysiloxane shell on ND surface. A polysiloxane coating is usually achieved through a Stöber process, which involves a silane hydrolysis in basic conditions followed by the reaction between hydrolyzed silane and hydroxyl groups on the ND surface and further polycondensation via creation of Si–O–Si bonds [31]. When ND surface contains –COOH groups instead of –OH groups, a hydrolyzed silane is more likely to react with OH-group of other silane molecules rather than with the –COOH group of the ND. Therefore, a probability of the reaction between carboxylated nanodiamond and hydrolyzed silane needs to be evaluated. Another direct functionalization of carboxylated NDs through the reaction with the epoxy group can be applied [24,32] based on the esterification reaction discussed in the literature [33,34]. However, such modification has been performed on NDs at 140 °C, which is still relatively high temperature.

The aim of the present study was to covalently attach the ND filler to the silicone matrix and promote the interaction between carboxylated NDs and the silicone matrix. Covalent bonding is

achieved by decorating NDs with vinyl- groups, which are able to participate in the curing process, and the compatibility with the matrix is improved by introducing alkoxysilanes to the ND surface. Here, two different routes of surface modification of carboxylated NDs are discussed: through silanization with a silane coupling agent and esterification reaction with a modifier containing an epoxy-group. In the study, the probability of ND-silane bond formation is argued in case of carboxylated diamond, but a simple and efficient method of ND surface modification was offered via reaction with an epoxy-group of the modifying agent at 40 °C. Furthermore, the effectiveness of modified NDs in lowering dielectric and viscoelastic losses of silicone composites is discussed. The present study indicates that the application of surface-modified NDs can be beneficial for the dielectric energy harvesting application and could potentially increase the efficiency of dielectric energy generators.

2. Materials and Methods

2.1. Materials

The study utilized NDs with carboxylated surface (uDiamond Molto Vox, Carbodeon Oy, Vantaa, Finland). According to the supplier, single ND particles are 4.2 nm in size and have an aspect ratio close to 1. According to the particle size distribution measurement conducted by the supplier, agglomerated NDs have a median size of 2.6 μm. The specific surface area of NDs is 330 m^2/g. More information about the properties of NDs is provided in Table S1. Vinyltrimethoxysilane (referred as VTMS, Sigma Aldrich, St. Louis, MO, USA) as well as 1,2-epoxy-9-decene (referred as ED, abcr GmbH, Karlsruhe, Germany) and 3-glycidoxypropyltrimethoxysilane (referred as GOPTMS, abcr GmbH, Karlsruhe, Germany) were used as surface modifiers. Structures of the used surface modifiers are shown in Figure S1. Glacial acetic acid (Sigma Aldrich) was used for the pH adjustment of the silanization reaction. The composites were prepared using two-component room temperature curable silicone (polydimethylsiloxane—PDMS) with Pt catalyst (Elastosil 601 RT, Wacker Munich, Germany) and 10 phr (parts per hundred rubber) of silicone oil (Rhodorsil 47 V 50, Solvay, Brussels, Belgium).

2.2. Nanodiamond Treatment

As-received, carboxylated NDs were oxidized in air at 425 °C for 4 h. Such thermal treatment is expected to increase the amount of surface carboxyl groups available for the further modification by oxidizing the existing oxygen-containing groups, such as lactones. The amount of oxygen-containing surface groups was determined by Boehm titration performed according to the procedure described elsewhere [35]. The total amount of the surface groups, which can be identified by the Boehm titration, was determined by the reaction with NaOH. The number of carboxylic groups—by the reaction with $NaHCO_3$, lactones—from the difference between NaOH and $NaHCO_3$ tests, and the number of phenolic groups from the difference between Na_2CO_3 and $NaHCO_3$ reacted with the functional groups of the carbon material

For the ED-based modification, 0.3 g of oxidized NDs were placed into a three-neck flask, dispersed in 80 mL toluene and brought to a constant temperature (40 °C or 100 °C). After temperature stabilization, ED was added slowly in excess molar amount (5:1 based on the amount of surface carboxyl groups on NDs). The reaction was allowed to proceed for 24 h, followed by filtration and washing with toluene. The obtained fillers were further purified in a Soxhlet extractor with toluene for 24 h and dried in an air-ventilated oven at 120 °C for 12 h. The modification of NDs with GOPTMS was performed at 40 °C following the same procedure as for ED.

The VTMS modification was performed as described in [30], with ND to silane mass ratio of 1 to 5, washed with acetone, filtered, purified in Soxhlet extractor with toluene and dried in oven for 24 h at 120 °C. In order to understand the probability of the reaction between the carboxylic groups of ND and the silanol groups of the modifier, additional surface modifications were performed with monoalkoxysilanes (vinyldimethylethoxysilane and octadecyldimethylmethoxysilane) following the same procedure as for VTMS. Monoalkoxysilanes have only one reactive site and cannot form a shell

around NDs. Therefore, the presence of these silanes on the ND surface indicates that the reaction between carboxylic- and silanol- groups is possible. When a condensation reaction occurs between two silane molecules, the resulting molecule cannot attach to the ND surface, and it is removed by the following filtration. Vinyldimethylethoxysilane was chosen due to its similarity to VDMS. However, the characteristic FTIR peak of a vinyl- group is often small, and it could remain unnoticed. Therefore, octadecyldimethylmethoxysilane was chosen as the second modifiers due to the distinctive FTIR peak of a long aliphatic chain that could identify the presence of the modifier on the ND surface. The details are provided in the Supplementary Information.

2.3. Composite Preparation

For the preparation of ND-PDMS composites, ND powder was dispersed in silicone oil by ultrasonication (FinnSonic m03) for 30 min at room temperature. NDs were used in 0.1 or 1 phr amounts. ND-containing oil was then added to the part A of a two-component silicone containing the catalyst and stirred for 5 min, then combined with part B silicone containing the crosslinker and stirred for another 2 min. The material was poured into molds to form both 1 mm and 0.5 mm thick sheets, and then degassed in vacuum for 30 min to eliminate air bubbles.

2.4. Characterization

Dielectric properties of 0.5 mm thick PDMS samples were measured with a Novocontrol Alpha-A dielectric analyzer at room temperature in a frequency range of $5{\cdot}10^{-2}$–10^{6} Hz using gold-plated electrodes (20 mm in diameter). The average value of minimum three specimens was reported for each sample. Between the measurements, the samples were stored in the darkness at room temperature. Dynamic mechanical analysis (DMA), stress relaxation and cyclic loading of the samples were performed with Pyris Diamond DMA (Perkin Elmer, Waltham, MA, USA) using the 1 mm thick samples. DMA samples were measured in the tension mode at 1 Hz with 20 µm displacement amplitude and 3 °C/min heating rate. For the stress relaxation measurement, samples were stretched to 10% and the change in force was recorded. The tensile cyclic loading was performed at ambient conditions at 6 mm/min rate for 10 mm test samples with a maximum elongation at 45 ± 1%. The hysteresis loss was calculated by subtracting the integrated loading and unloading curves and dividing the value by the area under the corresponding loading curves. Determination of moduli (stress at certain percent elongation) was performed on Messphysik Midi 10-20 universal tester equipped with a contact long-travel extensometer (MFE, Mess- & Feinwerktechnik GmbH, Velbert, Germany) at 200 mm/min rate. ISO 37 dumb-bell specimen type 3 with 10 mm test length and about 1 mm thickness were used in the test. The average value of three specimen was reported.

Fourier transform infrared spectra (FTIR) was obtained from the NDs with Bruker Tensor 27 in the attenuated total reflectance (ATR) mode in the range from 500 to 4000 cm^{-1} with a diamond crystal background and 4 cm^{-1} resolution. The ND powders were studied with a scanning electron microscope (SEM, Zeiss ULTRAplus, Oberkochen, Germany) equipped with an energy dispersive X-ray spectroscopy detector (EDS, Oxford Instruments X-MaxN 80, Abingdon, UK). The samples were coated with a thin carbon layer to prevent charging during SEM analysis. In the EDS analysis, the average of two-point measurements were reported. Thermogravimetric (TGA) data was obtained from the NDs with TG 209 F3 Tarsus (Netzsch, Selb, Germany) in nitrogen flow. The samples were kept at 125 °C for 30 min to remove loosely bound water and then heated to 850 °C with 20 K/min rate. The effect of NDs on the crystallinity of the PDMS was studied by means of differential scanning calorimetry (DSC) with DSC 214 Polyma (Netzsch) in N2 flow with 10 K/min heating/cooling rate. The degree of crystallinity was calculated by the DSC Proteus Analysis software based on the equation:

$$\% \text{ Crystallinity} = \frac{\Delta H_m - \Delta H_c}{\Delta H_m^{\circ}} \times 100\%, \quad (1)$$

where ΔH_m is the heat of melting, ΔH_c is the heat of cold crystallization and ΔH_m° is the heat of melting of a 100% crystalline polymer.

The apparent crosslink density (1/Q) of the PDMS was calculated for the 1 × 1 cm samples immersed in toluene in closed vessels for 72 h based on the equation [36]:

$$1/Q = 1/\left(\frac{m_s - m_d}{m_0}\right)\frac{F}{100}, \quad (2)$$

where m_s and m_d are the weight of the swollen and dried specimen, respectively, m_o is the initial weight of the specimen, and F is formula weight in phr. Toluene was renewed every 24 h during the measurement. Three parallel samples were used.

ND powder samples were designated as ND- "surface modifier abbreviation", for example, ND-VTMS. The PDMS sample without additives was designated as PDMS/0, and PDMS with 10 phr silicone oil - as PDMS_oil/0. In case of a ND filler addition, samples were marked as PDMS/"ND modifier type"_"phr amount", for example, PDMS_oil/VTMS_1.

3. Results and Discussion

3.1. Surface Modification of Nanodiamonds

An additional oxidation in air at 425 °C can be employed in order to increase the number of oxygen-containing groups, especially –COOH, on a ND surface [37,38]. During the treatment, ketones, aldehydes, and esters on the ND surface are converted into carboxylic acids, anhydrides, or cyclic ketones. Moreover, some sp^2 carbon is removed from the surface giving an access to the formation of oxygen-containing groups. The amount and type of oxygen-containing groups on the ND surface before and after oxidation is shown in Table 1. As the result of the oxidation treatment, the total amount of oxygen-containing groups was virtually unchanged, but the amount of carboxyl groups increased 2.5-fold. Such results are probably achieved by the oxidation of lactone groups and creation of new carboxyl-groups upon removal of few surface sp^2 carbon layers. Based on the titration results oxidized NDs were selected for further modification. Furthermore, the concentration of surface carboxylic groups was used to calculate the amount of the reagents.

Table 1. Oxygen-containing groups on nanodiamond (ND) surface determined by Boehm titration method.

	Surface Groups, mmol/g			
	Carboxyl	**Lactone**	**Phenolic**	**All Surface Groups**
ND reference	0.131	0.101	0.219	0.451
ND oxidized	0.329	0.018	0.127	0.475

The modification of the ND surface with vinyltrimethoxysilane (VTMS) was performed according to the procedure described in the literature [30]. However, a different mechanism of the reaction is suggested, as shown in Figure 1. During the reaction A, methoxy- groups were hydrolyzed and acetic acid was added to prevent a condensation. The suggested reaction B between the carboxylic and silanol groups was unlikely to proceed, which was confirmed by the use of silanes containing single silanol group, as seen from FTIR spectra and TGA curves depicted in Figures S2 and S3, where no additional peaks appeared. At higher temperature, the shell formation by silanol condensation was proceeded according to the reaction C, but a possibility of the reaction between carboxylic and silanol groups was not fully excluded.

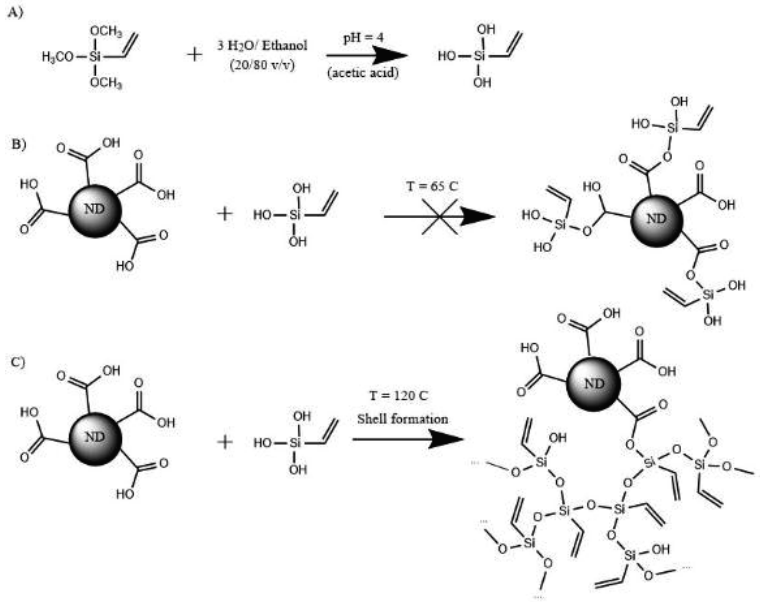

Figure 1. Modification process of carboxylated nanodiamonds (ND) by vinyltrimethoxysilane.

According to the literature, the reaction between epoxy and carboxyl-group is possible without a catalyst [34]. The probable reactions between carboxylated ND and 1,2-epoxy-9-decene (ED) are shown in Figure 2. Depending on the ring-opening mechanism, two different reaction products can appear. At high temperatures and acidic conditions, the products of the reaction A are prone to bond to ND-COOH via reaction B. In order to maximize the probability of the reaction A between ND-COOH and an epoxy-group, the reaction was performed in toluene at 40 °C and compared to the reaction at 100 °C in terms of the resulting ND surface functionalization. The resulting NDs modified with ED at 40 °C and 100 °C are designated as ND-ED(40C) and ND-ED(100C) respectively. The hydrolyzed epoxy compound and unreacted components were eliminated by filtration and purification stage. It was expected that at 40 °C the reactions A and C occur most probably, while higher temperature would result in more reaction B products and hydrolysis of the epoxy compound as the reaction proceeded. As the excess of ED was used, reaction D was also expected at higher temperature (100 °C).

The reaction between ND and GOPTMS was assumed to follow the same mechanism as for ED, as the direct reaction between carboxyl and silanol was found unlikely, especially at 40 °C (Figure 1, reaction B). Due to the steric effect, type A reaction was expected to be dominant. Moreover, as some water molecules could be present in the system, a condensation of silanol groups could occur upon purification and drying at elevated temperatures.

In the FTIR spectra in Figure 3, oxidized NDs (ND-COOH) show characteristic carbonyl peaks around 1780 cm^{-1} and 1300–900 cm^{-1} as a combination of overlapping peaks from multiple oxygen-containing groups [39]. The same peaks are present in all modified materials, but epoxy-modified materials have more pronounced carbonyl peaks. The presence of the –OH group could be specified at 3100–3600 cm^{-1} (stretching) and 1625 cm^{-1} (bending). All modified fillers have an indication of CH_2 groups due to peaks at 2860–2930 cm^{-1} and 1408/1453 cm^{-1}.

In the VTMS-modified ND spectrum shown in Figure 3a, a broad peak appeared at 1020 cm^{-1} with a shoulder up to 1110 cm^{-1}, corresponding to the overlapping Si–O–Si and Si–C bonds respectively. The appearance of Si-O-Si bonds is a result of the condensation of silanol groups. The intensity of the peaks suggests an extensive shell formation around ND clusters. Peaks at 1275 cm^{-1} corresponds to a Si–C stretching, and the broad peak around 1745 cm^{-1} to the C=O stretch. The broadening at

3200–3400 cm^{-1} confirms the presence of –OH groups and could be an indication of bound water. Peaks at 3062 cm^{-1} and 1601 cm^{-1} appear due to the C=C bond of the vinyl group, and the peak at 750 cm^{-1} – due to the C–H bend of the same group. GOPTMS-modified NDs shown in Figure 3a have distinctive peaks for Si–C bond at 1267 and 1098 cm^{-1} with a broadening towards 1050 cm^{-1}, which indicates the presence of Si–O bonds.

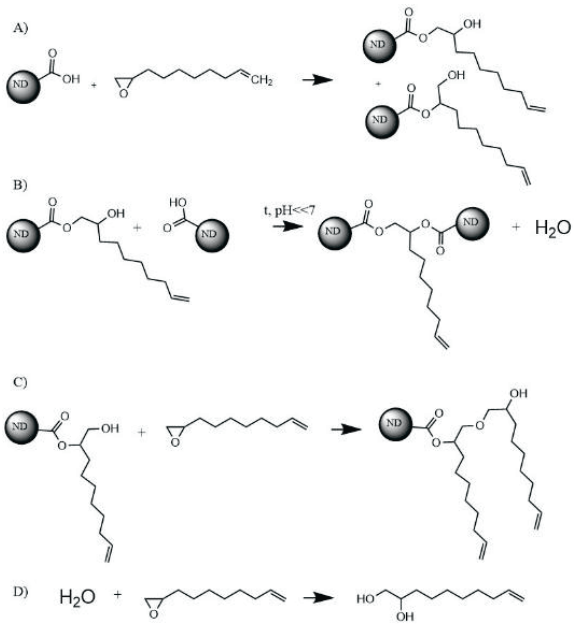

Figure 2. Possible reactions between 1,2-epoxy-9-decene and carboxylated ND (only one carboxyl-group is depicted for clarity).

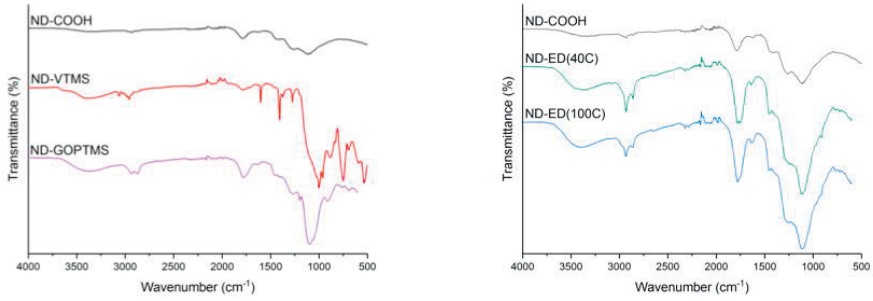

(**a**) (**b**)

Figure 3. FTIR spectra of NDs modified with: (**a**) silanes; (**b**) 1,2-epoxy-9-decene at different reaction temperatures. Spectra are vertically shifted for clarity.

The FTIR-spectra of ED-modified NDs shown in Figure 3b in comparison to ND-COOH. ND-ED(40C) and ND-ED(100C) spectra were almost identical to one another, except the small peak at 3080 cm^{-1} which is related to the vinyl group. This is more pronounced for the ND-ED(40C) than for the ND-ED(100C). Moreover, ND-ED(40C) had double peaks corresponding to the different antisymmetrically coupled C=O stretches (1780 cm^{-1} and 1750 cm^{-1}), which could indicate two different reaction A products in epoxy-modification.

According to [39,40], oxidized NDs have shown freely bound water release up to 120 °C and strongly bound water till 200–300 °C, but according to the TGA data shown in Figure 4, ND-COOH experienced no significant mass loss at the mentioned temperatures. Only ND-VTMS and ND-ED(40C) samples show 1% and 0.6% mass loss respectively during the dehydration step indicating the presence of water or solvent residues. When heated above 600 °C in inert atmosphere, unmodified ND first loses its oxygen-containing groups and then undergoes graphitization and sintering above 800 °C resulting in a mass loss up to 10–20% [41], which was observed also in the present study. Among the modified samples, only ND-VTMS has the same onset temperature for the release of strongly bound oxygen-containing groups, while the onset of others shifts to higher temperatures. This finding can indicate that the ND surface was not altered by the VTMS treatment, but a siloxane shell was formed around it.

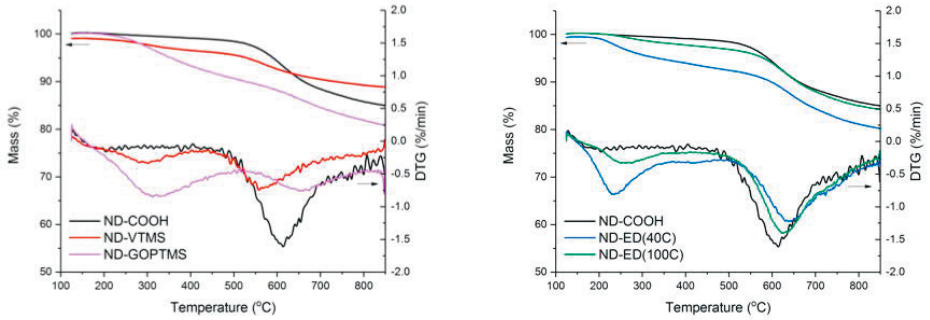

(**a**) (**b**)

Figure 4. Thermogravimetric (TGA) mass loss and decomposition rate curves of NDs modified with: (**a**) silanes; (**b**) 1,2-epoxy-9-decene, at different reaction temperatures.

Unlike ND-COOH, all modified samples show a mass loss in the range of 200–360 °C related to the decomposition of organic groups attached upon modification. The residual mass of a ND-VTMS sample, shown in Figure 4a, is higher than of a ND-COOH sample due to the higher silicon oxide content. Differences in TGA curves of the ED-modified samples are minor, as seen in Figure 4b. The ND-ED(40C) sample seems to have more organic groups attached to the ND, as could be suggested from the proposed reactions A and C (Figure 2). A lower modification temperature and probably more developed surface containing vinyl groups made ND-ED(40C) a good candidate for the further use in PDMS composites. Due to the higher modification temperature and potentially lower vinyl- group content, ND-ED(100C) was not used in PDMS composites.

The elemental analysis by EDS, presented in Table 2, confirms that the new elements were introduced to the fillers upon modification, and the ratio of the elements was changed. Exceptionally high silicon and oxygen content in ND-VTMS confirmed the extensive shell formation. The presence of a similar shell in the ND-GOPTMS sample is unlikely, as both the Si content and the Si:O ratio was low. The reaction of the epoxy- group with the ND surface is probably much more pronounced and thus the GOPTMS molecule is bounded to the surface and less likely to condense due to restricted mobility. The SEM images of ND powders shown in Figure 5 revealed that all the modified NDs are more agglomerated, and they show a broader range of particle sizes than the initial ND-COOH. Among the modified fillers, ND-VTMS samples have the largest agglomerates, which could be related to the silanol condensation and shell formation around the ND clusters.

Table 2. Energy dispersive X-ray spectroscopy detector (EDS) analysis of filler particles.

Sample	Element Content, %			
	C	O	Si	Others
ND-COOH	96.0	3.2	-	<1
ND-VTMS	54.6	18.0	27.3	<1
ND-ED(40C)	96.0	4.0	-	-
ND-GOPTMS	90.8	6.6	2.6	-

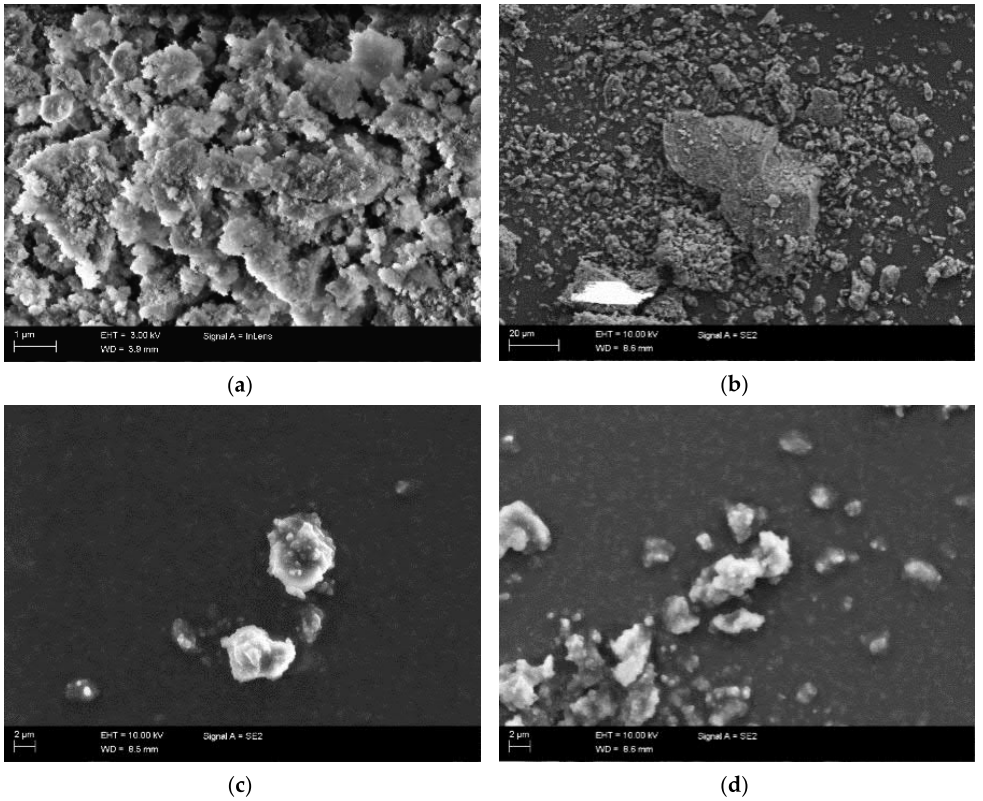

(**a**) (**b**)

(**c**) (**d**)

Figure 5. SEM images of ND powders: (**a**) ND-COOH; (**b**) ND-VTMS; (**c**) ND-ED(40C); (**d**) ND-GOPTMS.

3.2. Nanodiamond-Silicone Composites

Silicon oil added to the two-component PDMS served as the dispersion media for the NDs. This method helps to avoid common problems with solvent-based dispersion. The effect of oil addition and ND modification on dielectric properties of ND-silicone composites was studied with the focus on dielectric losses. As shown in Figure 6a, no significant difference is found between the non-plasticized PDMS/0 and plasticized PDMS_oil/0. However, the addition of 0.1 phr NDs results in reduced dielectric losses below 10 Hz. For example, the dielectric loss of PDMS_oil/ED_0.1 is $3.6 \cdot 10^{-3}$ at 1 Hz, which is about 5 times lower than of PDMS_oil/0. This effect can be related to the reduction of a DC-conductivity effect, which can be seen from the linear slope of the loss curve at low frequency area and from the frequency-independent part of the conductivity curve in Figure 6b. Such losses may be related to the impurities and mobile ions within the matrix that could be trapped and demobilized on the filler surface. For the PDMS_oil/COOH_0.1 sample, an additional broad relaxation peak is visible around a

frequency of 10 Hz. Such relaxation was related to the Maxwell-Wagner polarization appearing due to the permittivity and conductivity differences at the matrix-filler interface. As this interfacial relaxation is less pronounced for the modified ND samples, a stronger filler-matrix bond and a more uniform interface is suggested as explanation for this phenomenon. The shape of the curve and positions of the relaxation peaks of PDMS_oil/VTMS_0.1 are very similar to PDMS_oil/ED_0.1, and they lead to decreased dielectric losses four- and fivefold respectively when compared to PDMS_oil/0. Finally, the samples PDMS_oil/COOH, PDMS_oil/ED and PDMS_oil/GOPTMS were selected for further testing due to the differences in their dielectric behavior at the frequencies below 10 Hz.

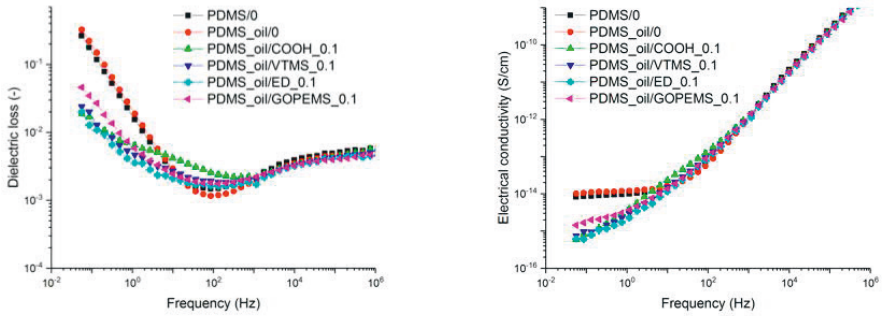

(**a**) (**b**)

Figure 6. (**a**) Dielectric loss and (**b**) AC electrical conductivity of PDMS samples containing 0.1 phr NDs.

When the filler amount was increased to 1 phr, an interfacial polarization becomes visible also in PDMS_oil/ED_1 and PDMS_oil/GOPTMS_1 samples (Figure 7b). Nevertheless, it is lower than for the PDMS/COOH_1 sample, which shows a very distinctive broad loss peak around 2 Hz. According to the Figure 7b, the addition of 1 phr of fillers results in a more linear AC conductivity curve, which implies that the reduction of losses is related to the conductivity effect. However, due to the stronger interfacial polarization that increased the losses at low frequencies of the mentioned compounds, it was decided to focus on the 0.1 phr composites, which are also preferable from the economical point of view due to comparably high costs of the nanofillers.

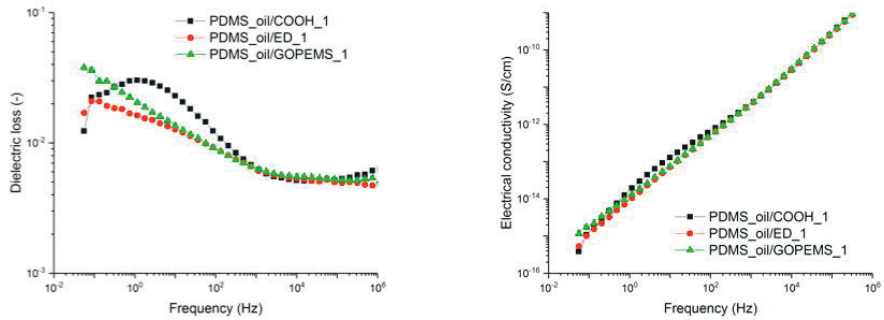

(**a**) (**b**)

Figure 7. (**a**) Dielectric loss and (**b**) AC electrical conductivity of PDMS samples containing 1 phr NDs.

Next, as the dielectric loss may change with time [42], the dielectric loss spectra of the samples were measured at different periods of time after curing. According to Figure 8a, the time affects the dielectric loss of PDMS_oil/0 by a small decrease of the relaxation peak around 0.1 MHz and a shift of that peak towards lower frequencies. This relaxation peak is associated with the chain mobility,

and herefore, the shift may be explained by a small increase in the degree of crosslinking [43,44]. More significantly, the losses associated with the DC-conductivity are reduced with time, and the largest loss reduction is visible between 1 day and 2 months. This may be related to the progressing crosslinking reaction and migration of ions to the surface of the sample. According to Figure 8b, the reduction in dielectric losses with time is not directly dependent on the filler amount. Moreover, the reduction in losses is less significant than for the reference sample. This suggests that the matrix material is more subjected to time-related changes. Moreover, as the loss properties of the matrix are reduced with time, the positive effect of modified NDs on losses is reduced as well.

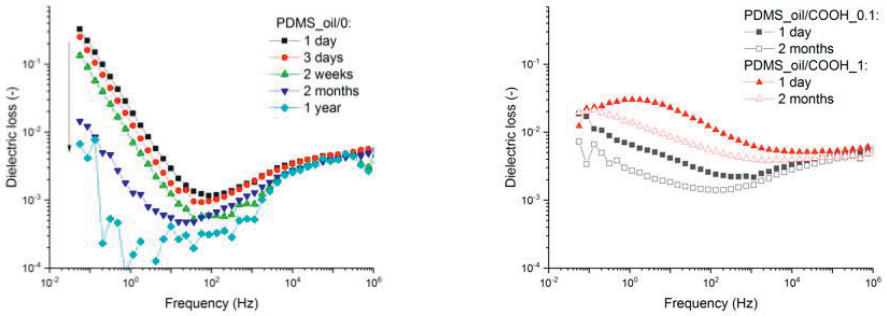

(**a**) (**b**)

Figure 8. Time-dependent dielectric loss of (**a**) PDMS_ref/0 and (**b**) PDMS with 0.1 and 1 phr of ND-COOH.

From the crosslink density results shown in Table 3, it can be suggested that the crosslinking process is most probably interfered by the presence of methoxysilane or –OH groups at the filler surface. The other ND compounds increased the apparent crosslink density to the level of non-plasticized PDMS, which may suggest certain interaction between the filler and matrix. Although the difference in apparent crosslink densities is notable, moduli change upon the plastification of PDMS and addition of NDs are marginal, as can be seen in Table 3. Due to the combination of low moduli and sufficient crosslink density, PDMS_oil/VTMS_0.1 and PDMS_oil/ED_0.1 have the highest potential for energy harvesting applications compared to the other samples.

Table 3. Moduli and apparent crosslink densities of silicone-ND composites (0.1 phr) and reference material.

Sample	Modulus, MPa			Apparent Crosslink Density 1/Q, -
	10%	50%	100%	
PDMS/0	0.12 ± 0.01	0.49 ± 0.03	1.34 ± 0.11	0.689 ± 0.005
PDMS_oil/0	0.12 ± 0.01	0.45 ± 0.01	1.38 ± 0.09	0.614 ± 0.003
PDMS_oil/COOH_0.1	0.11 ± 0.01	0.49 ± <0.01	1.13 ± 0.22	0.683 ± 0.003
PDMS_oil/VTMS_0.1	0.10 ± 0.01	0.47 ± 0.01	1.39 ± 0.02	0.674 ± 0.004
PDMS_oil/ED_0.1	0.10 ± 0.02	0.44 ± 0.01	1.38 ± 0.10	0.679 ± 0.003
PDMS_oil/GOPTMS_0.1	1 ± 0.01	0.45 ± 0.01	1.39 ± 0.03	0.554 ± 0.047

DMA is a helpful tool to study the chain dynamics and the damping properties of the materials, where the loss factor (tan δ) indicates the ratio of lost to stored dynamic energy. As seen from Figure 9, the glass transition temperature (Tg) determined at maximum tan δ is lowered upon the addition of plasticizer. The addition of fillers marginally shifts the Tg towards higher temperatures, and also lowers and broadens the transition peaks which is related to the restriction of chain mobility and the differences in the amount of amorphous phase. Additionally, it becomes clear from the insert, tan δ of the ND containing composites is lower than the reference compound indicating less energy loss. PDMS_oil/COOH_0.1 and PDMS_oil/VTMS_0.1 compounds show the lowest tan δ. Such behavior is preferable for the dielectric energy harvesting application, and maybe related to the reduced internal

friction as NDs could behave as dry lubricants facilitating the orientation of macromolecules upon the applied stress [7,45]. However, no information is available in the literature concerning the effect of filler-polymer interaction on the dry lubrication action of NDs.

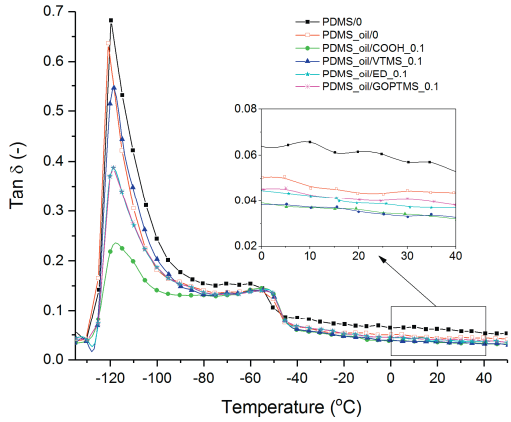

Figure 9. DMA loss tangent curves of PDMS/ND composites as a function of temperature.

According to the DSC study (Table 4 and Figure S4), both ND-COOH and modified NDs are expected to affect the orientation of the PDMS molecules. As the addition of 0.1 phr NDs resulted in the increased degree of crystallinity, NDs are expected to act as crystallization centers. Moreover, higher glass transition temperatures of PDMS_oil/VTMS_0.1 and PDMS_oil/ED_0.1 suggests stronger filler-matrix interaction, which can be due to the presence of chemical bonds. The compounds also show no cold crystallization peaks, indicating that the material was fully crystallized during the initial cooling. Although PDMS_oil/COOH_0.1 and PDMS_oil/GOPTMS_0.1 serve as crystallization centers and show similar melting behavior as the previous compounds, the increase in T_g is not very significant. This can be due to the physical nature of the filler-matrix interactions. Moreover, PDMS_oil/GOPTMS_0.1 has the highest cold crystallization peak and the lowest degree of crystallinity, which can be related to more branched and bulky modifier used for NDs.

Table 4. Glass transition temperature and crystallinity of silicone compounds measured by differential scanning calorimetry (DSC).

Sample	T_g, °C	Enthalpy, J/g		Degree of Crystallinity*, %
		Cold Crystallization	Melting	
PDMS/0	−127.0	3.26	3.84	0.9
PDMS_oil/0	−127.3	0.78	0.92	0.2
PDMS_oil/COOH_0.1	−124.8	1.45	15.37	22.7
PDMS_oil/VTMS_0.1	−120.6	-	15.47	25.2
PDMS_oil/ED_0.1	−121.6	-	14.90	24.3
PDMS_oil/GOPTMS_0.1	−126.6	9.57	13.58	6.5

* Based on the enthalpy of fusion of 100% crystalline PDMS = 61.3 J/g [46].

The mechanical losses of the samples at higher strains were studied by the cyclic loading and stress relaxation. Due to the low amount of fillers a low Mullins effect was expected. As can be seen from the Table 5, the addition of plasticizer to PDMS reduces the stress losses without notable changes in mechanical hysteresis measured at the 10th cycle. The addition of ND-COOH further reduces the stress loss percentage and hysteresis losses at the first cycle, but again resulted in no significant change after the 10th cycle. All the compounds filled with modified NDs experience a positive hysteresis reduction at the 10th cycle. For example, the hysteresis losses in PDMS_oil/ED_0.1 and PDMS_oil/GOPTMS_0.1 are 53% and 42% lower than the reference. Moreover, the stress loss after 1 and 5 min is decreased.

Such improvement can be related to the enhanced interfacial interaction between matrix and filler upon the filler surface modification. Reduction of the hysteresis loss together with smaller stress relaxation implies that the PMDS composites containing NDs are suitable candidates for the energy harvesting application.

Table 5. Hysteresis loss and stress relaxation of silicone compounds.

Sample	Hysteresis Loss, %		Stress Loss, %		
	1st Cycle	10th Cycle	after 1 min	after 5 min	after 1 h
PDMS/0	1.49 ± 0.17	0.63 ± 0.20	1.08 ± 0.04	1.77 ± 0.11	2.83 ± 0.47
PDMS_oil/0	2.21 ± 0.27	0.64 ± 0.15	0.78 ± 0.13	1.30 ± 0.28	2.26 ± 0.38
PDMS_oil/COOH_0.1	1.70 ± 0.25	0.64 ± 0.37	0.61 ± 0.17	0.96 ± 0.23	1.98 ± 0.38
PDMS_oil/VTMS_0.1	1.59 ± 0.66	0.46 ± 0.23	0.56 ± 0.09	0.86 ± 0.06	1.47 ± 0.16
PDMS_oil/ED_0.1	1.89 ± 0.71	0.30 ± 0.10	0.69 ± 0.04	1.22 ± 0.28	2.50 ± 0.41
PDMS_oil/GOPTMS_0.1	1.48 ± 0.37	0.37 ± 0.18	0.62 ± 0.12	1.07 ± 0.21	2.41 ± 0.37

4. Conclusions

The efficient surface functionalization of nanodiamonds allows coupling of the NDs to the silicone rubber matrix and can reduce the material-related losses of the composites. Carboxylated nanodiamonds were successfully modified with modifying agents containing epoxy-groups. The reaction between carboxylic and epoxy-groups at 40 °C offered a relatively easy way to decorate the ND surface with groups that can improve the interaction between ND and silicone matrix. In the case of 1,2-epoxy-9-decene containing vinyl-group ND can participate in the crosslinking process of the matrix, thus creating strong chemical interactions or in case of epoxy-compound containing silane an alkoxysilane group can be used for further surface modification. A direct reaction between carboxyl and silanol groups, however, was shown to be insufficient but due to the condensation of silanol groups a thick shell seems to be created around the ND clusters thus changing its surface.

Surface modification of NDs improved the dielectric properties of ND-silicone composites. Only 0.1 phr of NDs is enough to reduce the dielectric loss of silicones mostly due to the lower contribution from the DC-conductivity. The addition of higher amounts of NDs does not improve the properties further. Among the different modified NDs, the treatment with 1,2-epoxy-9-decene reduces the dielectric losses at 1 Hz fivefold compared to the reference, but the effect deteriorates with increasing time owing to the change in the loss properties of the matrix. The same compound also led to about twice-decreased hysteresis loss at 10th cycle and a meaningful reduction of the stress relaxation. Therefore, the application of small amounts of NDs, especially those modified with 1,2-epoxy-9-decene, can be considered beneficial to improve the efficiency of silicones applied in dielectric energy generators.

Supplementary Materials: The following are available online at http://www.mdpi.com/2073-4360/11/7/1104/s1, Table S1: Properties of carboxylated NDs, Figure S1: Chemical structure of the surface modifiers used in the study, Figure S2: FTIR-ATR spectra of the mono-silanol group modified NDs, Figure S3: TGA mass loss and mass loss rate curves for the mono-silanol group modified NDs, Figure S4: DSC curves of PDMS-ND compounds.

Author Contributions: Conceptualization, A.S., R.A., E.S., A.B. and J.V.; Methodology, A.S., R.A. and E.S.; Analysis, A.S., R.A., E.S., A.B. and J.V.; Investigation, A.S. and E.S.; Writing—Original Draft preparation, A.S.; Writing—Review and Editing, A.S., R.A., E.S., A.B. and J.V.; visualization, A.S.; supervision, E.S., A.B. and J.V.

Funding: This research was funded by Tampere University Graduate School.

Acknowledgments: This work made use of Tampere Microscopy Center facilities at Tampere University and the chemical laboratory facilities at the Elastomer Technology and Engineering chair at the University of Twente.

Conflicts of Interest: The authors declare no conflict of interest.

References

1. Dolmatov, V.; Fujimura, T. Physical and Chemical Problems of Modification of Detonation Nanodiamond Surface Properties. *Synth. Prop. Appl. Ultrananocrystalline Diam.* **2005**, *192*, 217–230.
2. Krueger, A. The structure and reactivity of nanoscale diamond. *J. Mater. Chem.* **2008**, *18*, 1485–1492. [CrossRef]
3. Zhang, Y.; Rhee, K.Y.; Hui, D.; Park, S.-J. A critical review of nanodiamond based nanocomposites: Synthesis, properties and applications. *Compos. Part B Eng.* **2018**, *143*, 19–27. [CrossRef]
4. Shakun, A.; Vuorinen, J.; Hoikkanen, M.; Poikelispää, M.; Das, A. Hard nanodiamonds in soft rubbers: Past, present and future – A review. *Compos. Part A Appl. Sci. Manuf.* **2014**, *64*, 49–69. [CrossRef]
5. Mochalin, V.N.; Gogotsi, Y. Nanodiamond–polymer composites. *Diamond Related Mater.* **2015**, *58*, 161–171. [CrossRef]
6. Shakun, A.; Poikelispää, M.; Das, A.; Vuorinen, J. Improved electromechanical response in acrylic rubber by different carbon-based fillers. *Polym. Eng. Sci.* **2018**, *58*, 395–404. [CrossRef]
7. Shakun, A.; Sarlin, E.; Vuorinen, J. Natural rubber-nanodiamond films for the minimisation of losses in dielectric energy harvesters. *Int. J. Exergy* **2018**, *26*, 170. [CrossRef]
8. Hoffstadt, T.; Graf, C.; Maas, J. Optimization of the energy harvesting control for dielectric elastomer generators. *Smart Mater. Struct.* **2013**, *22*, 94028. [CrossRef]
9. Chiba, S.; Waki, M.; Wada, T.; Hirakawa, Y.; Masuda, K.; Ikoma, T. Consistent ocean wave energy harvesting using electroactive polymer (dielectric elastomer) artificial muscle generators. *Appl. Energy* **2013**, *104*, 497–502. [CrossRef]
10. Kornbluh, R.D.; Pelrine, R.; Prahlad, H.; Wong-Foy, A.; McCoy, B.; Kim, S.; Eckerle, J.; Low, T. *From Boots to Buoys: Promises and Challenges of Dielectric Elastomer Energy Harvesting*; Springer Science and Business Media LLC: Berlin, Germany, 2012; pp. 67–93.
11. Kaltseis, R.; Keplinger, C.; Koh, S.J.A.; Baumgartner, R.; Goh, Y.F.; Ng, W.H.; Kogler, A.; Tröls, A.; Foo, C.C.; Suo, Z.; et al. Natural rubber for sustainable high-power electrical energy generation. *RSC Adv.* **2014**, *4*, 27905–27913. [CrossRef]
12. Ahnert, K.; Abel, M.; Kollosche, M.; Jørgensen, P.J.; Kofod, G. Soft capacitors for wave energy harvesting. *J. Mater. Chem.* **2011**, *21*, 14492–14497. [CrossRef]
13. Jean-Mistral, C.; Basrour, S. Scavenging Energy from Human Motion with Tubular Dielectric Polymer. Available online: http://dx.doi.org/10.1117/12 (accessed on 29 June 2019).
14. Kang, G.; Kim, K.-S.; Kim, S. Note: Analysis of the efficiency of a dielectric elastomer generator for energy harvesting. *Rev. Sci. Instruments* **2011**, *82*, 46101. [CrossRef] [PubMed]
15. Madsen, F.B.; Yu, L.; Daugaard, A.E.; Hvilsted, S.; Skov, A.L. Silicone elastomers with high dielectric permittivity and high dielectric breakdown strength based on dipolar copolymers. *Polymer* **2014**, *55*, 6212–6219. [CrossRef]
16. Madsen, P.J.; Yu, L.; Boucher, S.; Skov, A.L. Enhancing the electro-mechanical properties of polydimethylsiloxane elastomers through blending with poly(dimethylsiloxane-*co*-methylphenylsiloxane) copolymers. *RSC Adv.* **2018**, *8*, 23077–23088. [CrossRef]
17. Graf, C.; Hitzbleck, J.; Feller, T. Dielectric elastomer–based energy harvesting: Material, generator design, and optimization. *J. Intelligent Mater. System Struct.* **2014**, *25*, 951–966. [CrossRef]
18. Baidakova, M.; Vul', A. New prospects and frontiers of nanodiamond clusters. *J. Phys. D Appl. Phys.* **2007**, *40*, 6300–6311. [CrossRef]
19. Shenderova, O.; Jones, C.; Borjanovic, V.; Hens, S.; Cunningham, G.; Moseenkov, S.; Kuznetsov, V.; McGuire, G. Detonation nanodiamond and onion-like carbon: applications in composites. *Phys. Status Solidi (a)* **2008**, *205*, 2245–2251. [CrossRef]
20. Voznyakovski, A.P.; Kudoyarov, M.F.; Pozdnyakov, O.F. Self-organization and sedimentation stability of detonation nanodiamond suspensions. *Tech. Phys. Lett.* **2007**, *33*, 29–36. [CrossRef]
21. Kong, S.; Mariatti, M.; Busfield, J. Effects of types of fillers and filler loading on the properties of silicone rubber composites. *J. Reinf. Plast. Compos.* **2011**, *30*, 1087–1096. [CrossRef]
22. Neverovskaya, A.Y.; Voznyakovskii, A.P.; Dolmatov, V.Y. Structure of the dispersive medium and sedimentation resistance of suspensions of detonation nanodiamonds. *Phys. Solid State* **2004**, *46*, 662–664. [CrossRef]

23. Schrand, A.M.; Hens, S.A.C.; Shenderova, O.A. Nanodiamond Particles: Properties and Perspectives for Bioapplications. *Crit. Rev. Solid State Mater. Sci.* **2009**, *34*, 18–74. [CrossRef]
24. Krueger, A. Chapter 8 - current issues and challenges in surface chemistry of nanodiamonds. In *Nanodiamonds*; Arnault, J., Ed.; Elsevier: Amsterdam, The Netherlands, 2017; pp. 183–242.
25. Brochier Salon, M.; Bayle, P.; Abdelmouleh, M.; Boufi, S.; Belgacem, M.N. Kinetics of hydrolysis and self condensation reactions of silanes by NMR spectroscopy. *Colloids Surf. A Physicochem. Eng. Asp.* **2008**, *312*, 83–91. [CrossRef]
26. Altmann, S.; Pfeiffer, J. The Hydrolysis/Condensation Behaviour of Methacryloyloxyalkylfunctional Alkoxysilanes: Structure-Reactivity Relations. *Monatshefte Chemie-Chemical Monthly* **2003**, *134*, 1081–1092. [CrossRef]
27. Krueger, A.; Williams, O.A. (Eds.) *The Chemistry of Nanodiamond. Royal Society of Chemistry*; No. 2014-January; RSC Nanoscience and Nanotechnology: Cambridge, UK, 2014.
28. Krüger, A.; Liang, Y.; Jarre, G.; Stegk, J.; Kr?ger, A. Surface functionalisation of detonation diamond suitable for biological applications. *J. Mater. Chem.* **2006**, *16*, 2322–2328. [CrossRef]
29. Edgington, R.; Spillane, K.M.; Papageorgiou, G.; Wray, W.; Ishiwata, H.; Labarca, M.; Leal-Ortiz, S.; Reid, G.; Webb, M.; Foord, J.; et al. Functionalisation of Detonation Nanodiamond for Monodispersed, Soluble DNA-Nanodiamond Conjugates Using Mixed Silane Bead-Assisted Sonication Disintegration. *Sci. Rep.* **2018**, *8*, 728. [CrossRef] [PubMed]
30. Hajiali, F.; Shojaei, A. Silane functionalization of nanodiamond for polymer nanocomposites-effect of degree of silanization. *Colloids Surfaces A Physicochem. Eng. Asp.* **2016**, *506*, 254–263. [CrossRef]
31. Neburkova, J.; Vavra, J.; Cigler, P. Coating nanodiamonds with biocompatible shells for applications in biology and medicine. *Curr. Opin. Solid State Mater. Sci.* **2017**, *21*, 43–53. [CrossRef]
32. Li, Z.; Tatsuya, T.; Masaaki, I.; Naoko, K.; Takahide, K.; Naoki, K. Chromatographic Separation of Highly Soluble Diamond Nanoparticles Prepared by Polyglycerol Grafting. *Angew. Chem. Int. Ed.* **2011**, *50*, 1388–1392.
33. Huang, Z.; Ji, H.; Mays, J.W.; Dadmun, M.D. Understanding the Grafting of Telechelic Polymers on a Solid Substrate to Form Loops. *Macromolecules* **2008**, *41*, 1009–1018. [CrossRef]
34. Blank, W.J.; He, Z.A.; Picci, M. Catalysis of the epoxy-carboxyl reaction. *J. Coat. Technol.* **2002**, *74*, 33–41. [CrossRef]
35. Schönherr, J.; Buchheim, J.R.; Scholz, P.; Adelhelm, P. Boehm Titration Revisited (Part I): Practical Aspects for Achieving a High Precision in Quantifying Oxygen-Containing Surface Groups on Carbon Materials. *C* **2018**, *4*, 21. [CrossRef]
36. Tiwari, M.; Datta, R.N.; Talma, A.G.; Noordermeer, J.W.M.; Dierkes, W.K.; Van Ooij, W.J. Comparative Study of Plasma-Thiophene and -Acetylene Coated Silica in SBR and EPDM Reinforcement. *Rubber Chem. Technol.* **2009**, *82*, 473–491. [CrossRef]
37. Osswald, S.; Yushin, G.; Mochalin, V.; Kucheyev, S.O.; Gogotsi, Y. Control of sp^2/sp^3Carbon Ratio and Surface Chemistry of Nanodiamond Powders by Selective Oxidation in Air. *J. Am. Chem. Soc.* **2006**, *128*, 11635–11642. [CrossRef] [PubMed]
38. Bradac, C.; Gaebel, T.; Pakes, C.I.; Say, J.M.; Zvyagin, A.V.; Rabeau, J.R. Effect of the Nanodiamond Host on a Nitrogen-Vacancy Color-Centre Emission State. *Small* **2013**, *9*, 132–139. [CrossRef] [PubMed]
39. Stehlik, S.; Glatzel, T.; Pichot, V.; Pawlak, R.; Meyer, E.; Spitzer, D.; Rezek, B. Water interaction with hydrogenated and oxidized detonation nanodiamonds — Microscopic and spectroscopic analyses. *Diam. Relat. Mater.* **2016**, *63*, 97–102. [CrossRef]
40. Ji, S.; Jiang, T.; Xu, K.; Li, S. FTIR study of the adsorption of water on ultradispersed diamond powder surface. *Appl. Surf. Sci.* **1998**, *133*, 231–238. [CrossRef]
41. Efremov, V.P.; Zakatilova, E.I.; Maklashova, I.V.; Shevchenko, N.V. Thermal stability of detonation-produced micro and nanodiamonds. *J. Phys. Conf. Ser.* **2018**, *946*, 012107.
42. Casalini, R.; Roland, C. Aging of a low molecular weight poly(methyl methacrylate). *J. Non-Crystalline Solids* **2011**, *357*, 282–285. [CrossRef]
43. Roggero, A.; Dantras, E.; Paulmier, T.; Tonon, C.; Lewandowski, S.; Dagras, S.; Payan, D. Dynamic glass transition of filled polysiloxane upon electron irradiation. *J. Non-Crystalline Solids* **2017**, *455*, 17–23. [CrossRef]

44. Glatz-Reichenbach, J.K.W.; Sorriero, L.; Fitzgerald, J.J. Influence of Crosslinking on the Molecular Relaxation of an Amorphous Copolymer Near Its Glass-Transition Temperature. *Macromolecules* **1994**, *27*, 1338–1343. [CrossRef]
45. Dolmatov, V.Y. Polymer—Diamond composites based on detonation nanodiamonds. Part 3. *J. Superhard Mater.* **2007**, *29*, 199–205. [CrossRef]
46. Maus, A.; Saalwächter, K. Crystallization Kinetics of Poly(dimethylsiloxane) Molecular-Weight Blends—Correlation with Local Chain Order in the Melt? *Macromol. Chem. Phys.* **2007**, *208*, 2066–2075. [CrossRef]